THERMAL AND HYDRODYNAMIC STUDIES OF A ROTATING FLUIDIZED BED DRYER WITH STATIC GEOMETRY

A Thesis

Submitted in Partial Fulfilment of the Requirements for

The Award of the Degree of

DOCTOR OF PHILOSOPHY

by

PAVITRA SINGH

(REGISTRATION NUMBER: 166151001)

SCHOOL OF ENERGY SCIENCE AND ENGINEERING

INDIAN INSTITUTE OF TECHNOLOGY GUWAHATI

GUWAHATI-781039

March, 2021

This thesis is dedicated to my parents

Late Smt. Ramashri Devi

and

Late Shri Chhitar Singh

Declaration

I hereby certify that the information presented in this thesis is entirely my own account of my research and contains at its main content work except where otherwise stated, which has not previously been submitted for a degree or diploma at this institute or any tertiary educational institution.

Date: 1-03-2021

Pavitra Singh

Regd. No. 166151001

School of Energy Science and Engineering

Indian Institute of Technology Guwahati

Guwahati - 781039, India

School of Energy Science and Engineering
Indian Institute of Technology Guwahati
Guwahati-781039
INDIA

Certificate

It is certified that the work contained in the thesis entitled **Thermal and hydrodynamic studies of a rotating fluidized bed dryer with static geometry** by **Pavitra Singh (Regd. No. 166151001)**, a student in the **School of Energy Science and Engineering, Indian Institute of Technology Guwahati, India**, for the award of the degree of the **Doctor of Philosophy** has been carried out under our supervision and this work has not been submitted elsewhere for a degree.

Prof. Pinakeswar Mahanta
Professor
Department of Mechanical Engineering
Indian Institute of Technology Guwahati
Guwahati-781039, India

Dr. Pankaj Kalita
Assistant Professor
School of Energy Science and Engineering
Indian Institute of Technology Guwahati
Guwahati – 781039, India

Acknowledgement

First of all, I take this opportunity to express my profound gratitude and deep regards to my supervisors, Professor Pinakeswar Mahanta and Dr. Pankaj Kalita for his exemplary guidance, monitoring, constant support and encouragement throughout my doctoral research tenure. The blessing, help, guidance and advice given by him, are the key factors in shaping this work to its present form.

I would like to thank my doctoral committee members, Professor U.K. Saha, Dr. Harsh Chaturvedi, and Dr. R. Anandalakshami, for their valuable suggestions at different stages of my research.

I would like to thank Professor Kaustubha Mohanty H.O.S, School of Energy Science and Engineering, Indian Institute of Technology Guwahati for his valuable help and guidance.

I would like to extend my gratitude to Dr. Ankita Gaur, Dr. Lepakshi Barbora, Mr. Debarshi Baruah and Mr. Dhiren Huzuri, for their constant support and technical advice. I also thank Mr. Paragjyoti Sharma, and all the staff of School of Energy Science and Engineering, IIT Guwahati for their help.

I wish to thank Mr. Dilip Chetri, and other staff members of Central Workshop for helping me in various stages of the experimental setup fabrication. Without their timely support, this work could not have been accomplished.

I am thankful to many friends at IIT Guwahati. Special mention to acknowledge, Mr. Abinash Mahapatro, and Mr. Rishiraj Purkayastha, for their suggestion, technical support and help during my experiment time. Dr. Pankaj Kalita, Dr. L. Barbora (Scientific Officer) School of Energy Science and Engineering, IIT Guwahati, Rituraj Saikia, and Mr Abinash Mahaparto here are being with me in good and difficult times through these years. Special thanks to Dr. Anita Mahanta for her kind support and encouragement in my social life, which is unforgettable forever. I am very much grateful to my beloved parents, family members, my wife Mrs. Suneeta Singh, son, Shreyash Singh and daughter Shreya Singh and all other relatives for their immeasurable love, understanding and unwavering support, which has made this feat possible.

Last but not the least I place a deep sense of gratitude to my parents and family, who have been a constant source of inspiration throughout this project.

Pavitra Singh

ABSTRACT

Lack of supply of good quality food worldwide is a major problem from the point of view of imbalance in production and consumption. Post-harvest losses in developing countries have reached 10%, and food preservation is the only way to reduce food losses. Drying of food is an essential energy-intensive technique to reduce damage to the product and increases its shelf-life by inhibiting the growth of enzymatic reactions, microorganisms, and other deteriorating reactions. Most dryers available in the literature are low-efficient and requires large space. The fluidized bed technique is one of the emerging drying techniques that reduces the drying time, by maintaining the product quality and nutritional value. However, conventional fluidized beds are well-performing dryers and have been in use for many years. Nevertheless, few demerits such as large in size, expensive, need for rotating seal, difficulty in solid loading, and unloading during the operation were incorporated with these dryers. All the drawbacks of traditional fluidized beds were eliminated in the recently developed rotary fluidized-bed (RFB) dryer. Nevertheless, few demerits of RFBs such as vibration during operation, wear-tear of moving elements, and particle breakage reduce their significance. To minimize the demerits of RFBs, an innovative technique of a RFB dryer with static geometry was reported. Though RFB-SG dryers have salient features, there is a need to increase system capacity at the commercial level, which is quite difficult due to system complexity. The present research is focused on the development and performance analysis of a rotating fluidized-bed dryer with static geometry (RFB-SG) without slit. In the present study, the performance of the RFB-SG dryer with and without slit has been evaluated experimentally numerically. Further, the experimental results of the RFB-SG dryer without slit and RFB-SG dryer with slit are compared. For the drying of 400 g paddy at the operating temperature of 338 K, and air flowrate of 600 m^3/h the drying efficiency of the RFB-SG dryer without slit is found to be 20.45% higher than RFB-SG dryer with slit. Also, numerical findings of RFB-SG unit without slit were experimentally validated. Based on the experimental results, the scale-up of the best performing laboratory level RFB-SG unit without slit has been carried out for the solid loading capacity of 3370 g.

Contents

Nomenclature

A	:	Cross sectional area (cm^2)
a_c	:	Centripetal acceleration (m/s^2)
C_D	:	Drag coefficient
C_{pda}	:	Specific heat of dry air (kJ/kg K)
D	:	Diameter of the vortex chamber (cm)
D_j	:	Diameter of the jacket (cm)
E	:	Bed voidage
Ex	:	Exergy of the system
F_D	:	Drag force (N)
g	:	Acceleration due to gravity (m/s^2)
I	:	Solid inventory (g)
K	:	Thermal conductivity (W/m K)
K_1, K_2	:	Drying constant (min^{-1})
L	:	Length of dryer (cm)
L_r	:	Bed height (cm)
dM/dT	:	Moisture gradient
ΔMC_p	:	Moisture content difference of product
m_a	:	Mass flowrate of drying air (m^3 /h)
m_i	:	Initial weight of (paddy) sample (kg)
m_f	:	Final weight of sample at end of drying (kg)
$m_{f\,u}$	:	Minimum fluidization velocity (m/s)
m_p	:	Mass flowrate of product (g/s)
m_w	:	Mass flowrate of water (g/s)
m_{wp}	:	Mass of the wet paddy (kg)
N	:	Drying parameters
n	:	Number of slots
n_{rot}	:	Number of rotation
p_d	:	Mean particle diameter (mm)
ΔP	:	Pressure difference (m bar)
Q_g	:	Volumetric gas flow rate (Nm^3 /h)
R_e	:	Reynold's number
s	:	Slot-width (mm)

T_a	:	Air inlet temperature (K)
T_o	:	Atmospheric temperature (K)
T_1	:	Operating temperature of the air (K)
T_2	:	Dry product temperature (K)
T_3	:	Outlet temperature in (K)
t	:	Drying time (min)
U_g	:	Non dimensional fluidizing velocity
U_{mf}	:	Minimum fluidization velocity (m/s)
U_{sf}	:	Superficial velocity (m/s)
U_{sup}	:	Superficial velocity (m/s)
U_t	:	Terminal velocity (m/s)
u_{tg}	:	Gas tangential velocity (m/s)
t_u	:	Terminal velocity of particle (m/s)
V	:	velocity of the fluidizing air (m/s)
X	:	Moisture content ratio
Y	:	Scaling parameter
ϕ_{am}	:	Moisture of the ambient air
ρ_{da}	:	Density of dry air (kg/m^3)
ρ_{dp}	:	Density of dry paddy grain ((kg/m^3)
ρ_{ma}	:	Density of moist air ((kg/m^3)
ϕ_{wp}	:	Moisture of the wet paddy (g water/kg air)
ϑ_{fc}	:	Volume of the vortex chamber (m^3)
β	:	Drag-coefficient
λ	:	Force ratio
φ	:	Relative humidity
A	:	Cross sectional area (cm^2)
a_c	:	Centripetal acceleration (m/s^2)
C_D	:	Drag coefficient
C_{pda}	:	Specific heat of dry air (kJ/kg K)
D	:	Diameter of the vortex chamber (cm)
D_j	:	Diameter of the jacket (cm)
Ex	:	Exergy of the system
F_D	:	Drag force (N)

g	:	Acceleration due to gravity (m/s^2)
I	:	Solid inventory (g)
K	:	Thermal conductivity (W/m K)
L	:	Length of dryer (cm)

Abbreviations

AFR	:	Air flow rate
BFP	:	Biomass Feeding Pipe
DAS	:	Data Acquisition System
EUR	:	Energy Utilisation Ratio
FMC	:	Final Moisture Content
IMC	:	Initial Moisture Content
MC	:	Moisture Content
RH	:	Relative Humidity
RFB-SG	:	Rotating Fluidized-Bed with Static Geometry

List of figures

List of tables

CHAPTER-1

INTRODUCTION

1.1 MOTIVATION

Food is essential in daily life to provide nutrients to our bodies. From this point of view, rice is considered to be staple food in South-East Asian countries. South-East Asia ranks first in rice cultivation, and India is the second-largest rice-producing country worldwide. India cultivates around 285.01 million tons of food grain annually, including paddy around 115.63 million tons (MT), wheat about 101.20 million tons (MT), coarse cereals 43.33 million tons and pulses about 23.22 million tons (MT). Post-harvest technology related to the processing of food grain is highly expensive. Unfortunately, a large amount of food-grain (around 10% of total grain) is lost during post-harvesting process, from drying-place to the market. This is a tremendous loss which is equivalent to approximately 4000 million Indian rupees. Improper and uneven drying operation of food grain leads to deteriorating quality, cracks in the grains, and also a loss of nutrients. Though sun-drying is the cheapest and traditional method, it is not a good quality process due to being completely weather dependent which causes the damage of foods by birds and rodents as well as mould growth [Prasad et al. (2006)]. An efficient and economic natural convection dryer for a range of input parameters has reported but it takes significantly large drying time [Mohaparta and Mahanta (2012)]. Moreover, solar drying is cost-effective, more hygienic, and faster than sun drying, but the major disadvantages of this dryer is its low drying capacity and no control over the process [Ayensu (1997)]. Mechanical driers are also gaining importance due to better control over-drying parameters such as close control of temperature, drying rate, moisture content, etc., but these dryers are comparatively higher in cost. Fluidized bed drying is one of the technologies emerging out to the market which has higher heat and mass transfer capabilities. Fluidized bed dryers offer easy materials transport, higher thermal efficiency due to heat exchanging phenomena without overheating of the particles. As compared to the conventional fluidized bed drying a new concept of a rotating fluidized-bed (RFB) technique was developed which has the higher heat and mass transfer capabilities due to higher gas-solid slip velocity. However, RFB

dryers have high heat and mass transfer capacity through small-sized dryers. Nevertheless, a few imperfections such as vibration, particle breakage, higher cyclic-maintenance, wear-tear of parts, etc. disgrace its reliability.

The present work is an endeavour towards the development of rotary fluidized bed dryer with static geometry without slit so as to achieve better performance in drying of cereal grain.

1.2 PURPOSE OF DRYING

A freshly-harvested crop contains a lot of moisture and natural respiration that causes the deterioration of the grain quality. Also, the presence of high moisture in the grains arises the development of moulds and harmful insects in food grains. The prescribed moisture content (MC) level for safe storage of grain is shown in the following Table 1.1.

Table 1.1 Safe MC level required in paddy storage [IRRI (2005)].

Period for safe storage	Level of required % of MC in paddy for the safe-storage	Various potential problems
2-3 weeks	14-18%	Respiration loss, moulds and dis-coloration,
Around 8 to 12 months	13% or less	Insect harm
More than 12 months	9 % or less	Loss of viability

The following three conditions must be met for long-term storage and preservation of grains:

[1] Safety of grain from insects and rodents.

[2] Protection of grain from re-wetting by rain or atmospheric moist air.

[3] The moisture content (MC) in stored grains should be lower than the safe MC level (13–14%) of that food grain, but it experiences rapid loss of mold growth and viability [IRRI (2005)].

1.3 PRINCIPLE OF DRYING PROCESS

Drying is the process of removing moisture of wet-solids by circulating hot air. The hot drying air evaporates the moisture contained in the food grains and the drying air carried it away from the surface of the grain as shown in Fig. 1.1. For the effective drying of paddy, the air must be hot and dry, and the moisture must be trans-migrated from food grain (paddy) to its surface, as this is where moisture is exchanged with the air.

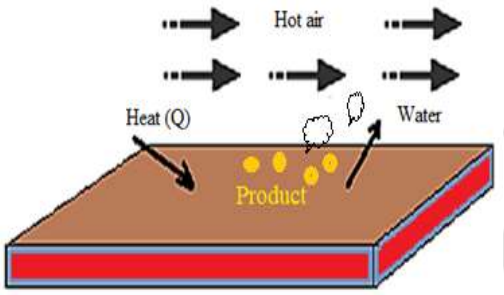

Figure 1.1 Air movements over the surface of food grain being dried [Sankat (2006)]

There are several methodologies to dry agricultural products such as steam or freeze-drying, infrared drying, chemical methods, microwave drying, mechanical, and fluidization methods, etc. Drying with the circulation of hot air is the most popular and economical method [Jangam (2011)]. Even waste heat of any thermal unit may be a source of this hot air. Hot air passing over the surface of the food grain forms a thermal boundary layer with a steep thermal gradient with the grain surface rendering evaporation of moisture from a grain surface. Thus, the hot air drying involves the contemporary action of heat and mass transfer. To maintain uniformity in drying operation, a thin layer of the product (thickness < 20 cm.) is most suitable [Chakraverty (1981)]. The variations of moisture contents of a product have been represented in the standard drying curve, as shown in Fig. 1.2 [Mujumdar (2007)]. The drying process is completed in two stages, the first phase of which is to remove the 'surface moisture,' and the second phase is to remove the 'internal moisture' from the food grains. There are two different rules of operation of drying which are as follows: (1) constant rate period A-B and (2) Fall rate period B-C.

1.3.1 CONSTANT RATE PERIOD

During the constant rate period, the surface of the grain is still wet, and the drying rate is controlled by evaporation of free moisture from the surface of the product or near-surface areas. The shape and size of the particles, air velocity, and air temperature, can significantly

influence the drying rate [Sankat (2006)]. As the name suggests, the gradient of moisture removal rate remains constant. The phenomenon incorporates equalizing the vapor-pressure at the grain-surface with saturated vapor-pressure, at the temperature of grain-surface. The process of food grain drying is subjected to the rate of vigorous heat and mass transfer. Concentrated heat transfer is a predominating mode in this regime. The moisture removal rate from the product surface can be expressed in equation (1.1) given by [Zaman and Bala (2001)].

$$\frac{dM}{d\tau} = -k\,A\,\left(M_g - Me\right) \tag{1.1}$$

where M_g, M_e, k, τ and $dM/d\tau$ are moisture content of the grain, equilibrium moisture content (EMC), drying constant, drying time and the moisture gradient, respectively. It can be witnessed in figure 1.2 that the moisture removal rate at point B remains constant. Also, it is known as critical moisture content (CMC) of the product.

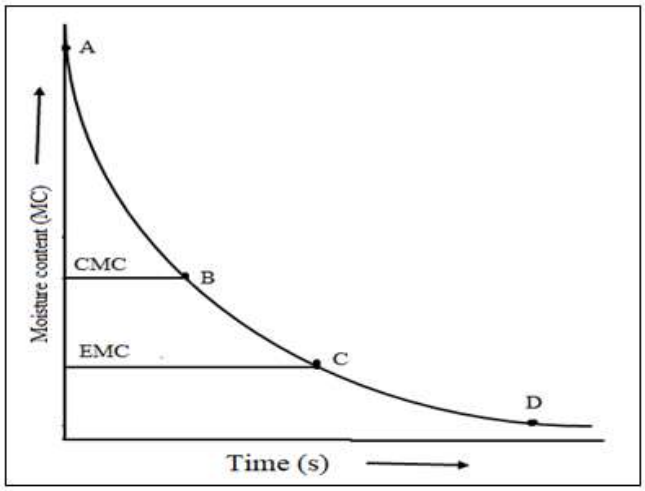

Figure 1.2 Drying Process [Mujumdar (2007)]

1.3.2 FALLING RATE PERIOD

It is a second stage of the drying operation, once it starts, the vapor-pressure at grain-surface drops below the saturated vapour pressure. Alternatively, the falling rate period commences subsequent to the crossing of critical moisture content (CMC). The temperature of the particle surfaces no longer remains constant; rather, there will be an increase in temperatures both at the surface and the core of the product. During this period, the rate of moisture removal can be determined by intra-particle diffusion limitation. This is the phase at which the rate of transfer of water from the inner surface to the particle surface decreases

with the evaporation rate of water from the surface. However, the properties of the product or particle do not affect the duration of the constant rate. Point D showed in Fig. 1.2 states that the product comes to a state of equilibrium with the ambient at a particular state of moisture. Also, it is called equilibrium moisture content (EMC). Some of the recommended EMC values with different periods of paddy storage are enlisted in Table 1.1 [IRRI (2005)].

1.4 DIFFERENT TYPES OF DRYER AND DRYING METHODS

Many methods have been devised for drying of agricultural products or grains, yet no ideal dryer seems to have been developed. Each drier has its own inherent abilities and demerits. A various selected dryers and drying methods are listed below in Table 1.2 and Fig. 1.3.

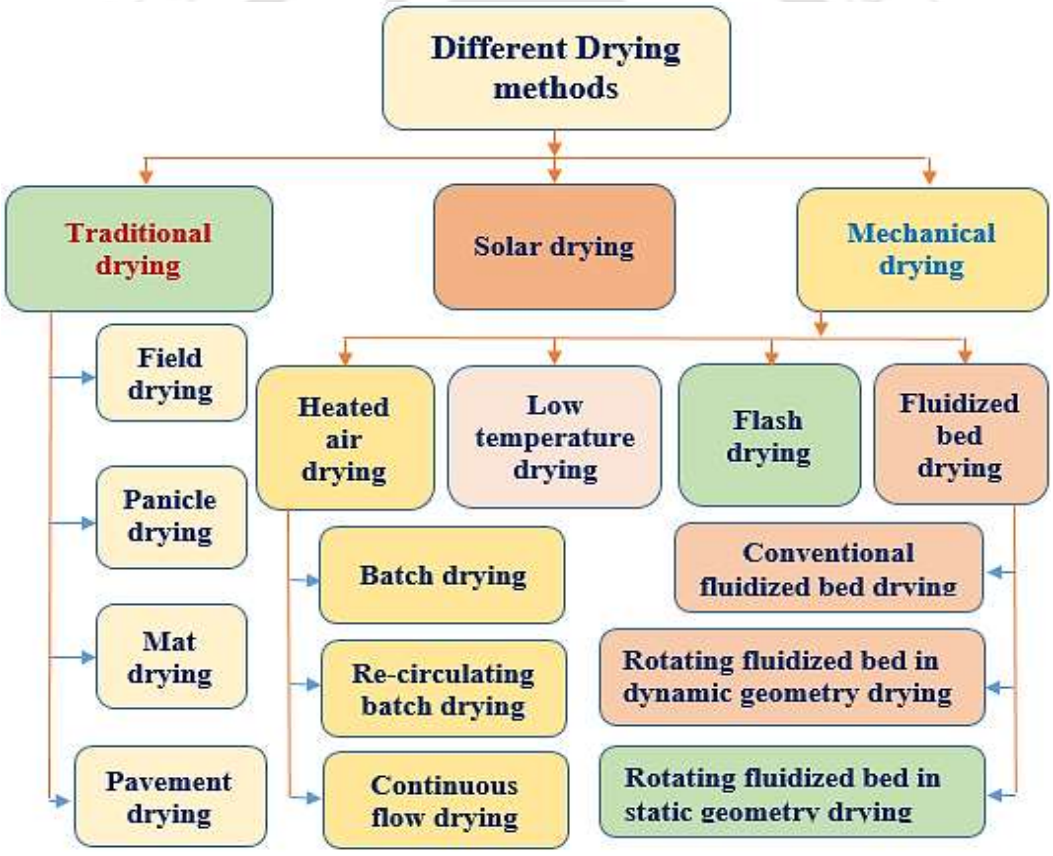

Figure 1.3 Schematic diagram of dryer classification

Table 1.2 Different type of dryers and drying methods

Dryer and drying methods	Description	Advantages/disadvantages
Traditional drying		
Open sun-drying	It is the oldest technique of reducing the MC of food grains by dispersing the grains in the sun. The sun heats both the surrounding air and the grains.	Limited drying capacity, labor-intensive, and unavailability of the sun at night and in the rain. Due to this delay fungal growth in the seeds, Re-wetting or overheating of grains can result in low milling quality, cracks in the kernels.
Field drying	The paddy that dries in the field is spread over an open field before it is pierced. This can reduce the moisture content by about 1% per day	Damage to rodents and birds when it spreads in the area. When the paddy poured as the pile and it re-wetted with straw in a pile
Panicle drying	This is a sun-drying method for a small amount of grain or cereal.	Moisture removal rate inside the panicle is very slow.
Pavement drying	Pavements are need to be constructed to perform drying. It is frequently used by traders, grain collectors, millers, and better-off farmers, use this drying method.	However, it has high capacity, and it can partially mechanize, but it has few demerits of pollution with dirt transpire in cereal.
Woven mat drying	It is one of the hygienic methods of sun drying. In	The main disadvantage of this process is the Re-wetting of paddy

	this method of cereal or grains are placed in nets, mats, or plastic sheets.	in the bottom location by the moisture of the soil.
Solar drying		
Direct solar dryers	In this process, air is heated in the drying chamber that acts as both the solar collector and the dryer. The sun's radiation passes through the roof of the transparent dryer, normally glazed with plastic foil and heats the dryer chamber, which is ideally black painted for the purpose of maximum absorption of heat. It can be used in coconut, fish, and chili drying.	This drier is cheap in cost, comparatively more hygienic, and drying faster than sun drying. The efficiency of this dryer declines during rainy or cloudy weather and is difficult to use at night. The major hindrance of this drier is the low drying capacity and no control over.
Indirect solar-dryer	Solar dryer comprises two parts, namely the solar collector and solar drying cabinet. The solar collector first receives the sun's radiation and transfers it to the connected drying container. In the collector zone, the air is heated. Subsequently, the density difference results in natural air circulation.	Efficiency of this dryer declines during rainy or cloudy weather and is difficult to use at night. It is difficult to extend the limit of solar dryers without re-building fragile structures. A mixed dryer was taken into consideration to overcome these problems.

Mixed solar dryers	In this dryer, burning fuel is used as a back-up source of heat to free it to deal with conditions that do not have a favorable weather condition. A wide range of products is dried in these dryers and have better drying control as well as greater drying capacity than solar dryers.	A major disadvantage of these dryers is the higher cost as compared to direct solar dryers.
Mechanical dryers are gaining importance due to close control of temperature, drying rate, moisture, etc. can be maintained.		
Batch dryers	Airing temperature is maintained according to the type of material used for batching the material. The dyeing process is completed in about 6-12 hours, and its capacity is 1 to 3 tons per day. In this dryer, rice bran or kerosene is used as fuel.	These dryers are simple but expensive and labor-intensive. In addition, there is a wide variety of moisture in the vertical direction of the drying tray.
Re-circulating batch dryers	These are automatic process type dryers that can be installed on a low floor and also provide excellent quality of the grain.	Their drying capacity is 4–12 tonnes per batch for 8 hours per day
Continuous flow dryers	Wet paddy was introduced from its top, which continuously flows through the drying chamber where	This is the low impact of high investment costs as they are able to dry quickly in large quantities; the operating cost per ton can be

	the hot air is passes through across it. This dryer is designed in such a way that it takes 15-30 minutes to pass through the dryer. Meanwhile, the moisture of the product decreases by 1-3%.	compared with both large-sized batch dryers and re-circulating dryers.
Fluidized bed drying		
Fluidized bed dryers	In this drying technique, either the hot air is supplied across the fluidized beds of granular materials. These are applicable to a wide range of non-heat sensitive and heat sensitive products. Under controlled fluids (approximately 2.3 m/s), the air is passed through the product layer of thickness of 10 cm to form a fluidized bed. It is the state in which the particle is exposed to dry air for about 10–15 minutes. The capacity of the commercial drying unit is 1–10 tons/hour.	The fluid bed drying method has significant advantages compared to other methods of particle drying. Particle liquefaction prevents easy material transport, a high rate of heat transfers at high thermal efficiency, and excess heat of particles. A rice hull furnace or diesel burner can be used as a heat source. It improves the efficiency of the drying system, by recycling of 50–70% drying air.
Rotating fluidized bed (RFB) dryers	These are different from the conventional type of fluidized bed because their body force in the centrifugal	These are capable of flowing a large volume of air withstanding the particle bed without bubble formation. It results in better

	bed, is adjustable by the radius and rotating speed of air distributor when the conventional fluidized bed has a fixed gravity field. In the RFB, the strong centrifugal field is much higher than gravity.	contact among gas and solid phases at an airflow rate.

1.5 ORGANIZATION OF THE THESIS

This thesis comprises seven Chapters. Chapter 1 introduces the motivation, background, and outline of the thesis. Comprehensive literature concerning drying techniques and processes are presented in Chapter 2. Based on the literature survey, the research gaps were identified, and the objectives of the thesis were formulated. Furthermore, the research that has been carried out on drying at IIT Guwahati is also described in this chapter. The description of the experimental setups, and experimental procedures, are presented in the Chapter 3. In Chapter 4, numerical simulations of a three-dimensional model of a RFB-SG unit without slit is performed. In Chapter 5, parametric studies on paddy drying in both the dryers viz. RFB-SG with and without slit have been carried out. The quality of the product (particle breakage) was tested in terms of milling index. Furthermore, the numerical outcomes of RFB-SG dryer without slit are validated with the experimental outcomes. On comparison of drying performance of lab scale setups, the RFB-SG dryer without slit has been found best performing dryer. Hence, scale-up of lab scale RFB-SG unit without slit is carried out numerically in terms of length to diameter (L/D) ratio. In Chapter 6, a detailed thermodynamic and thermo-economics analysis of the developed dryers have been carried out. Summary of the research findings and scope for the future works are presented in Chapter 7.

CHAPTER-2

LITERATURE REVIEW

2.1 INTRODUCTION

This chapter highlights the worthwhile efforts of researchers, reviewing their literature on quality maintenance of food grains, a parametric study on quality drying of grains, considering various aspects of drying techniques, such as open sun drying, solar drying, hybrid drying, fluidized bed drying, rotating fluidized bed with static geometry (RFB-SG). Food grain drying is an energy-intensive operation by which the water content of the grain is reduced. Drying process prolongs the shelf-life of bio-genesis product (grain) by reducing the bad effect of water in the grain. A summary of the literature review and scope of research works is presented at the end of the chapter.

2.2 PARAMETRIC STUDY OF QUALITY OF DRIED FOOD

There are two ways to determine the food quality either by objective [IRRI, (2002)] or subjective. In the subjective method, an individual can determine the quality based on the requirement, such as the appearance, taste, and smell of the product. On the other hand, the objective method comprises the characterization of chemical and physical attributes. Bakker-Arkema and Salleh (1995) and IRRI (2002) determined the quality of paddy on the basis of different physical characteristics, namely varietal purity, moisture content maturity, discoloration, cracks, and breakage. Also, some other characteristics of grain quality such as head rice yield (HRY), cooking qualities, and colour were also considered [Zhang et al. (2003)].

Biochemical changes occur in the grains during the drying process, which results in colour change and odour of the paddy, as well as heat, moisture, and insect deteriorate the quality of paddy [Bakker-Arkema et al. (1985); IRRI, (2002)].

Over exposure of food grains to mechanical effects and uneven drying temperatures causes cracks in the kernels that lead to the development of insects and mould [Dong and Zhihuai (2003)]. Also, it was found that the removal of grain's moisture content at high temperature

reduces the concentration of the aroma constituent of the grain that results in degradation of grain quality [Wongpornchai et al. (2004)].

2.3 PARAMETRIC STUDY ON DRYING

2.3.1 EFFECT OF RELATIVE HUMIDITY (RH)

Henderson (1957) investigated the influence of relative humidity (RH) in the range of 8-65%. They found that the high rice yield (HRY) of total grain was decreased with the decrease of relative humidity (RH), and increase of the operating temperature. Kunze and Prasad (1978) had studied the effect of humidity on the harvested paddy and reported that a low moisture paddy fissures more when it subjected to high relative humidity. Also, a similar study was carried out by Tabassum and Jindal (1992), and they noticed that moisture removal rate was faster at a lower RH as compared to higher RH.

Chakraverty (1994) had conducted an experimental investigation on the effect of relative humidity. He reported that the moisture removal rate was decreased slightly, while the effect of RH was very less as compared to the effect of increase of operating temperature.

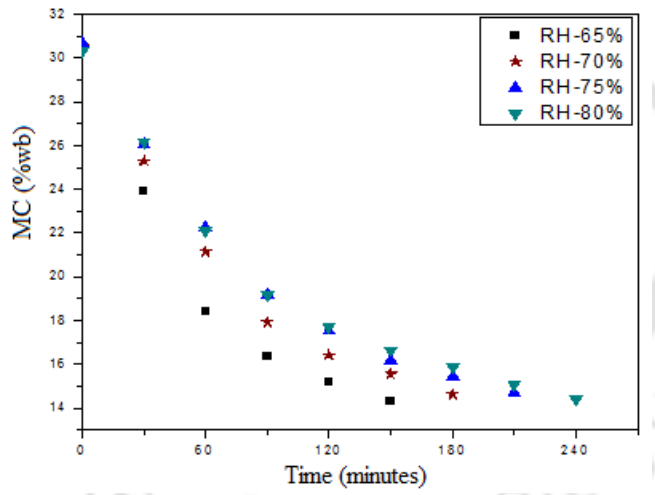

Figure 2.1 Variation of average moisture content with time at different RH [Mohapatra and Mahanta (2012)]

The low RH and high-temperature surrounding the kernel caused rapid evaporating capability and the moisture gradient was also found to be increased [Nag (2008)]. Mohapatra and Mahanta (2012)] had accompanied experimental analysis of drying a natural convection dryer (NCD) as illustrated in Fig. 2.1. They reported that with the increase of relative humidity from 65% to 80%the moisture removal rate was decreased and the drying time increased from 150 - 240 minutes.

2.3.2 EFFECT OF DRYING AIR TEMPERATURE

Thompson et al. (1955) had studied the effect of temperature (24–60°C) on the drying characteristics of small size paddy-grains. They proclaimed that both the high rice yield (HRY) and drying time were lessened by increasing the drying air temperature.

Chakraverty (1975) had conducted experiments to investigate the effect moisture removal rate at different operating conditions by exposing paddy grains. It was reported that the percentage of the moisture content of 13.5%,12.5%, 11.5%, and 10.5% were obtained in the short duration of time of 5-20 minutes, at the inlet air temperature of 45- 85°C. Also, they reported that both the high rice yield (HRY) and the percentage of moisture content were decreased by increasing drying air temperature.

Tabassum and Jindal (1992) studied the effect of drying air temperature on the moisture removal rate of the grain. They affirmed insignificance of the moisture removal rate at an operating temperature of 40°C. Nevertheless, Yadollahinia et al. (2008) studied the effect of the air temperature of 30-70°C on paddy drying and stated that with the increase of air temperature, the drying rate of paddy was increased. Also, the hot air drying is the most commonly used technique in dehydration of the food products, they observed that the quality of food products is sensitive to the drying air temperature [Luangmalawat et al., (2007)].

2.3.3 EFFECT OF AIR FLOW RATE

Henderson, (1961) had reported the significance of a natural convection dryer on the influence of the airflow rate on the moisture removal rate. Also, he reported that the airflow rate had no noticeable effect on thin-layered wheat drying for the turbulent flow of the drying air. Also, it was reported that the airflow rate significantly affected the drying rate of paddy and corn. Furthermore, in a similar kind of observation drying air temperature was found to have the highest effect on the drying rate followed by air velocity as well as initial moisture content of the grains [Hustrulid (1962, 1963)].

Tabassum and Jindal (1992) had studied the effect of air flow rate (0.2-0.52 m^3/s) on the moisture removal rate as shown in Fig. 2.2. They reported the significance of drying rate under the effect of airflow rate.

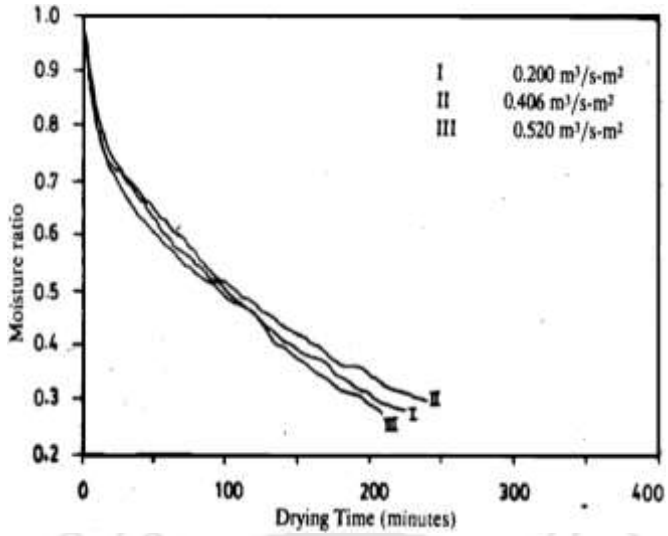

Figure 2.2 Effect of airflow on moisture removal rate [Tabassum and Jindal (1992)]

Akpinar et al., (2003) and Yadollahina et al., (2004) had conducted experimental investigation on the moisture removal rate of paddy, considering the effect of air velocity on the drying time. They reported that a very low effect of drying air velocity on the moisture removal rate was observed. Also, Ndukwu (2009) reported that the drying air flow rate plays a significant role in the moisture removal rate in case of forced convection drying.

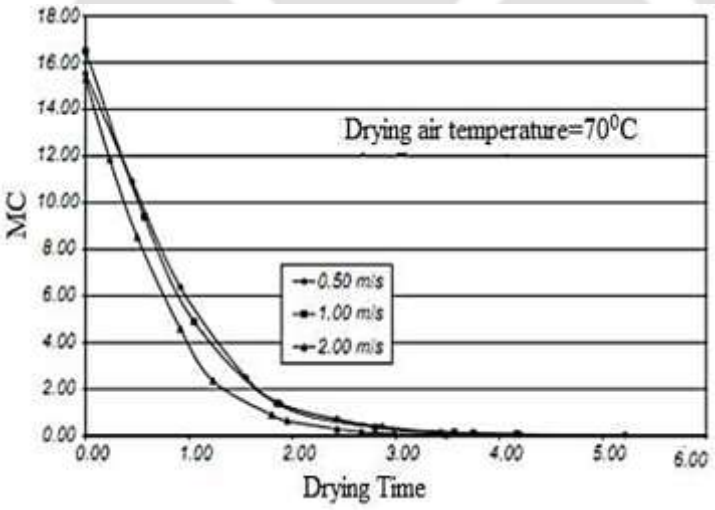

Figure 2.3 Effect of air velocity on drying time [Ertekin and Yaldiz (2004)]

A drying experimentation in the eggplant was carried out in view of many variables such as drying time, temperature, and air-velocity as shown in Fig 2.3. They reported that with the increase of drying air velocity from 0.5-2 m/s at the drying temperature of 70°C, the drying time was found to be decreased by 2 hours [Ertekin and Yaldiz (2004)]. In addition,

wheat drying in a fluidized bed dryer in batch was conducted, considering different operating parameters such as air inlet temperature, drying time, and the mass flow rate of the air. It was reported that the moisture removal rate was increases with the increase of the mass flowrate of drying-air from 0.1-0.264 kg/s and the drying temperature of 40-70°C [Özbey, M. and Söylemez (2005)].

2.4 TRADITIONAL DRYING

In general, traditional sun drying is the most popular method widely used in Asia and other tropical and subtropical countries [Togrul and Pehlivan (2002)]. Zaman and Bala (2001) reported that it is a very time-consuming drying method, during which so many complications were observed to maintain the quality of the product due to fluctuation of temperature. It needs many more days to dry grain in the cloudy and rainy season [(Zaman and Bala, 2001)]. However, this drying method is economical but the workforce required for a long time of 1-3 days after threshing makes the product costly. Quality is also not found satisfactory [Imoudu and Olufayo (2000)]. It was also reported that sun drying is not suitable for large scale drying due to improper process and control of the operation [Basunia and Abe (2001); Toğrul and Pehlivan (2004)].

2.5 DRYING CHARACTERISTICS OF DIFFERENT TYPES OF DRYER

Open sun drying is not preferable for quality drying of the grains due to unfavourable climatic conditions in the rainy season and night. Because the drying temperature is tough to control, which fixes the drying time and drying delays the loss of grain and deterioration of quality, it motivated the researchers to develop newer paddy dryers worldwide.

2.5.1 NATURAL CONVECTION DRYERS

Ayensu (1997) and Gbaha et al. (2007) had developed an experimental set-up of a solar dryer easily at a meager cost, using locally available materials such as wood, metals, and glass. It was reported that it could potentially operate at a low temperature. Ayensu (1997) had reported that the moisture content (MC) in solar drying is reduced to 14% by using atmospheric air of 32°C temperature and RH of 80%, respectively. Gbaha et al. (2007) conducted drying operations experimentally in the natural convection dryer, using drying material cassava and bananas. They reported the MC of cassava and bananas was reduced significantly from 80% to 13%. Forsona et al. (2007) had conducted a drying operation in a

dual kind of dryer using a mixed-mode of natural convection and solar dryer. They had also reported that the MC of cassava was significantly reduced.

Basunia and Abe (2001) had studied a mixed-mode type natural convection solar dryer for rough rice drying in thin layer. They also stated that the relative humidity of the surroundings was decreased from 57.9-34.5% for the drying air temperature range of 22.3-34.9°C. Diamante and Munro (1993) had implemented drying data with Page model-based ratios of the differences between the initial moisture content and equilibrium moisture content of the drying material. They had proclaimed an error of 0.38% ±db in moisture contents.

El-Sebaii et al. (2002) had developed an indirect kind of flat-plate natural convection solar air heater and conducted drying operations using agricultural products like tomato, green peas, apple, and seedless grapes. They used sand as a thermal storage medium to improve the dryer process and observed that the drying time was significantly reduced at the air temperature of 45.5-55.5°C. A natural convection solar-energy driven dryer was developed comprising of a drying chamber with the solar air heater. They found an energy-intensive drying process that reduced the drying time by 4 days, as compared to shade drying (15 days) and open sun drying (7 days) [Pangavhane et al. (2002)].

Mohaparta and Mahanta (2011) had conducted paddy drying experimentation in a thin layer of drying material in an Indirect kind of a Natural Convection Dryer. They conducted drying operations of 10 kg, 15 kg, 20 kg, and 25 kg paddy of initial moisture content 30.5% and reported that the average moisture content was reduced to14.69% (wb). A natural convection dryer developed, using sensible heat storage material (pebbles) and phase-change material (paraffin wax). The use of sensible heat-storage materials improved the drying by delivering air at a constant temperature. Parametric study of the natural convection grain dryer had done. The drying time required to reach the safe moisture content of paddy for storage was reported to be high [Mohaparta and Mahanta, (2012)].

2.5.2 FORCED CONVECTION DRYERS

Reviewing, section 2.5.1 it is concluded that the natural convection dryers consume much more time in the drying operation. In the forced convection dryers, heated air from heat-source is flown through the product to be dried. The remarkable researches had done by

many researchers to improve the drying methodology using forced convection drying [Mujumder (2007)].

The experimental studies had been conducted on drying using the forced convection dryer. On the basis of the experimental outcomes of forced convection drying it was reported that both the operating cost of dryer and drying time were found to be reduced. Moreover, they observed better control of drying temperatures in these dryers [Tiris et al. (1994) and Pangavhane et al. (2002].

A large-scale forced convection solar drying system at large had was developed by [Pawar et al. (1995)]. This drying system comprises three drying cabinets with blower and an array of forty solar collectors. They had evaluated its feasibility and capability to save substantial amounts of fuel. They reported that this dryer had the capable of product drying in a shorter period as compared to open sun drying.

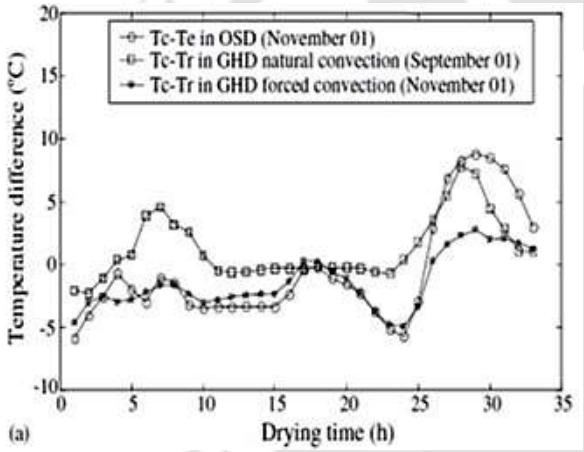

Figure 2.4 Drying time vs. temperature difference (cabbage)

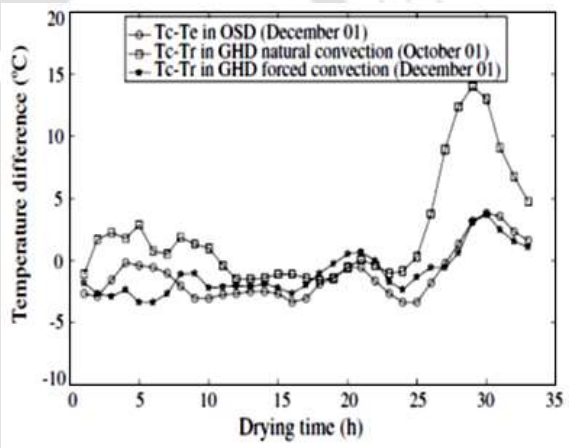

Figure 2.5 Drying time vs. temperature

A comparative study on forced convection drying, an open sun-drying (OSD) and greenhouse sun-drying (GSD) was conducted, as shown in Figs. 2.4, and 2.5. They reported that drying time was decreased to half in case of an open sun drying. Also, they found that in case of forced convection drying the convective mass transfer coefficient was significantly affected the drying process. They also established curve drying time vs. temperature for cabbage and peas, using an exponential curve model [Jain and Tiwari (2004)].

Anwar and Tiwari (2001) had conducted drying experiments on various food products, such as white gram, potato, onion, green peas, green chili, cauliflower, green peas, onion,

potato. Further, they had validated numerical findings with experimental results. They also found the uncertainty error of 7-24% and 6-20% in the results of natural and forced convection drying. Also, they reported the significant role of convective heat transfer coefficient in drying. Similarly, a comparative study between free and forced convection drying was done by [Kudal et al. And (2009)].

Sreekumar et al. (2008) had developed a forced-convection solar-dryer, using a double chamber and dried bitter gourds. They reported that the moisture content of bitter gourd was reduced from 95% to 5% within 6 hours at a maximum air temperature of 78.1°C. In these dryers the hot air is supplied to dry the products by coupling an electric motor with the blower. In the case of indirect forced convection type dryers, drying operation is conducting in similar way but the air is heated separately, preventing combustion flue gases from reaching the drying product [Fudholi (2010)].

2.5.3 HYBRID DRYERS

A forced convection hybrid solar dryer was developed using a fan driven by the diesel engine. They reported that the consumption of diesel was observed 16 liters to reduce the moisture 1% of 1-tonne paddy. The corresponding drying rate of paddy was observed to be 0.5% wet-basis per tonne of dry paddy per hour, with a maximum capacity of 10 tonnes. Also, they reported that the drying process was economical only when two paddy crops cultivated per year in the field, while the payback period was estimated at 2.3–14.8 years [Soponronnarit (1995)].

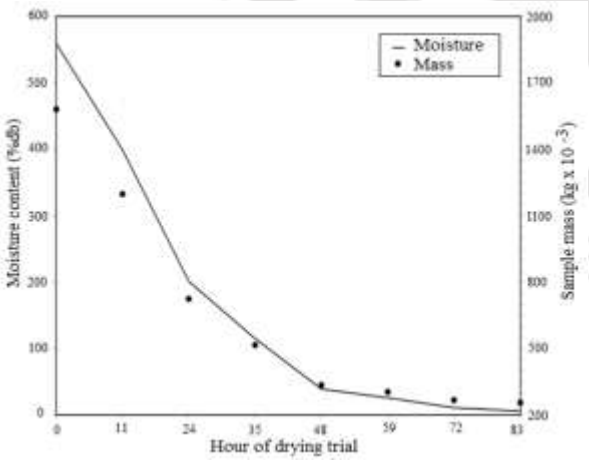

Figure 2.6 Percentage of moisture content (% db) and mass of sample during drying trial, [Bena and Fuller 2002]

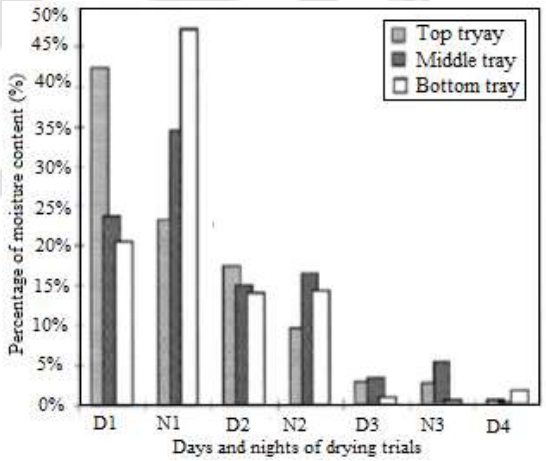

Figure 2.7 Moisture content (% db) and drying time (day/nights), [Bena and Fuller 2002]

A natural convection dryer was developed using energy sources like solar and biomass energy. It was observed that the drying efficiency of the dryer was found to be increased by 9% by using biomass energy, while the overall drying efficiency was observed 27% using solar and biomass energy. Also, it was reported that the combination of both biomass and solar energy makes the drying technology suitable for non-electrified areas of developing countries worldwide, as shown in Figs. 2.6 through 2.9 [Bena and Fuller (2002)].

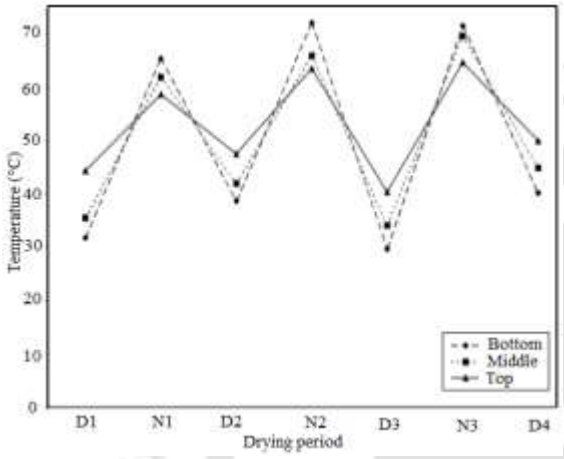

Figure 2.8 Maximum air temperatures above three trays during drying trial [Bena and Fuller 2002]

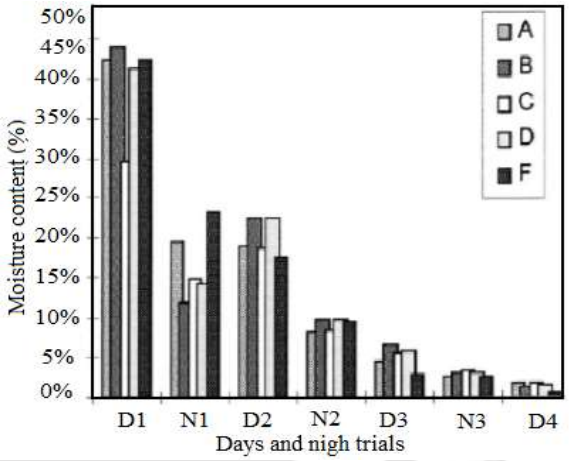

Figure 2.9 Percentage of total moisture lost by the slices in sampled locations on top tray [Bena and Fuller 2002]

A solar coupled biomass-fuelled dryer was developed to dry turmeric, by flowing hot air into the dryer continuously at operating temperature from 55-60°C. They stated that the solar biomass drier took only 1.5 days to dry turmeric, while the drying time was noted 11 days in open sun drying. Also, they reported a better quality of the product in this dryer as compared to other conventional methods, with the overall drying efficiency of 28.57% [Prasad et al. (2006)].

Amer et al. (2010) had developed a hybrid kind of solar dryer as a heat exchanger cum heat storage device and stated that it could be operated in normal sunny and cloudy days. To operate it in the night and unfavourable climatic condition and the heat energy stored in the water in day (sunshine hours) time was released. The solar dryer's efficiency was found to be increased by 65% (approx.) on recycling the drying air in the solar dryer, while a minimal amount of energy was found to be lost outside of the dryer. They reported that the moisture of 30 kg banana slice was reduced from 82% to 18% (wb) on sunny days in 8 hours, while in the open sun drying method, moisture was reduced to 62% (wb) only, as

shown in Figs. 2.10 and 2.11. Also, they found better texture, aroma, and colour of the dried products than the sun drying products.

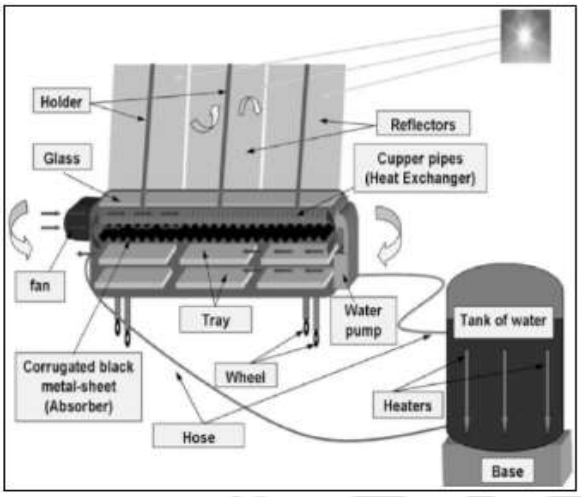

Figure 2.10 Schematic diagram of a solar hybrid dryer [Amer et al. 2010]

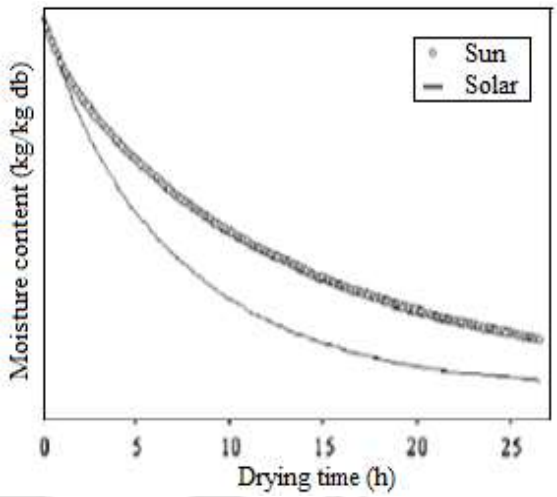

Figure 2.11 Comparison of solar and sun drying of banana slices in bad weather

2.5.4 FLUIDIZED BED DRYERS

Fluidized bed drying (FBD) techniques have extensively been employed in moisture removal of wet particulate and granular materials such as paddy, coconut, chili, black tea, and coal, etc. Fluidized bed dryers have various advantages, like high rate of heat, and mass transfer, uniform removal of moisture content and fineness of the products, protective control of final moisture content, better mixing of solids, automatically operate, compact in size, easy material transport, fast pre-drying, high drying capacity and able to increase milling yield. McLeod et al. (1999) had conducted experimental investigations on the drying process. They reported that their drying system reduces the moisture content (MC) up to 18% only for pre-drying, while the high cost of power consumed besides heat to maintain operating temperature.

Daud (2008) reported that the main advantage of the fluidized bed drying that it has large contact surface between gas and solids, good mixing of solids, the high thermal inertia of solids, rapid transfer of heat and moisture between gases and solids phase. A comparative study had carried out on the drying quality in the conventional and bubbling fluidized bed dryer. They had observed that the fluidized bed dryer reduces head rice yield (HRY) of the paddy, and the colour of the dried paddy gets faded [Karbassi and Mechdizadeh (2008)].

The concept of the RFB-SG dryer was conceptualized from Ye-Mon Chen's (1987) work in which he had experienced an influence of the centrifugal force in the rotating cylindrical drum around its axis. It was reported that the layer-wise motion of the gas-solid in the radial direction in the reactor improved drying rate.

De Wilde and de Broqueville, (2007) introduced the concept of rotating fluidized beds with static geometry. The distributor plate of this dryer had promoted an increase in the particle's radial dispersion and reduced the high concentration zones inside the dryer volume. Moon et al. (2006) had performed an experimental study of the fluidization behaviour of fine particles and reported difficulty in fluidization. Similarly, Nakamura et al. (2013) had reported the fluidization behaviour of C-type Geldart particles (micro particles).

Sobrino et al. (2008) had conducted experiments on drying of ginger slices of a mean diameter of 300 µm and a density of 2600kg/m^3 in a rotating distributor fluidized-bed. They had stated that the control of the rotational speed could control the fluidization, while bed height influenced the initial bed mass inventory.

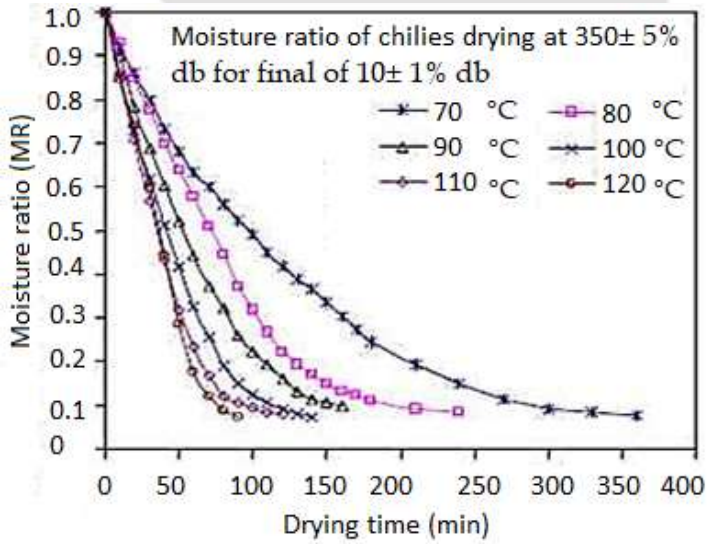

Figure 2.12 Variation of drying time with MR for drying air inlet temperature [Dongbang et al. 2010].

Dongbang et al. (2010) had carried out a chilly drying operation in a rotating fluidized bed dryer at the drying operating temperature of 70-120°C and the air velocity of 1.8 m/s, respectively as shown in Fig. 2.12. Chilies containing the initial moisture content (IMC) of 35 °C ± 5%db were dried till the reduction of moisture content (MC) level to 10±1%db.

They had also compared their results with traditional sun-drying. However, the quality of the chilies appeared deep dark red due to the higher operating temperature.

Ambrosio-Ugri and Taranto (2007) had investigated the drying characteristics of 2-hydroxybenzoic acid (cohesive particulate material) in the RFB dryer. They observed the fluidization difficulties associated with these Geldart's group 'A' particles due to their strong, cohesive force in a wet condition. Also, they reported a reduction in drying time with high-quality drying products.

However, the RFB with dynamic geometry allows a significantly higher gas flow rate, and these were found considerably more efficient than the traditional fluidized-beds [Quevedo et al., (2006)]. Still, the overall reliability of RFBs is diminished due to remarkable imperfections, namely wear-tear of the moving elements, leakage of lubricating oil, high cyclic maintenance, and vibration of the setup [Zhang, (2009)]. Using 1G-Geldart B-type salt particles and 1G-Geldart D-type polymer particles, Wilde and Broqueville (2008) had conducted experiments in fluidization chambers of two different diameters of 24 cm and 36 cm, respectively. They also reported that the polymer particles form a dense and uniform bed. Also, they found that the salt particles tend to form a less uniform and less dense bubbling bed. With both types of particles, slugging and channelling occur at too low solids loading.

Trujillo and Wilde (2012) had conducted a numerical study on fluid catalytic cracking in the rotating fluidized bed with static geometry. They stated that simulation demonstrates the significance of accounting for multi-air inlet slots for the gas distribution via gas-chamber. The results demonstrate the ability of the proposed computationally traceable approach to account for catalytic coke material distributor function and confirm that the latter has no pre-described functional form.

The gas-solid behaviour was analyzed numerically using multi-phase model. The key variations were emphasizing the requirement of further improvement of a dense discrete particle and a two-phase model [Chen and Wang (2014)].

Kovacevic et al. (2015) reported that a gas-solid vortex reactor (GSVR) exhibited superior heat and mass transfer ability. Developing GSVR on an industrial scale requires, amongst others, good insight and understanding of the hydrodynamics of the granular flow. They

developed a cold flow pilot-scale set-up and evaluated its performance. All the operating conditions were examined in the process of change of granular flow by performing PIV. They also reported that the rotating fluidized bed could change from a smoothly rotating, dense fluidized bed to a highly bubbling rotating fluidized bed, depending on the operating conditions. In this investigation, the bubbling diminishes with increasing solids density and particle diameter. Experimental measurements of azimuthal particle velocity fields in a GSVR were reported first time.

Weber et al. (2017) developed a rotating fluidized bed for High-G intensified particle separation. It reported that the chemical looping combustion (CLC) operation was successfully carried out in a rotating fluidized bed, using solid fuels. Both the carbon capture efficiency and recyclability of oxygen career were found to be improved on separating ash from the oxygen career. It has been theorized that solid-solid and gas-solid separation in rotating the fluidized bed increases the process efficiency compared to the conventional fluidized beds.

CFD simulations in a sectioned part (around 40°) of the cylindrical chamber were carried out, using software FLUENT v.14a® applying Eulerian-Eulerian approach. A well-established solid-bed was noticed at the higher gas flow-rates over a particle's density and diameter. At the same time, a more condensed bed achieved by raising "centrifugal force to radial force ratio" [Niyogi et al. (2017)].

A CFD-aided process intensification investigation was conducted for fast pyrolysis of biomass with particle-image velocimetry in the vortex reactor. Also, the numerical analysis had been carried out on the fast biomass pyrolysis using Eulerian-Eulerian and Euler-Lagrange approach. The gas was acknowledged as a continuous phase and the solid-phase discrete phase. "Due to a very high slip velocity, and extreme heat and mass transfer between phases, the yield of bio-oil were found to be higher (70 wt%). They also reported that by using Euler-Lagrange approaches, intra-particle participation, such as segregation, breakage, mixing, thermochemical degradation, shrinkage, etc., were resolved" [Kulkarni et al. (2018)].

The gas-solid hydrodynamics had been studied in a 3-D model of a vortex reactor. The investigations were conducted with particle and without particles to investigate gas-particle flow behaviour, volume fraction of solid, velocity of solid, the axial, and radial

pressure distribution in the vortex chamber fluidized bed. The hydrodynamic behaviour of gas-solids in the vortex reactor mainly depends on the particle size, slot width, and the number of gas inlet slots. It was reported that the smaller particles were thrown out from the chamber via chimney-outlet and large particles were observed to be fluidized partially. However, the large particles were not fluidized properly which could be fluidized with the increase of number of slots [Dutta et al. (2018)].

Chokphoemphun and Chokphoemphun (2018) conducted the numerical and experimental investigations of paddy drying in a rectangular fluidized-bed dryer, creating vortex flow. They conducted drying experimentation in three different configurations. Each case study has performed at two inlet air velocities (2.24±0.02 m/s and 2.52±0.02 m/s), and the temperatures of 60°C and 80°C, respectively. They reported the significant effects of inclined baffles on the rate of moisture removal, which was reduced by 7-18% as compared to the smooth surface fluidized-bed dryer. Also, they had made the prediction to defined the regression coefficient of 0.99556 with a mean absolute error of 0.00127 and square error of 1.988×10^{-4}.

A small size RFB-SG reactor with 8 inlets and eight chimney outlets was numerically examined by using ANSYS FLUENT 18.0 software. To obtain proper fluidization of particles, a sufficiently high velocity (35-70 m/s) air was supplied into vortex-chamber via air inlets, making an angle of inclination 15° or 30° with its tangential direction. It was reported that with an increase of solid loading capacity, the quality of fluidization was improved, but it increases the pressure drop. Also, it was found that the quality of the fluidization improved by increasing velocity at higher solid loading. Simultaneously, the tangential inlets allow more vigorous fluidization than the inlets at the angle of 15° or 30°. Also, it was observed that on stopping the solids injection, particles were immediately evacuated from the freeboard and the chimney region. It resulted in losses of the smaller particles via the chimney and allowed whirlwind in this zone to recover the strength [Lavrich et al. (2018)].

A 3-D CFD simulation model of the vortex chamber was developed in order to analyze the effect of solid-loading for different variables such as the gas-solid separation behaviour, density of the particle-bed, and solid-bed consistency [Hardy et al. (2019)]. For granular

flow, kinetic theory is given by Lun et al., (1984), and Gidaspow, (1994), which was founded from the theory for non-ideal and dense gases by [Chapman and Cowling (1970)].

Syamlal and O'Brien (1988) had developed a hydrodynamic computer model to describe multi-particle fluidization, identifying the density and diameter of each group of particles. For particle fluidization, they did computer coding to solve mass and momentum balance equations. They used their model to simulate particle layer inversion in the fluidized bed and observed that the denser particle size was smaller in the binary mixture of the particulate material. Also, they reported that the larger particles were segregated in the top layer at low velocity, while they sank at the higher fluid velocity. Furthermore, the results of the computational study had been experimentally validated.

Ogawa et al. (1980) had reported the equations for fully developed fluidization of the particulate materials, and the set of these equations had properties similar to the turbulence equations. Also, they had observed that the steady 1-D gravity flow was similar to the experimental outcomes.

However, rotating fluidized bed (RFB) dryers were more efficient than the conventional fluidized bed dryers. These dryers are still incorporated with few notable imperfections such as vibration, requirement of packing to prevent leakage of lubricating-oil, and higher cyclic maintenance of the system, diminish their importance.

To overcome above mentioned drawbacks a new version of RFB dryer was tried by researchers in static geometry. However, limited work is available in the published literature.

2.6 RESEARCH ON DRYING AT IIT GUWAHATI

Mahapatra and Mahanta (2012) had developed a natural convection drying mechanism with a sensible and latent heat storage system for quality drying, as illustrated in Fig. 2.13. It consists of (1) rectangular brick chamber, (2) biomass feeding pipe (BFP), (3) biomass burner, (4) tray containing phase change material (PCM), (5) air inlet vents, (6) perforated drying tray, (7) sensible heat storage materials (SHSM) and (8) flue gas pipe. In this dryer, a conical furnace of mild steel sheet was used to fabricate its core, and this furnace was established in the mid of the furnace at the height of 22 cm. Also, this furnace's platform was made of GI sheet with the facility of air supply via 1700 holes of 5 mm diameter. To

maintain the required drying temperature, wood-chips were supplied into the furnace via an inclined air inlet. Furthermore, the top of this furnace was connected to the exhaust pipe. Besides, as the phase change material (PCM), a paraffin wax tray was placed on the top of the dryer to maintain a constant temperature by absorbing and releasing stored energy. The lower section of the furnace is surrounded by pebbles of 5-7 cm diameter as sensible heat storage material (SHSM) to prolong the heat supply period.

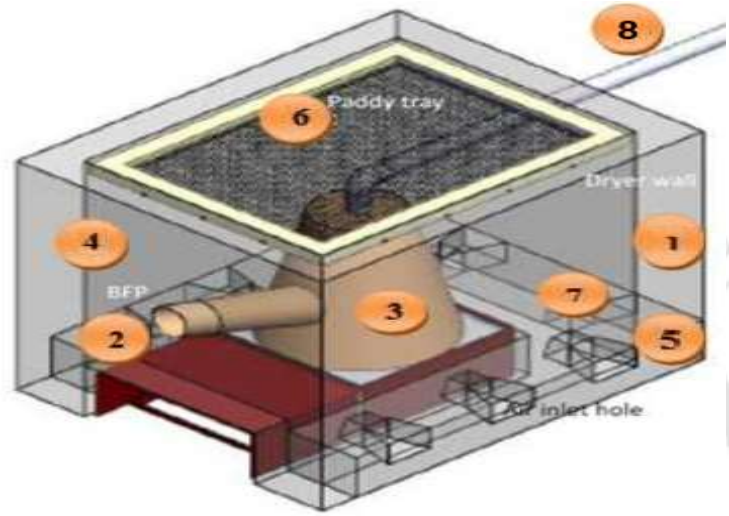

Figure 2.13 Schematic of natural convection dryer (NCD) [Mahapatra and Mahanta (2012)]

Pati et al. (2016) had been performed drying experiments in a laboratory level RFB-SG dryer of 0.24 m diameter and length of 0.05 m. The fluidization air enters via multi air inlets and leaves the chamber through the chimney outlet of the inner and outer diameter of 70 mm, and 120 mm. They performed paddy drying experimentation for 300-600 g paddy, at the operating temperature of 50-65°C and an airflow rate of 400-600 m^3/h, respectively. Each slot is sized to 0.05 m width, 5 mm breadth, and the gap between the two slots was 3 mm. They reported that the drying rate was very high compared to the conventional fluidized bed dryers and modifying the chimney outlet to reduce the losses of particles through the chimney outlet.

Preliminary experimentation was performed in a RFB-SG chamber of 240 mm diameter and 50 mm length for drying inventory of 200-300 g at CFB Lab, IIT Guwahati. There were various demerits of the existing RFB-SG dryer, such as non-uniform bed, low drying capacity, high complexity, maintenance of slit, and product damage. To overcome the insignificance of the existing RFB-SG dryer with slits, an RFB-SG dryer without slit is developed with eight air inlets of the rectangular cross-sectioned area spiral chimney outlet

as shown in Fig. 2.14. Further, the performance of both the RFB-SG dryer without slit and RFB-SG dryers have been compared.

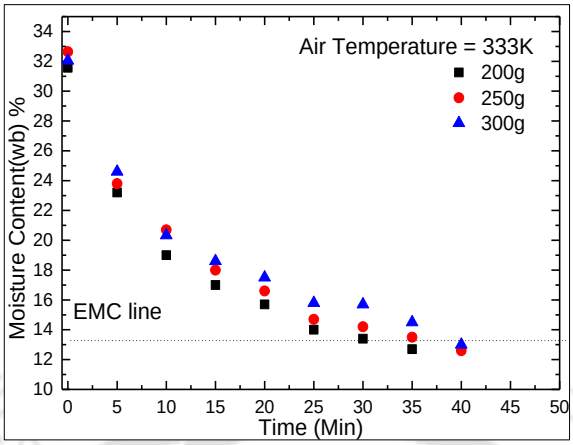

Figure 2.14 Variation of MC with time for different inventory (T_a= 333K)

2.7 RESEARCH GAP

A comprehensive literature review has been carried out on drying involving natural, convection forced convection, hybrid, and fluidized bed dryers. This study highlighted numerous information related to the drying performance, environmental conditions, and input parameters. Preliminary experiments on paddy drying were carried out at IIT Guwahati in the laboratory scale RFB-SG dryer. It was observed that the drying capacity and drying rate were lower (300 g), while the system complexity and cyclic maintenance, needed further improvement. Hence, further improvements such as system capacity enhancement by reducing cost complexity, drying air requirement, and drying time are need to be studied. Moreover, detailed thermodynamic (energy and exergy) and economics analysis of RFB-SG dryer are found to be limited. Hence, there is a necessity to examine the RFB-SG dryer's feasibility without slit for grain drying. The present research attempts towards grain (Paddy) drying in RFB-SG dryer with and without slit by replacing of circular cross-sectional inlets with the rectangular cross-sectional air-inlets. In addition, thermodynamic (energy, and exergy) and thermo-economics analysis are to be performed.

2.8 OBJECTIVES

The objectives of the present work are as follows:

- ✓ Performance investigation of RFB-SG dryer without and with slit.
- ✓ Numerical study on heat transfer and hydrodynamic of gas-solid phase in RFB-SG without slit.
- ✓ Experimental validation of numerical results of RFB-SG dryer without slit.
- ✓ Scale-up and optimization of the best performing RFB-SG unit without slit, numerically in terms of varying "length to diameter ratio".
- ✓ Thermodynamic (energy, and exergy) and economics analysis of RFB-SG dryer with and without slit.

2.9 SUMMARY

The in-depth literature review has been carried out and discussed in the present chapter. Based on the performance and demerits of all discussed dryers, the problem has been identified for the existing work. Theoretical background, experimental set-up, and procedure of experimentation have been discussed in the succeeding chapter.

CHAPTER-3

THEORETICAL BACKGROUND AND EXPERIMENTAL SETUP

3.1 INTRODUCTION

Drying is the process of removing moisture from a wet solid material by circulating hot air through it. The hot air first evaporates the grain moisture and then moves this moisture away from the grain surface, as shown in Fig. 3.1. For effective drying, the moving air must be hot, and dryer and moisture must be transported from within the grain to the surface of the product, as this is where moisture is exchanged with the air. Drying bears, a simultaneous functional relationship with the conditions of the inlet air, grain temperature, and the humidity of the environment, etc. This chapter includes the theories associated with heat and mass transfer in the RFB-SG dryer and experimental setup description. The procedures for performing the experiments are also presented in the chapter.

3.1.1 ROTATING FLUIDIZED BED WITH STATIC GEOMETRY (RFB-SG)

Conventional fluidized beds work under the influence of the Earth's gravitational field. These fluidized beds are known for their heat transfer features, and the fluidization gas can later be used for heating or cooling operations. The mass, momentum, and heat transfer rate are limited because the velocity of the gas-solid slip cannot exceed the terminal velocity of the solid particles under the effect of Earth's gravitational field. In the traditional fluidized beds, the gas-solid velocity or air flow rate cannot exceed certain limit however in the case of RFB-SG dryer works at the higher air velocity. Also, there are some other difficulties in the fluidization of fine adhesive particles in conventional fluidized beds due to the popular Vander Waals force, are shorted out in the RFB-SG dryer. To dealing with the above issues, a RFB-SG has been developed [de Wilde and de Brockville (2007); De Brockville (2014)]. This provides the ability to overcome the restriction of existing conventional fluidized beds (CFBs) with heat transfer coefficients of solid concerning the gas flow rate and fluidization. In the RFB-SG dryer, the vortex chamber is used to attain tangential and radial fluidization of the particles against a very high acceleration due to the gravity effect. Compared to other drying techniques, the drying capacity of a rotating

fluidized bed dryer is more advantageous due to the higher heat and mass transfer through it.

3.1.2 WORKING PRINCIPLE OF RFB-SG DRYER

The hot fluidization air was supplied tangentially into the vortex dryer via multiple gas inlets, as illustrated in Fig. 3.1. Tangentially injected air fluidizes the particles along tangential direction and induces the rotary motion of a cylindrically shaped particle bed. The mixture of air-particle at any location in the fluidization chamber will be subjected to drag force and inertia forces. The resulting centrifugal force has been reacted by the radially inwards drag force of the gas-solid phase while Coriolis force aligns the mixture of air-solid to be in a circular motion. The resultants of these forces determine the rate of the gas-solid mixture to leave the fluidization chamber via a centrally located chimney outlet. The forces exerted on the particles are balanced by drag, buoyancy, and centrifugal force, while the value of gravity in the dryer is about 9 times of acceleration due to gravity. Unlike a traditional fluidized-bed, the RFB can carry a higher centrifugal force, and hence the drag force needed to fluidize (lift) the particles further becomes larger to meet the force equilibrium.

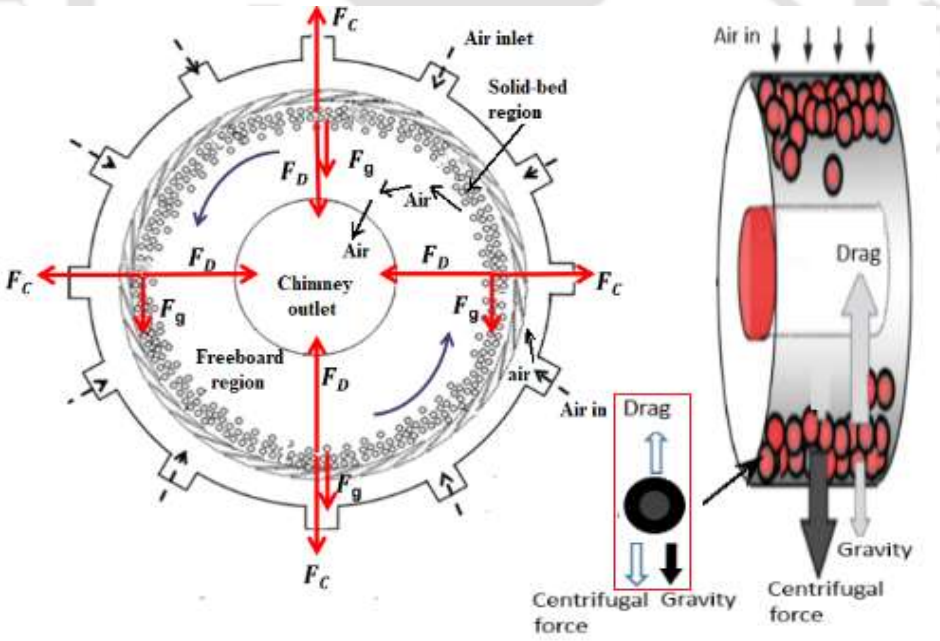

Figure 3.1 Schematic diagram of principle of working of RFB-SG dryer

3.1.3 DESIGN AND HYDRODYNAMIC OF RFB-SG DRYER

By considering two forces, such as centrifugal force and drag force, in balance, a fluidization chamber can be fully designed. Therefore, the theoretical formulation of gas-solid drag forces, centrifugal forces, terminal velocity, and minimum velocity of fluidization is the major function of the total volumetric gas flow rate [De Broqueville and De Wilde (2009].

The centrifugal force per unit volume of fluidization is given by the equations or relations.

$$f_c = \varepsilon_s \rho_s a_c \tag{3.1}$$

where centripetal acceleration, $a_c = \dfrac{u^2_{s,t}}{r} = \dfrac{(s_{gs} u_{g,t})^2}{r}$ (3.2)

where

$u_{g,t}$: Tangential velocity of the gas,-phase

$u_{g,s}$: Tangential velocity of solid-phase,

S_{gs} : Tangential gas-solid slip factor (a constant)

The tangential velocity of the gas-phase is concerned with the total volumetric gas flowrate.

The tangential velocity of gas, $u_{g,t} = \dfrac{Q_{g,t}}{S_t} = \dfrac{Q_{g,t} n_{rot}}{S_t} = \dfrac{Q_{gt} n_{rot}}{\varepsilon \left[D/2 - R_f \right] L}$ (3.3)

where

D : Diameter of fluidization chamber

L : Length of fluidization chamber

R_f : Radial position of freeboard region

S_t : Surface area of the gas phase

n_{rot} : Number of rotation of the gas phase

Q_g : Volume flow rate

ε : Voidage factor

Using equation (3.2) and (3.3), the centripetal acceleration can be expressed as;

$$\bar{a}_c = \left[\frac{2\pi \bar{n}_{rot} S_{g,s} Q}{\bar{\varepsilon}_g \, v_{bed}} \right] . \bar{\Gamma} \tag{3.4}$$

The centrifugal force is consequently can be written as;

$$\bar{f}_c = \rho_g \bar{\varepsilon}_s \left[\frac{2\pi \bar{n}_{rot} S_{g,s} Q}{\bar{\varepsilon}_g v_{bed}} \right]^2 . \bar{\Gamma} \tag{3.5}$$

The radial drag force per unit volume of fluidization chamber is expressed as;

$$f_{d,r} = \beta\,(u_{g,r} - u_{s,r}) \tag{3.6}$$

where β is the drag coefficient in the fluidization bed [Gidaspow (1994)], both the drag and pressure drop of the denser fluidized bed are explained by the following two equations [Ergun (1952)].

$$\beta = \frac{3}{4} C_D \frac{\varepsilon_s \varepsilon_g \rho_g}{d_p} \beta\left|(u_g - u_s)\right| .\varepsilon_g^{-2.65} \quad \text{for } \varepsilon_s \le 0.2 \tag{3.7}$$

$$\beta = 150 \frac{\varepsilon_s^{\,2} \mu_g}{\varepsilon_g d_p^{\,2}} + 1.75 \frac{\varepsilon_s \rho_g}{d_p}\left|(u_g - u_s)\right| \quad \text{for } \varepsilon_s > 0.2 \tag{3.8}$$

In equation (3.9), the drag coefficient is correlated with the particle's Reynolds number and the radial velocity of the gas phase is related to the gas flow rate by the surface area provided for the radial motion for the gas phase.

Reynolds number, $$\mathrm{Re} = \frac{\rho_g \varepsilon_g d_p}{\mu_g}\left|u_g - u_s\right| \tag{3.9}$$

Drag coefficient, $$C_D = \frac{24\,(1+0.15\mathrm{Re}^{0.687})}{\mathrm{Re}_p} \quad \text{for} \quad \mathrm{Re_p} \le 1000 \tag{3.10}$$

and $$C_D = 0.44 \quad \text{for} \quad \mathrm{Re_p} \ge 1000 \tag{3.11}$$

From equations (3.11) and (3.12), the minimum fluidization and terminal velocities can be calculated as [Froment et al. (1990), De Wilde and De Broqueville, (2007)].

$$u_t = \sqrt{\frac{4\bar{a}_c(\rho_s - \rho_g)}{3\rho_g C_D}} \tag{3.12}$$

Wen and Yu (1966) has given the following correlation for minimum fluidization velocity

$$u_{mf} = \frac{\mu_s}{\rho_g d_p}[33.7\,(1+0.000037A_r)^{0.5}] \tag{3.13}$$

3.1.4 DESIGN OF GAS INLET SLOTS

For the design of the gas inlet slots, an important factor is known as force ratio (λ) given by [Kochetov et al. (1969)], and this relation is used in the slot design of the RFB-SG as expressed in Eqn. (3.14);

$$\lambda = \frac{\text{Centrifugalforce}}{\text{Dragforce}} = \frac{n.S}{\pi D} \tag{3.14}$$

where D, s, and n are the vortex chamber diameter, width, and the number of gas inlets, respectively.

The number of inlet slots should be high enough to ensure the tangential uniformity of gas flow along with the solid particle distribution and the circumference of the fluidization chamber. The value of force ratio in the design estimations is the best suitable in the range of 0.025-0.038.

3.1.5 SELECTION OF PARTICLE SIZE

For proper liquefaction of granular particles, the density of the particle bed should be more or less the same everywhere, in the vortex chamber. According to the behaviour of the particle fluidization, the particles are classified in four categories types, as represented in Fig. 3.2 and appendix A [Geldart (1973), Geldart and Abrahamsen (1978)]. Also, Kunii and Levenspiel (1969) stated that the classification of the particle depends on the equivalent mean diameter of the solid particle and an apparent density $\left(\rho_s - \rho_g\right)$.

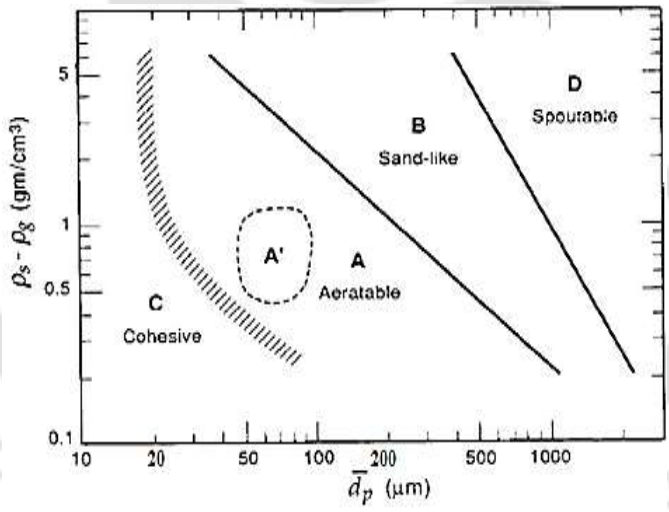

Figure 3.2 Geldart classification of the particles [Geldart (1973); Geldart and Abrahmsen (1978)]

3.1.6 CALCULATION OF MOISTURE CONTENT IN PADDY

The percentage of MC available in paddy is calculated using Eqns. (3.15) and (3.16) given by [Zaman and Bala (2001); IRRI (2005)].

Percentage of MC on dry basis and wet basis can be calculated as;

$$MC_{w.b.} = \frac{m_i - m_f}{m_i} X\ 100\ \% \tag{3.15}$$

$$MC_{d.b.} = \frac{m_i - m_f}{m_f} X\ 100\ \% \tag{3.16}$$

where m_i, m_f, MC_{wb} and MC_{db} are the initial weight of paddy, the final weight of paddy, moisture content of paddy (wet basis), and moisture content of paddy (dry basis), respectively. It can be said as the MC is a function of independent variables.

3.2 EXPERIMENTAL SET UP AND PROCEDURE

The experimental setup with two different drying chambers have been designed and fabricated viz. the RFB-SG dryer without slit and rotating fluidized bed in static geometry with slit at IIT Guwahati. The procedures of paddy drying in the RFB-SG dryer without slit and the SFB-SG dryer with slits are described systematically. To obtain better uniformity of bed, fast-drying, efficiency improvement, and capacity enhancement as RFB-SG without slit is used. Furthermore, the scale-up of RFB-SG dryer without slit has been completed.

3.2.1 EXPERIMENTAL SETUP DESCRIPTION

The schematic diagram and photograph of the RFB-SG dryer and without slit experimental setups for batch drying are illustrated in Figs.3.3 and 3.4, respectively. The experimental setup consists an electric motor, rotary blower, flow control valve, air bypass valve, manometer, orifice plate, air heating unit, air distribution chamber, air inlets, solid inlet, solid outlet, vortex chamber, and chimney outlet. A stainless steel RFB-SG (with slit) vortex-chamber of inner diameter (ID) 240 mm, length (L) is fabricated with a transparent cover of the polycarbonate sheet. A slit of 36 slots is mounted inside the chamber, while the solid injection system is attached to the front cover of the chamber. A centrally located chimney is attached in the rear-side of the chamber and 8 air inlets are attached with the periphery of the reactor in the transverse direction. A total of 8 nos. of rectangular cross-sectioned air inlets of width 6 mm are provided on the periphery of the dryer making angle of 30° with its tangential direction. A solid outlet is provided for solid unloading or sample collection during the drying operation. The fluidization air is supplied to the RFB-SG house through the air distribution unit by the high-pressure centrifugal blower and a compressor for particle injection (Make: Ingersoll Rand, Model No.: S-01480). In the air heating unit, three heating elements of rating 2 kW each was covered around an insulated heating-chamber pipe of 76.2 mm diameter and the length of 800 mm. An adequate layer of thermal insulator (Ceramic-wool) and an electrical insulator (mica sheet) were used to reduce the losses. A total of 12 numbers of thermocouples were used for temperature measurement at

several locations such as at the multiple air-inlets, outlet, surface of the vortex chamber, in solid-bed region, and freeboard region. A data acquisition system is employed to record data in the attached PC. The air is conditioned in an air heating chamber in the temperature range of 328-338K. The airflow rate (AFR) is measured by the standard (BS1042) orifice meter, and air controlled vale is used to regulate the airflow rate. A bypass valve is also arranged to bypass the access air. Static pressure, the temperature in the radial direction, and suspension density in different four directions were investigated. Fine wire mess of size 200 mm and filters of the cigarette ends were used at the pressure probes tapping ends, to avoid the escape of food grain (paddy) from the chamber and to minimize the pressure fluctuation. A measured quantity of paddy (after towel drying) was kept ready for injection loading. The conditioned (hot) air was injected into the vortex chamber via 8 air inlets, which is passed through 36 slots deviated along the tangential direction of the chamber wall. Further, this drying reactor is connected with other components such as the air distribution chamber, air heating unit, U-tube manometer, moisture analyzer, weighing machine, data acquisition system, PC, blower, compressor, and stopwatch. A detachable polycarbonate glass cover is used for the purpose of flow visualization of the particles in the vortex chamber. The particles injected into the reactor are fluidized by the high-velocity gas and formed a solid rotating bed inside the vortex chamber, near to its periphery. Due to the rotating motion of the particles, radially outward force acts on the particles due to the radially inward gas-solid drag force is also acted on the particles because of the gas moment from the chamber periphery to its central chimney.

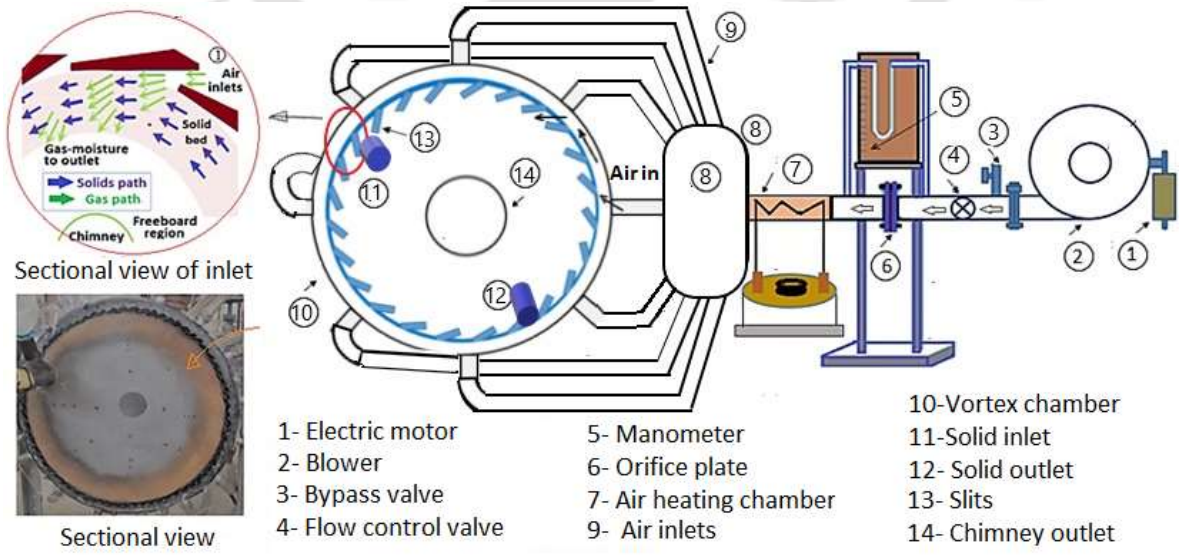

Figure 3.3 Schematic view of a RFB-SG dryer with slit

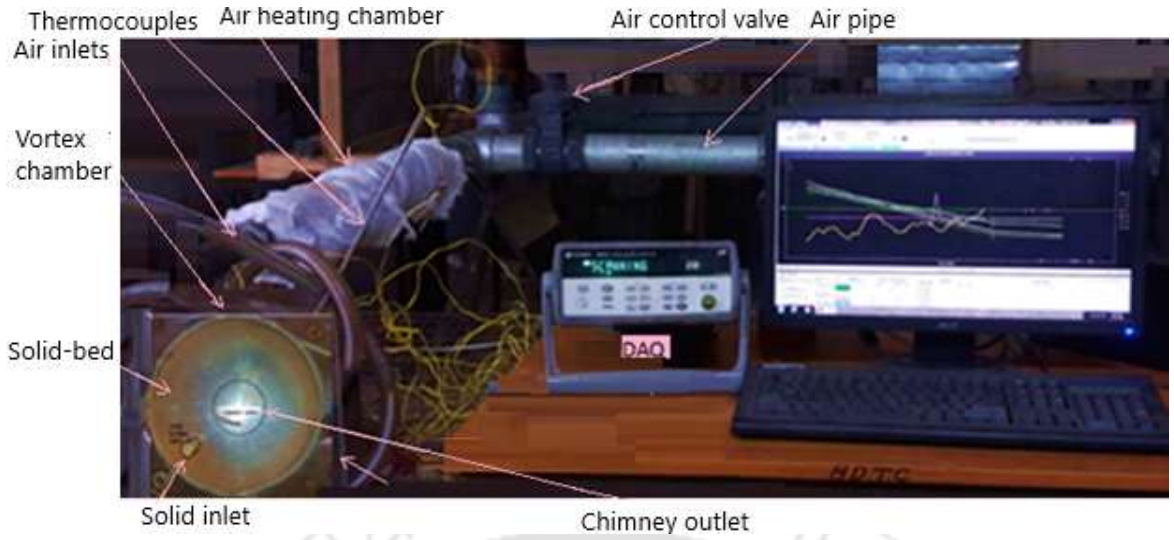

Figure 3.4 Photograph of RFB-SG dryer without slit

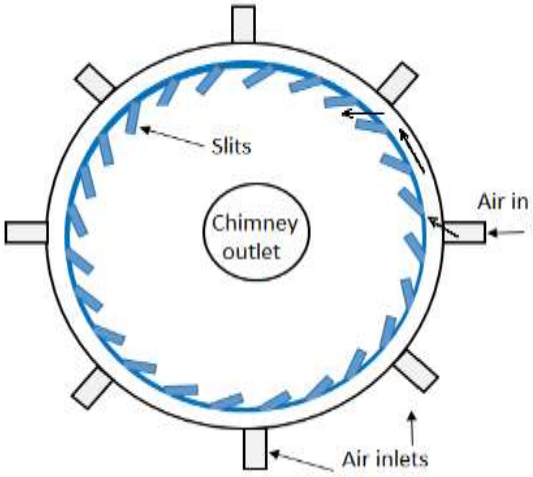

Figure 3.5 Schematic of the RFB-SG dryer with slit

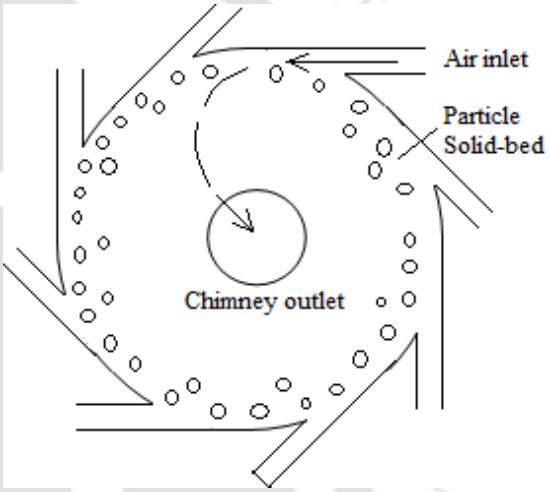

Figure 3.6 Schematic of the RFB-SG dryer without slit

A stable solid-bed formation against the chamber wall is possible only when radially outward centrifugal force dominates over. Gas–solid drag force acting in a radially inward direction. The balance of the radial force on the fluidized particles is made up of equilibrium of both the centrifugal force and drag force. On the other hand, RFB-SG without-slit is developed arranging the air inlets in tangential direction to the vortex-chamber without use of slit as shown in fig. 3.4. also, the schematic diagram of RFB-SG dryer without slit and RFB-SG with slit are shown in figs. 3.5 and 3.6. in case of the RFB-SG dryer without slit the air inlets are fitted with the vortex-chamber tangentially, while in other case of RFB-SG dryer with slit, the fluidization air is injected into the vortex chamber via air inlets in transverse-direction and this air is diverted in tangential direction by using slit.

An adequate electrical insulator (mica sheet) was used to separate the steel pipe from electric heating elements. In contrast, ceramic wool was used as a thermal insulator to reduce the heat loss from the experimental setup. Necessary temperature probes (celebrated thermocouples) are facilitated to measure temperature in the solid bed region, freeboard region, chamber surface, air inlet, and chimney outlet as shown Fig.3.7. The requirement of energy varies on the increasing quantity of inventory, airflow rate, and operating temperature. For the drying experimentation in RFB-SG dryer, a temperature check facility is connected with the data acquisition system using k-type celebrated thermocouples (appendix B) for temperature display. Besides, temperature variation (328-338K) over time was associated with computers.

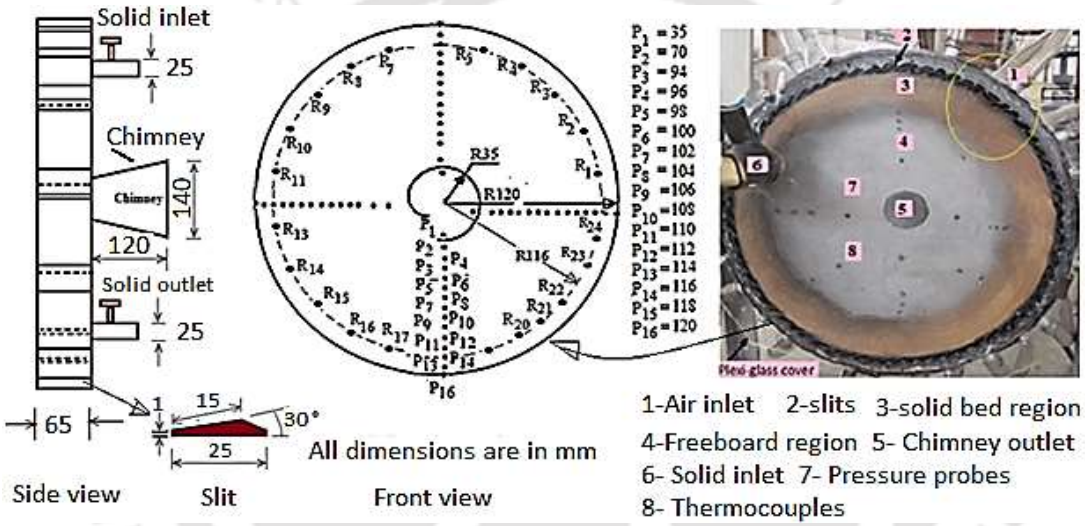

Figure 3.7 Locations selected to measure the temperature along radial direction

3.2.2 DRYING PROCEDURE

The preliminary trial multiple food grains such as coriander, ground, tea, and paddy were fluidized in the developed dryer. Further, an extensive investigation on drying paddy characteristics has been carried out considering various parameters such as drying air temperature, airflow rate, inventory, and drying time. To conduct the drying operation in the RFB-SG dryer, the fluidization-air was injected via multiple air inlets and switched on the air heating unit. When the desired air operating temperature was obtained, a measured quantity of paddy was injected into the dryer via a solid injection system, which partly followed the gas path and formed a solid-bed. In the present study, seventy-two experiments were conducted, and in each experiment, numbers (4 to 9) of samples were

collected for moisture measurement at the time interval of 5 minutes. Also, a plunger-pump type facility was provided separately for the loading and unloading of inventories. A pictorial view of the various components of the experimental setup is presented in Fig. 3.8 and appendix C.

(a) Air blower

(b) Electric air heating chamber

(c) Air distributor

(d) Data acquisition system

Figure 3.8 Components of the experimental setup

3.3 SUMMARY

In this chapter, the theoretical background of a rotary fluidized-bed dryer with static geometry without slit and with slit, and experimental setup have been described. The concept of design and mathematical equations related to heat and mass transfer have also been discussed. Also, the experimental procedure and instrumentation of RFB-SG dryer without slit and RFB-SG with slit dryers have been described in the present Chapter. CFD simulation model and numerical results of RFB-SG dryer without slit is presented in the next chapter.

CHAPTER-4

NUMERICAL INVESTIGATION OF RFB-SG UNIT WITHOUT SLIT

4.1 INTRODUCTION

The present simulations are mainly concerned with the behaviour of particle fluidization and heat transfer features of two phases (gas-solid) in a three-dimensional RFB-SG model. To predict the maximum fluidization capacity as well as heat transfer characteristics, the effect of fluidization air velocity, pressure, operating temperature, and size of the unit was numerically analyzed. The flow is turbulent at a higher gas velocity, so the Reynolds-averaged approach has been used [De Wilde (2009)]. An effect of turbulence is accounted for through the realizable k-ε model [Shih et al. (1995)]. Nevertheless, C_μ is no longer remains constant; still, it is a function of turbulence fields mean-strain and rotation rates. Coupling between both the gas-sold phases has managed through turbulent momentum exchange.

4.1.1 GAS-SOLID CFD SIMULATION MODEL

In this study, the gas-solid model has adopted furthermore the gas-phase was supposed to be an incompressible-fluid. It is multi-phase flow, based on the generalization of N-S equations, so it is known as the Eulerian-Eulerian approach [Anderson and Jeckson, (1967)]. The mass, momentum equations are solved for each of the phases. Kinetic theory-granular flow [Lun at al., 1984; Gidaspow, (1994)], was originated from the theory [Chapman and Cowling, (1970)] for non-ideal dense gases are used to close the equations of the solid phase. The basic model CFD has been summarized by the constitutive equations, addressed in this chapter for the fluid-solid phase which consists of the balance of the mass, momentum and energy. The boundary conditions used in the simulations and various parameters are listed in the Table 4.1

Reynolds number (20000) for higher inlet velocities is calculated using equation (4.1) as;

Reynolds number, $$R_e = \frac{\rho_f v_g L_c}{\mu_f} = \frac{v_g L_c}{\nu_f} \quad (4.1)$$

Hence, the heat transfer coefficient, $h = \frac{N_u k_g^{eff}}{d_s}$ (4.2)

where k_g^{eff} = an effective thermal-conductivity for gas-phase.

Nusselt number $Nu = \left(7 - 10\varepsilon_g + \varepsilon_g^2\right) + \left(1 + 0.7 Re_s^2 Pr^{0.33}\right) + \left(1.33 - 2.4\varepsilon_g^2\right) Re_s^{0.7} Pr^{0.33}$ (4.3)

$$Re_s = \frac{\rho_g \varepsilon_g d_s}{\mu_g}\left|\left(\vec{v}_g - \vec{v}_s\right)\right| \text{ and } Pr = \frac{\mu_g C_{p,g}}{k_g} \quad (4.4)$$

Within Eulerian equations, a mathematical interpretation is needed to differentiate the overall bulk thermal conductivity into the gas and solid phase thermal conductivity. Kuipers et al. (1992) utilized an effective thermal conductivity (k_g^{eff}) for gas-solid which is founded from augmentation of [Syamlal and Gidaspow (1985)].

4.1.2. MASS CONSERVATION EQUATION

For gas-phase $$\frac{\partial}{\partial t}(\varepsilon_g \rho_g) + \nabla.(\varepsilon_g \rho_g \vec{v_g}) = 0 \quad (4.5)$$

For solid-phase $$\frac{\partial}{\partial t}(\varepsilon_s \rho_s) + \nabla.(\varepsilon_s \rho_s \vec{v_s}) = 0 \quad (4.6)$$

4.1.3. MOMENTUM CONSERVATION EQUATION

For the gas-phase [Anderson and Jeckson, (1967)]

$$\frac{\partial}{\partial t}\left(\varepsilon_g \rho_g \vec{v_g}\right) + \nabla.\left(\varepsilon_g \rho_g \vec{v_g}\vec{v_g}\right) = -\varepsilon_g \nabla p_g + \nabla.\bar{\bar{\tau}}_g + \varepsilon_g \rho_g \vec{g} + \beta_{gs}\left(\vec{v_s} - \vec{v_g}\right) \quad (4.7)$$

For solid-phase

$$\frac{\partial}{\partial t}\left(\varepsilon_s \rho_s \vec{v_s}\right) + \nabla.\left(\varepsilon_s \rho_s \vec{v_s}\vec{v_s}\right) = -\varepsilon_s \nabla p_g - \nabla p_s + \nabla.\bar{\bar{\tau}}_s + \varepsilon_s \rho_s \vec{g} + \beta_{gs}\left(\vec{v_g} - \vec{v_s}\right) + \vec{S_s} \quad (4.8)$$

In equations (4.9) and (4.10), show the effect of shear, gravity, pressure, and momentum transfer between the gas and solid phase.

Gas-phase stress tensor $$\bar{\bar{\tau}}_g = \varepsilon_g \mu_g \left(\nabla \vec{v}_g + \nabla \vec{v}_g^{T}\right) \quad (4.9)$$

Solids-phase stress tensor $$\bar{\bar{\tau}}_s = \varepsilon_s \mu_s \left(\nabla \vec{v}_s + \nabla \vec{v}_s^{T}\right) + \varepsilon_s \left(\lambda_s - \frac{2}{5}\mu_s\right) \nabla \vec{v}_s \bar{\bar{I}} \quad (4.10)$$

4.1.4. k-EPSILON TWO-EQUATION TURBULENCE MODEL

To govern dissipation rate (ε) and kinetic energy (k), two equations, (4.11) and (4.12) can be written as;

$$\frac{\partial}{\partial t}(\rho k)+\frac{\partial(\rho k u_j)}{\partial x_j}=\frac{\partial}{\partial x_j}\left[\left(\mu+\frac{\mu_t}{\sigma_k}\right)\frac{\partial k}{\partial x_j}\right]+G_k+G_b-\rho\varepsilon-Y_M \tag{4.11}$$

$$\frac{\partial}{\partial t}(\rho\varepsilon)+\frac{\partial(\rho\varepsilon u_j)}{\partial x_j}=\frac{\partial}{\partial x_j}\left[\left(\mu+\frac{\mu_t}{\sigma_\varepsilon}\right)\frac{\partial\varepsilon}{\partial x_j}\right]+\rho\varepsilon S C_1-\rho C_2\frac{\varepsilon^2}{k+\sqrt{\nu\varepsilon}}+C_{1\varepsilon}\frac{\varepsilon}{k}C_{3\varepsilon}G_b \tag{4.12}$$

where

$C_1=\max[0.43, \eta/(\eta+5)]$, $\eta = S(k/\varepsilon)$, $S=(2S_{ij}S_{ij})^{0.5}$, $C_{1\varepsilon}=1.44$, $\sigma_k=1, \sigma_\varepsilon=1.2$ and $C_2=1.9$.

Lift forces are neglected.

Phase densities are differed by the factor >10^3.

Gas-phase shear tensor,

Solid shear viscosity (ε_s) has three contributions, as mentioned below:

Collision kinematic viscosity between the particles,

$$\mu_{s,coli}=\left[\frac{4}{5}\varepsilon_s\rho_s d_p g_{o,ss}\left(\frac{\Theta_s}{\pi}\right)^{0.5}(1+e_{ss})\right] \tag{4.13}$$

Kinetic shear viscosity of solid is expressed as [Syamlal et al. (1993)];

$$\mu_{s,kin}=\left[\left(\frac{\varepsilon_s\rho_s d_p.\sqrt{\Theta_s.\pi}}{6(3-e_{ss})}\right)\left\{1+\frac{2}{5}\varepsilon_s g_{o,ss}(1+e_{ss})(3e_{ss}-1)\right\}\right] \tag{4.14}$$

Frictional-viscosity of solids is written as [Schaeffer (1987)];

$$\mu_{s,fric}=\frac{p_s\sin\varphi}{2\sqrt{I_{2D}}} \tag{4.15}$$

where φ = Angle of initial-friction

Solid bulk viscosity equation (4.16) is for resistance to compression and expansion of particles written in equation [Lun et al. (1984)].

$$\xi_s=\frac{4}{3}\varepsilon_s\rho_s d_p g_{o,ss}\left[1+e_{ss}\left(\frac{\Theta_s}{\pi}\right)^{0.5}\right\}\right] \tag{4.16}$$

There are two terms under solid pressure, namely asynchronous terms in the regime of dense-phase as well as the kinetic terms in it.

$$P_s=\varepsilon_s\rho_s\Theta_s+2\rho_s(1+e_{ss})\varepsilon_s^2 g_{o,ss}\Theta_s \tag{4.17}$$

where Θ_s = Granular temperature.

Radial gas distribution function contribution is written [Ogawa et al. (1980)] as;

$$g_{o,ss} = \left[1 - \left(\frac{\varepsilon_s}{\varepsilon_{s,max}}\right)^{1/3}\right]^{-1} \tag{4.18}$$

This equation is considered that it consists of two individual contributions, as given below:

Kinetic-term: It dominates in dilute flow regime.

Collision terms: Phase regime have importance in the regimes of dense-phase.

The Syamlal-O'Brien model [Syamlal-O'Brien, (1989)] is used for the coefficient of inter-phase momentum exchange is given in Eqs. (4.19) & (4.20), [Syamlal and O'Brien, (1989)]. The drag friction

$$\beta = \frac{3\varepsilon_s \varepsilon_g \rho_g}{4 v_r^2 d_p}\left(\frac{Re_s}{v_{t,s}}\right)\left|\left(\vec{v}_s - \vec{v}_g\right)\right| \tag{4.19}$$

$$C_D = 0.63 + 4.8/\sqrt{\frac{Re_s}{v_{t,s}}} \tag{4.20}$$

The continuity equation for the solid phase needs the calculation of the granular temperature Θ_s. So one additional transport equation is to be solved, as given in the equation (4.21);

$$\left(-P_s \bar{\bar{I}} + \bar{\bar{\tau}}_s\right) : \vec{\nabla} v_s - \lambda_{\Theta s} + -3\beta\Theta_s) = 0 \tag{4.21}$$

Dissipation of kinetic-energy fluctuation given by [Lun et al. (1984)] is written in Eq.(4.22) as;

$$\gamma_{\Theta s} = \frac{12\left(1 - e_{g,s}^2\right) g_{0,ss}}{d_p \sqrt{\pi} \rho_s \varepsilon_s^2 \Theta_s^{3/2}} \tag{4.22}$$

1st term in the transport in the drastic collision of particles, [Lun et al. (1984)], and the last term represents the energy exchange between both the phases. Restitution coefficient for the collision of particles (e_{ss} = 0.9), [Rong et al. (1999); Tsuji et al. (2008)] for both the polymer and glass particle.

The energy equation for gas phase

$$\frac{\partial}{\partial t}\left(\varepsilon_g \rho_g H_g\right) + \nabla.\left(\varepsilon_g \rho_g \vec{v_g} H_g\right) = \nabla.\varepsilon_g k_g^{eff} \nabla T_g - h_{gs}\left(T_s - T_g\right) \tag{4.23}$$

The energy equation for the solid phase

$$\frac{\partial}{\partial t}\left(\varepsilon_s \rho_s H_s\right) + \nabla.\left(\varepsilon_s \rho_s \vec{v_s} H_s\right) = \nabla.\varepsilon_s k_s^{eff} \nabla T_s - h_{sg}\left(T_s - T_g\right) \tag{4.24}$$

4.1.5 NUMERICAL PROCEDURE

In the present investigation, finite volume method and 1st order implicit unsteady formulation was used.

The discretization of the convective fluxes is 1st order upwind.

Phase coupled SIMPLE algorithm is used to solve the equations for a 3-D simulation model of the RFB-SG unit without slit [Vasquez (2000)].

4.1.6 PHYSICAL MODEL DESCRIPTION

In the present simulations, the three-dimensional model of the RFB-SG unit without slit has been selected, as shown in Figs. 4.1 and 4.2. The dimensional details of the vortex unit, such as the diameter of the chamber, breadth of the spiral chimney outlet, length of the unit, the width of the air inlet, and the number of air inlets are 240 mm, 70 mm, 50 mm, 6 mm, and 8, respectively. Multiple air inlets attached to the unit periphery are attached at an angle of 30° with its tangential direction. The particle size is assumed to be of diameter 0.0025 m and other details related to the particle is listed in Table 4.3.

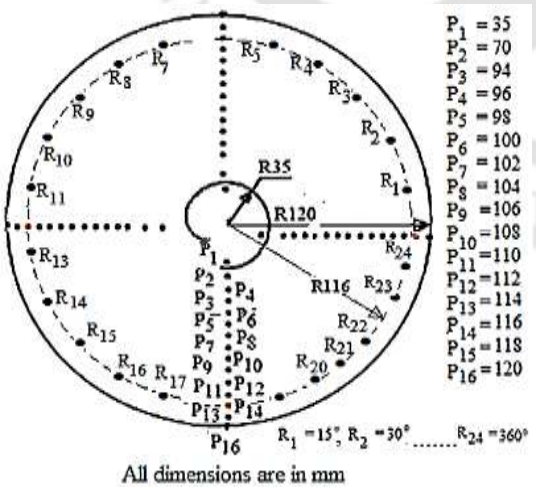

Figure 4.1 Dimensions of the RFB-SG unit without slit

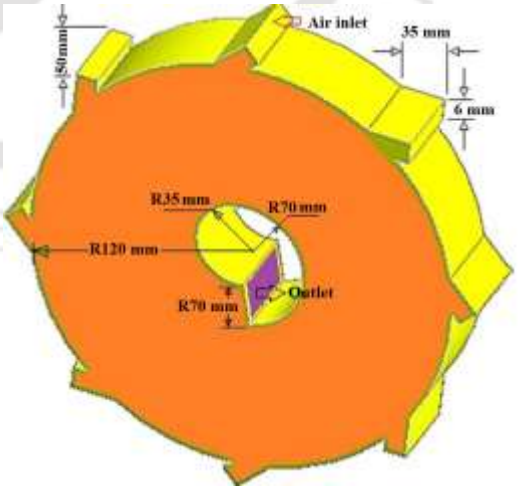

Figure 4.2 3-D geometry of a RFB-SG unit without slit

4.1.7 SIMULATION PARAMETERS AND BOUNDARY CONDITIONS

Boundary conditions, simulation-parameters, and thermo-physical parametric details of the gas-solid phase are illustrated in Table 4.1, 4.2, and 4.3. The isothermal condition is considered throughout the system and the pressure at the outlet is assumed to be atmospheric.

Table 4.1 Boundary conditions for simulation model

Setup description	Types of BCs.	Explanations
Inlet	Velocity inlet	Uniform distribution for gas phase No particles enter for solid phase
Outlet	Pressure outlet	Atmospheric
Chamber periphery	Stationery wall	No-slip for gas and Free slip for solid phase
Front wall	Stationery wall	No-slip for gas and Free slip for solid phase
Rear wall	Stationery wall	No-slip for gas and Free slip for solid phase
Chimney wall	Stationery wall	No-slip for the gas-phase and Free-slip for solids

Table 4.2 Parameters used in the simulations

Description	Selected value
Two phase model (gas-solid)	Eulerian-Eulerian approach, with kinetic theory
Pressure-velocity coupling	Phase-coupled SIMPLE
Discretization scheme	Second order upwind-scheme
Time step used	0.002 s
Convergence criteria	0.0001 for momentum and 0.000001 for energy
Under relaxation factors	For pressure 0.5, momentum 0.2, and volume 0.2.
The angle of internal friction	30°
Restitution coefficient	0.9
Maximum limit of solids packing	0.63
Air flow rate	600-800 m^3/h
Inlet air temperature	338 K

Table 4.3 Thermo-physical parametric details of the gas-solid phase

Phases	Density of gas-solid phases (kg m-3)	Thermal conductivity (W/mK)	Specific-heat capacity of gas-solid phases (J/kgK)
Gas-phase	1.2250	0.02420	994
Solid-phase	800	0.04540	737

4.2 RESULTS OF NUMERICAL SIMULATION OF RFB-SG UNIT WITHOUT SLIT

4.2.1 INTRODUCTION

The results of the experiments performed based on the methodology described in Chapter 3 are presented systematically in this chapter. In the present work, numerical simulations have been conducted to analyze the behavior of particle fluidization and heat transfer features of two phases in the RFB-SG unit without slit and scaled-up RFB-SG unit without slit. Predicting the capacity and heat transfer characteristics of RFB-SG unit without slit, an experimental drying setup has been developed to evaluate its performance using paddy.

The present study is mainly concerned with the behavior of particle fluidization and heat transfer features of two phases in the RFB-SG unit without slit. To predict the maximum fluidization capacity as well as heat transfer characteristics, the effect of fluidization air velocity, pressure, operating temperature, and size of the unit was numerically analysed. A comparative study of RFB-SG unit without slit and RFB-SG unit with slits has also made.

4.2.2 NUMERICAL ANALYSIS OF RFB-SG UNIT WITHOUT SLIT

CFD simulations has been performed to investigate the gas-solid hydrodynamics and heat transfer characteristics and the solid loading capacity of the unit, considering several parameters, such as temperature difference, heat transfer coefficient, and effect of fluidization air velocity. An experimental study on paddy drying has also been conducted in detail, verifying the capacity of solids fluidization and its flow pattern in the RFB-SG unit without slit.

4.2.3 TEST OF GRID INDEPENDENCE

This examination, the convergence criteria are established as 10^{-3} and 10^{-6} for physical variable residual and the energy residual values, respectively. Grid independence tests for three grids, namely G1, G2, and G3, have been accomplished by measuring suspension density for the number of the grid-cells of 80000, 94500, and 116610, respectively as shown in Fig. 4.3. Also, suspension density variations for the three densities G1, G2, and G3 are observed to be more or less similar in the number of cells. Consequently, grid G2 is selected in further simulations, accepting the estimation time and accuracy.

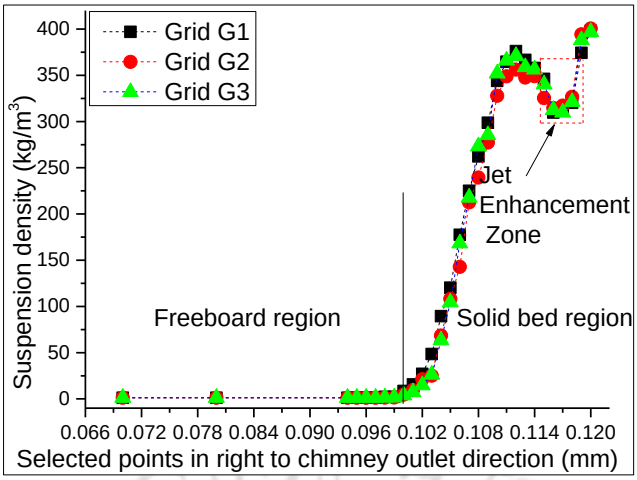

Figure 4.3 Grid independence test

4.2.4 NUMERICAL STUDY ON THE EFFECT OF DIFFERENT PARAMETERS

In the present study, CFD simulations have been performed under the effect of several operating parameters such as pressure deviation in different locations of the unit, velocity-distribution in the radial direction, particle fluidization velocity, and capacity.

4.2.4.1 VARIATION OF VOLUME FRACTION OF SOLID

The volume fraction of solids of solid-bed region and freeboard region is investigated from right, top, left, and bottom to the chimney outlet directions, as shown in Figs. 4.4 and 4.5. The volume fraction of solid first decreases from 0.4 to 0.35 in the bed-thickness of 120-118 mm by the impact of air, and in remaining bed thickness 118-116 mm, it increased to 0.385. It seems that the solid density is more stable in the location far from air inlets.

4.2.4.2 VARIATION OF PRESSURE IN SOLID-BED REGION

Fig.4.6 shows the pressure variation in four directions, namely right inlet, top inlet, left inlet, and bottom air inlet to chimney outlet. In each of the four directions, various location points (P1-P16) have been selected to analyze pressure distribution (see contour Fig.4.7). Initially, the higher velocity air comes into contact with the dense solid bed near the inlets where pressure seems to be very less. Initially, the higher velocity of air induces to rotate solid particles in the solid-bed region (120-116 mm), and the pressure is reached to its peak of 350 Pa. Further, the pressure is falling continuously in the solid-bed region (116-106 mm). However, at the end of the solid bed region, the pressure seems to be rise slightly, but it decreases again in the freeboard region. The pressure is falling in the right and top direction near to the chimney outlet, on the other hand, it increases in the left and bottom location.

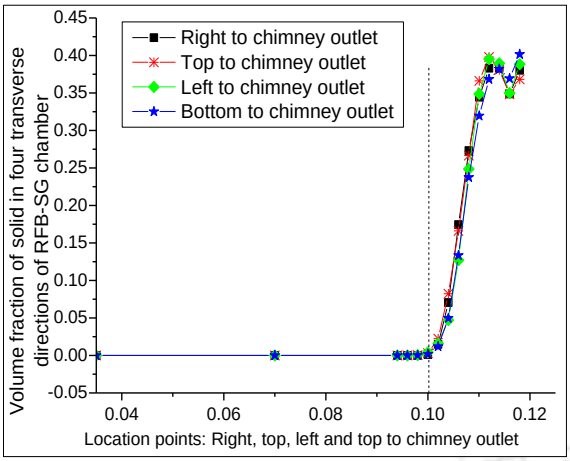

Figure 4.4 Variation in the volume fraction of solid

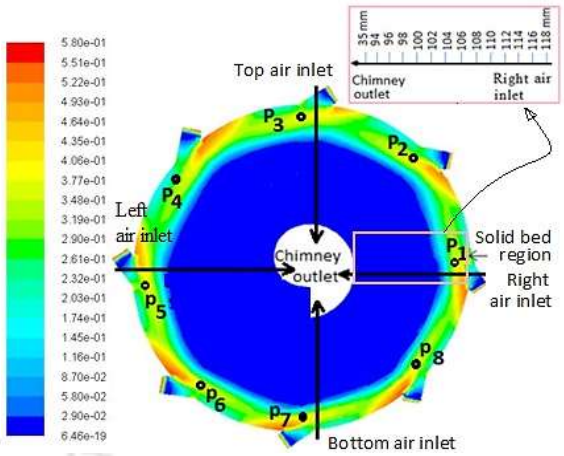

Figure 4.5 The contour volume fraction of solid

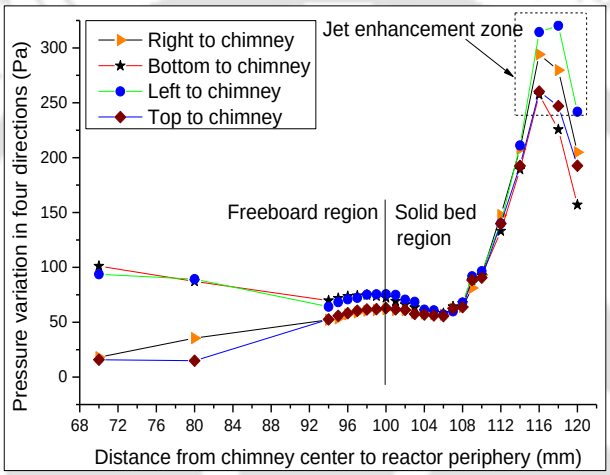

Figure 4.6 Pressure variation in four directions right, top, left, and bottom to outlet

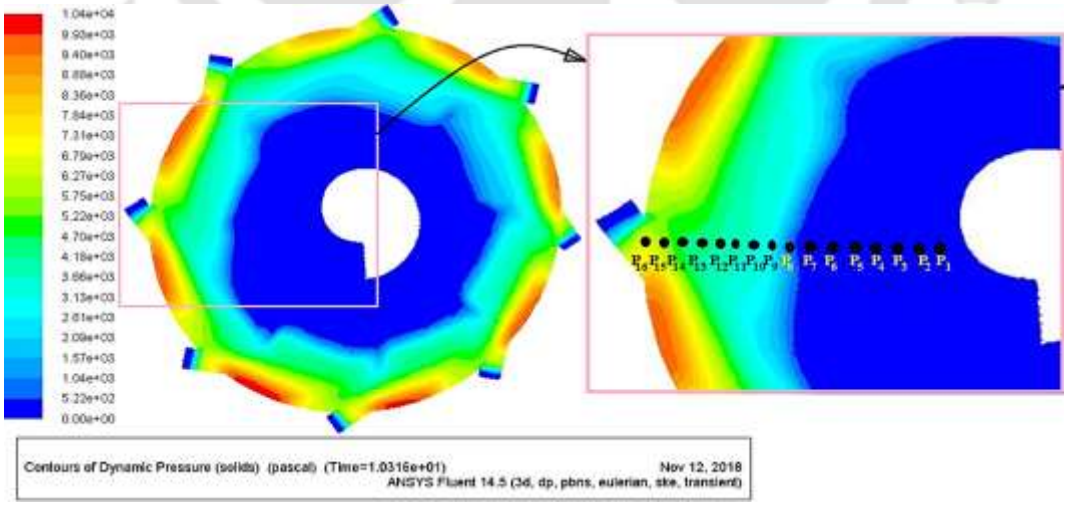

Figure 4.7 Contour of dynamic pressure of solids

4.2.4.3 EFFECT OF AIR VELOCITY IN RADIAL-DIRECTION

Figures 4.8 and 4.9 present the air velocity variation along the radial direction at various location points selected on two radii of 116 and 35 mm, respectively. The air velocity in the radial direction of the unit is fluctuating in the web form in the similar manners. It is observed higher at the radius of 35 mm near to air inlets location, while it is comparatively low at the location points selected on the radius of 116 mm. Also, the air velocity is increased to 110 m/s, near to the chimney outlet as shown in highlighted in Fig.4.8.

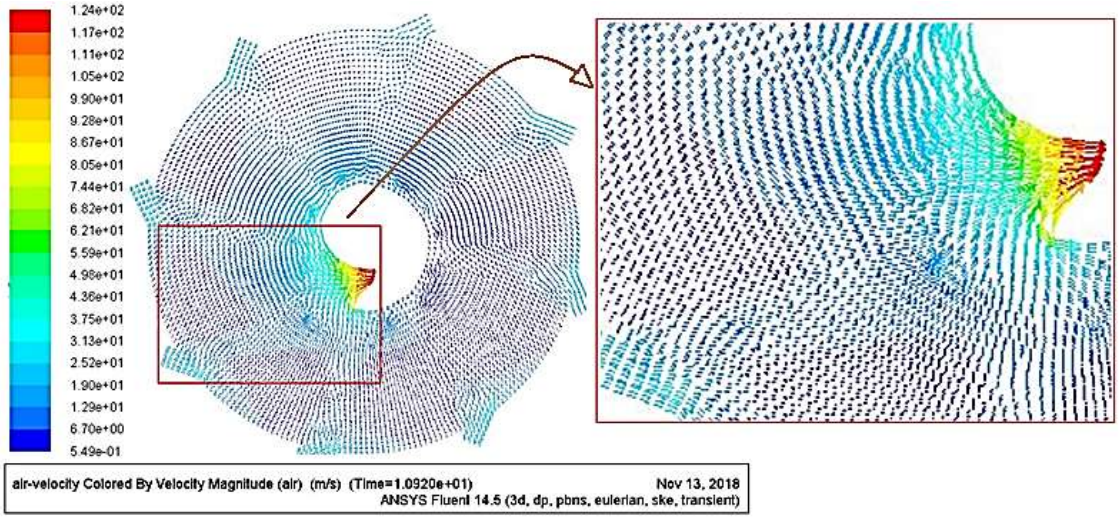

Figure 4.8 Contour of air velocity vector

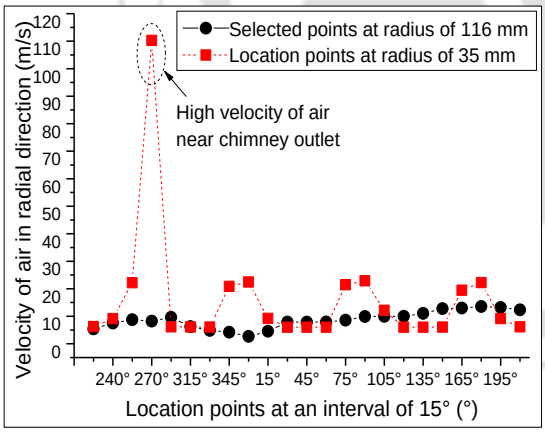

Figure 4.9 Effect of velocity in the radial direction at radius 35 and 116 mm

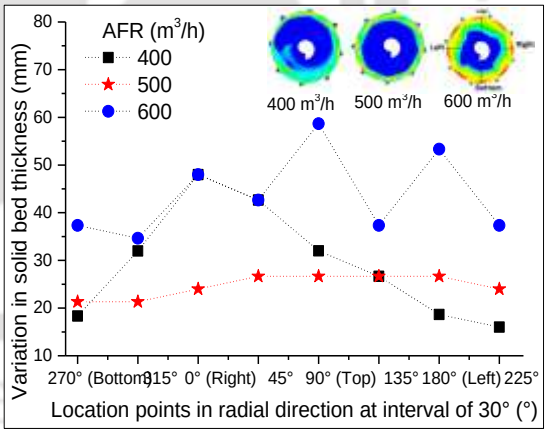

Figure 4.10 Effect of AFR on the fluidization capacity

4.2.4.4 INFLUENCE OF AIR FLOW RATE ON SOLID LOADING CAPACITY

Figure 4.10 illustrates the solid bed-thickness at the selected locations, such as 0°, 4°, 90°, 135°, 180°, 225°, 270°, and 315° angle of the vortex chamber. For the solid loading of 300 g, 400 g, and 500 g, the solid-bed thickness is varying in various selected locations of the

vortex chamber at the air flow rate of 400, 500, and 600 m^3/h, respectively. A non-uniform solid-bed is formed at the air flowrate of 400 m^3/h for 300 g solid loading, while a stable solid-bed of uniform thickness is obtained at the air flowrate of 500 m^3/h, for the solid loading of 400 g. Furthermore, on increasing solid loading capacity more than 500 g, the non-uniformity of bed is observed, fluidization of particles seems to be collapsed.

Figure 4.11 shows the temperature distribution in the radial direction in RFB-SG unit on various points selected at different two radii 116 and 46 mm, respectively. The slight temperature difference in the radial direction indicates that the gravity force is less dominated. The temperature is almost constant (337.9 K) on the selected locations on the radius of 116 mm, while the temperature gradient is varying in the web forms at a radius of 45 mm. The maximum temperature has been observed 337.95 K, in the left-bottom location (at an angle of 210-degree angle on radius 45 mm) near to the chimney outlet.

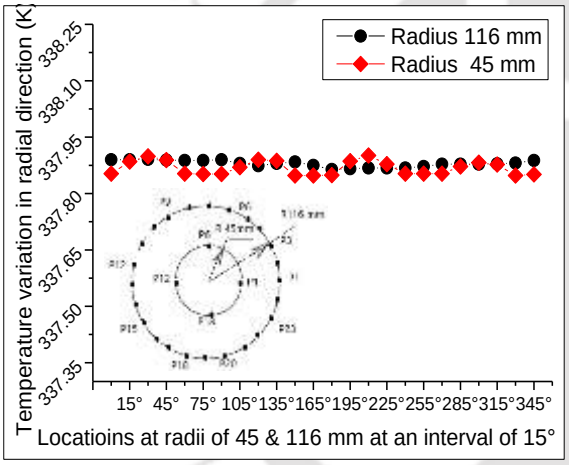

Figure 4.11 Temperature variation in radial direction

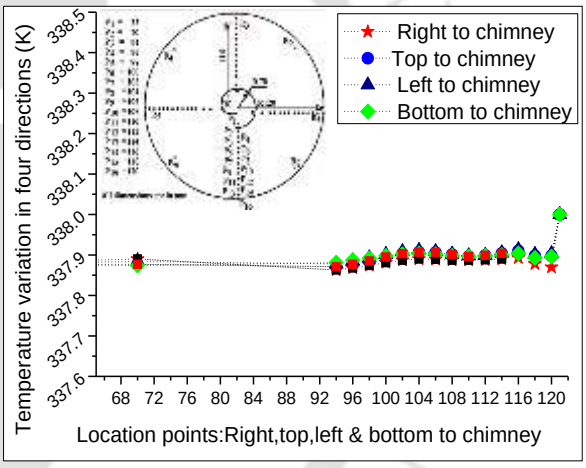

Figure 4.12 Temperature variation in four different directions

Figure 4.12 illustrates the temperature distribution in the selected directions, such as right, top, left, and bottom to chimney outlet. These 16 location points (P_1-P_{16}) are selected in each of all four directions. The pattern of temperature distribution seems similar in all four directions, while the temperature is observed higher in the right to chimney outlet and lower in the direction left to chimney outlet. When the air was injected into the vortex chamber, the air temperature decreased rapidly due to the dense bed of particles near to the air inlet, especially on the right side (120-115 mm) of the RFB-SG unit where the gravity effect is comparatively higher than the other three locations of the unit. Further, a minor

variation of temperature of 0.05 K (337.85-337.90 K) was noticed in the bed-length of 20 mm (115-95 mm) onward in all four locations.

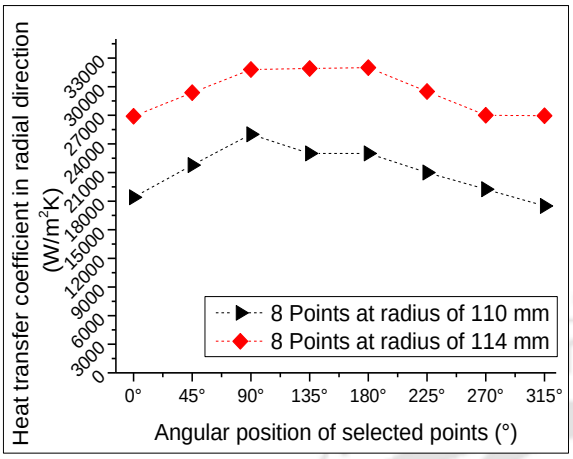

Figure 4.13 Heat transfer coefficient in radial direction at an interval of 45° angle

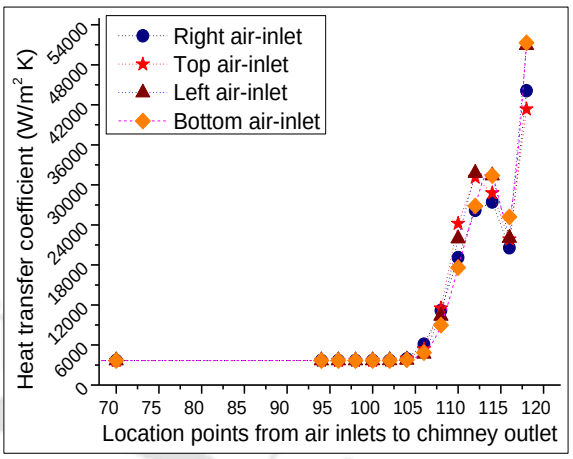

Figure 4.14 Heat transfer coefficient in four different directions

Figure 4.13 illustrates the difference of heat transfer coefficient in radial directions at two different radii of 110 mm and 114 mm, respectively. In both the curves at radius of 110 mm and 114 mm, the heat transfer coefficient at the top location of the RFB-SG unit is higher (31800 and 25000 W/m^{2}K) as compared to the other three locations of the vortex chamber while it is seen lowest in the bottom location.

Figure 4.14 shows the variation of heat transfer coefficient, in four different directions such as right, top, left, and bottom to chimney outlet. The pattern of the heat transfer coefficient variation seems similar in all four directions, while it is observed maximum of 51301.7 W/m^{2}K towards the bottom-inlet to chimney outlet direction and lowest of 41338.6 W/m^{2}K in the top-inlet to chimney outlet direction. When the air injected into the vortex chamber, the heat transfer coefficient decreases (51301.7-25198.4 W/m^{2}K) rapidly, due to the higher density of particles near to the air inlet, especially (41338.6-20568.7 W/m^{2}K) in the right side (120-116 mm) of the RFB-SG unit where the gravity effect is observed comparatively higher than the other three locations of RFB-SG unit. Further, the variation of heat transfer coefficient is recorded 27.721.98 W/m^{2}K, in the length of 20 mm (115-95 mm) onward in along chimney outlet direction. The heat transfer coefficient is almost constant (3679 W/m^{2}K) in the freeboard region of the unit. Figures 15, 16 and 17 show different contours of volume fraction of solid at the air flow rate of 400 m^3/h, and 600 m^3/h, and pressure variation.

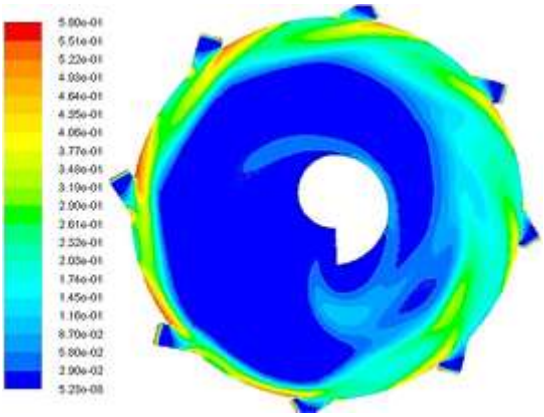

Figure 4.15 Contours of volume fraction of solid at t =20s, AFR = 400 m³/h and I = 400 g

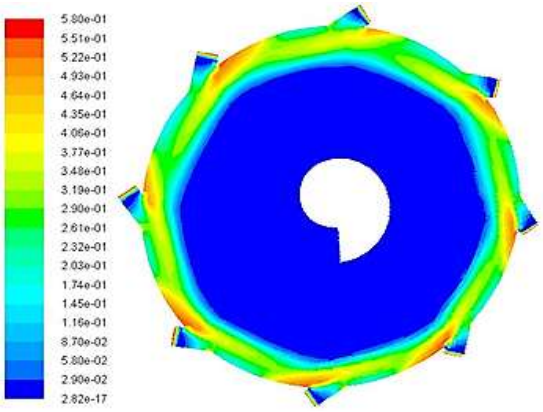

Figure 4.16 Contours of volume fraction of solid

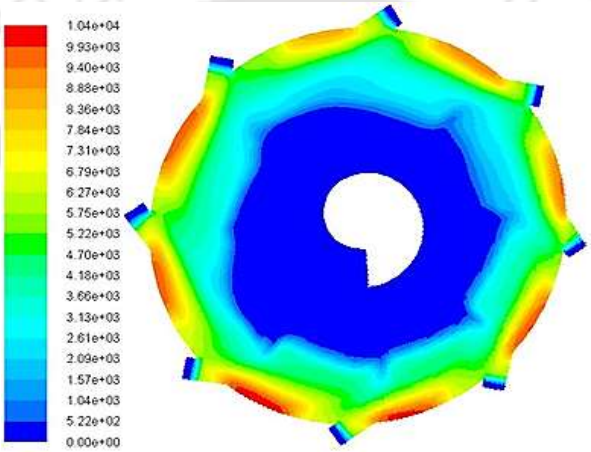

Figure 4.17 Contours of pressure variation at t = 20 s, and solid loading of 500 g

4.3 SUMMARY

In this Chapter, the numerical simulation model of RFB-SG unit without slit has been described in detail. Also, the dimensional detail, model descriptions, simulation parameters, and boundary conditions are explained. In chapter 5, experimental results and discussion on drying, comparative analysis of RFB-SG unit without and with slit, experimental validation of RFB-SG without slit and scale-up of RFB-SG dryer without slit are discussed in terms of length to diameter ratio (L/D).

CHAPTER-5

RESULTS AND DISCUSSION ON INVESTIGATION OF RFB-SG UNIT WITH AND WITHOUT SLIT

5.1 INTRODUCTION

Parametric studies on paddy drying have been conducted in a rotating fluidized bed with static geometry (RFB-SG) unit with and without slit. In this chapter, effect of various parameters on the drying characteristics has been studied in two distinct sections 5.5.2 and 5.5.3. Experimental input variables for RFB-SG dryer without slit and with slit are illustrated in Table 5.1.

Table 5.1 Experimental input variables for RFB-SG dryer without slit and with slit

Experimental conditions		
1	Ambient air temperature	300-304 K
2	Inlet air temperature	328-338 K
3	Relative humidity (RH) in the Lab	55-65%
4	Inventory RFB-SG dryer without slit	300–500 g
6	The initial moisture content of grains	29±4% (wb) approx.
7	The controlled final moisture content of paddy	13±0.8% (wb)
8	The electrical energy input for air heating	3-6 k We
9	Airflow rate (from the main duct) in RFB-SG dryer without slit	400–600 m^3/h

5.2 EXPERIMENTAL INVESTIGATION OF RFB-SG DRYER WITHOUT SLIT

Based on the experimental procedure described in the chapter 3, series of experiments were carried out in the RFB-SG dryer without slit. Initially, a few trials of multiple food grain fluidization such as coriander, black pepper, tea, and paddy were carried out. Whereas the performance evaluation of the developed dryer has been carried out using readily available food grain paddy. Results of the experiments of batch drying are discussed in the different subsections.

5.2.1 INFLUENCE OF AIRFLOW RATE ON DRYING TIME

At 10 minutes, the observation of paddy drying, the superficial moisture is rapidly removed within 2-3 minutes. Figures 5.1, 5.2, and 5.3 show the effect of air flow rate (600–800 m^3/h) on the drying time of 400 g paddy at the operating temperatures of 328, 333, and 338 K, respectively. It is observed that the drying time is reduced by 18%, 25.4%, and 40 % at the operating temperature of 328, 333, and 338 K, respectively. Figure 5.3 clearly shows that the drying time is significantly lower (17 min) at air temperature of 338 K to reach the safe moisture content (MC) level of (13±0.8 %) with an error of 4.8% as shown in appendix D.

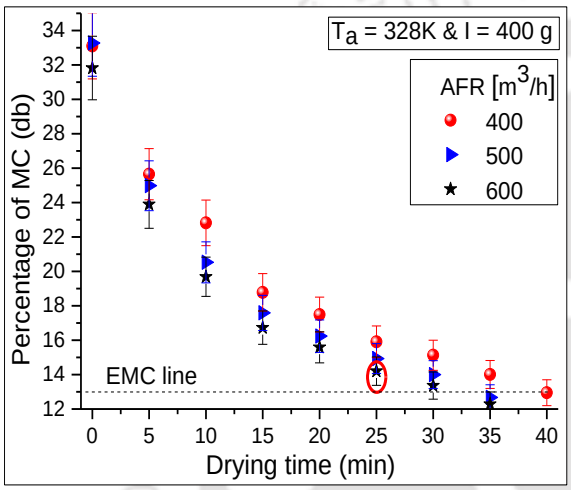

Figure 5.1 Effect of air flow rates on drying time at temperature of 328 K and I=400 g

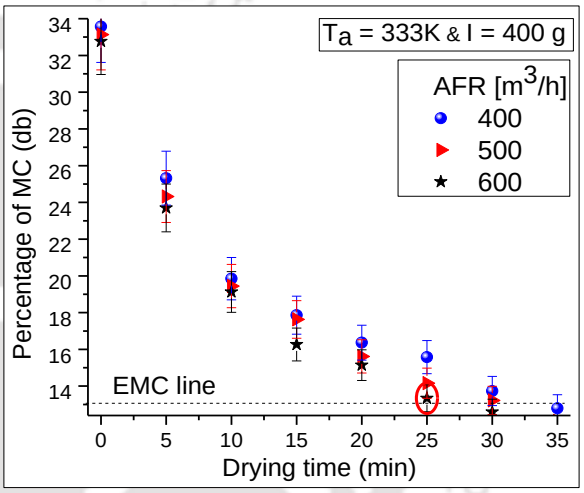

Figure 5.2 Effect of air flow rate on drying time at temperature of 333 K and I=400 g

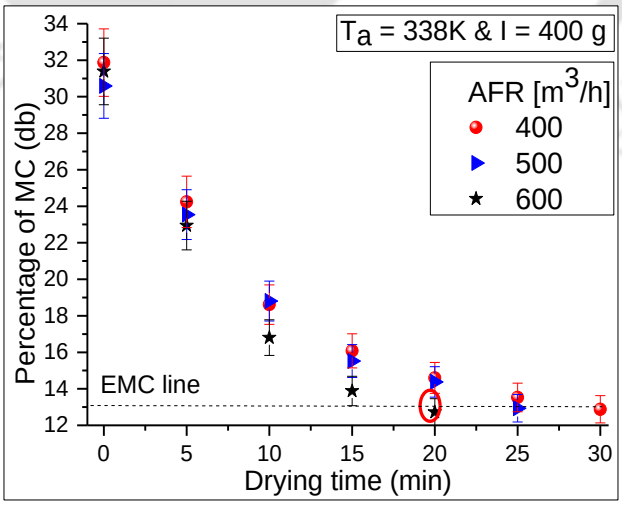

Figure 5.3 Effect of air flow rate on drying time at temperature of 338 K and I=400 g

5.2.2 INFLUENCE OF INLET AIR TEMPERATURE ON DRYING TIME

The slope of curves at varying air temperatures of 328, 333 and 338 K, are representing the percentage of moisture contents (MC) concerning time, as shown in the Figs. 5.4, 5.5, and 5.6. In the entire experimental investigations, the time of drying initialization is considered just after the end of the solid (paddy) feeding process. Figure 5.4 shows that on increasing drying air temperature from 328-338 K, the drying time is reduced by 43% in 29-15.5 min to reach a safe moisture content of paddy i.e. 13±0.8%db for inventory of 300 g and the air flow rate of 600 m^3/h. Figure 5.5 shows that on increasing drying air temperature from 328-338 K, the drying time is reduced by 40% in 32-19 min for an inventory of 400 g and the air flow rate of 600 m^3/h.

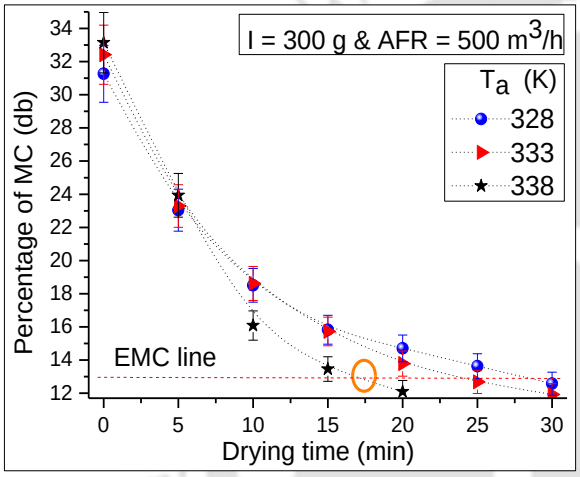

Figure 5.4 Effect of temperature on drying time at 600 m^3/h and I= 300 g

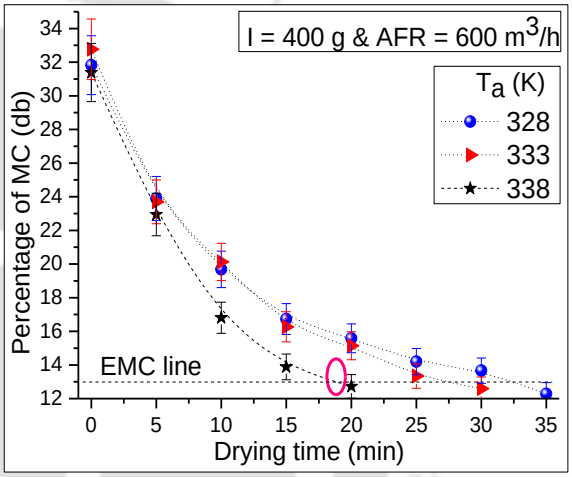

Figure 5.5 Effect of temperature on drying time at 600 m^3/h and I= 400 g

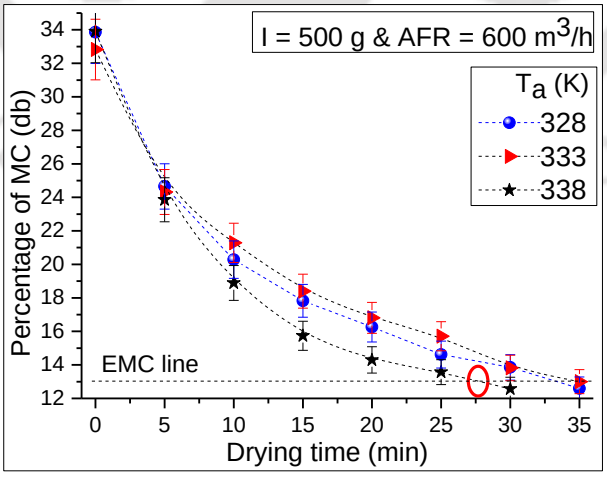

Figure 5.6 Effect of temperature on drying time at 600 m^3/h and I= 500 g

Similarly, Figure 5.6 shows that with the increase of air temperature from 328 to 338 K, the drying time is reduced by 35% in 34 to 22 min for the inventory of 500 g and the air flow rate of 600 m^3/h with an error of 4.4%. Although the drying rate increases when the temperature rises, paddy drying at temperature more than 338 K reduces the nutritional value of the paddy [Pati et al. (2016)].

5.2.3 INFLUENCE OF INVENTORY ON DRYING TIME

Figures 5.7 and 5.8 show an indicative influence of inventory of 300-500 g at the air inlet temperatures of 328 K and 338 K, respectively. It is observed that an increase in solid feeding rate lowered the specific drying rate in paddy. An effective air utilization method to reduce air consumption has been introduced in this investigation. The drying time of 300 g paddy is increased by 15.6% at the operating temperature of 328 K, while the drying time of 500 g paddy is increased by 23.5% at the air temperature of 338 K. However, the drying time of paddy increases with inventory, but the percentage increase in drying time is less as compared to the percentage increase in the inventory. Hence, the overall drying time is reduced with an error of 5.1%. Therefore, it is evidently stated that the drying is still being far from saturation, especially at the last stage of the drying operation.

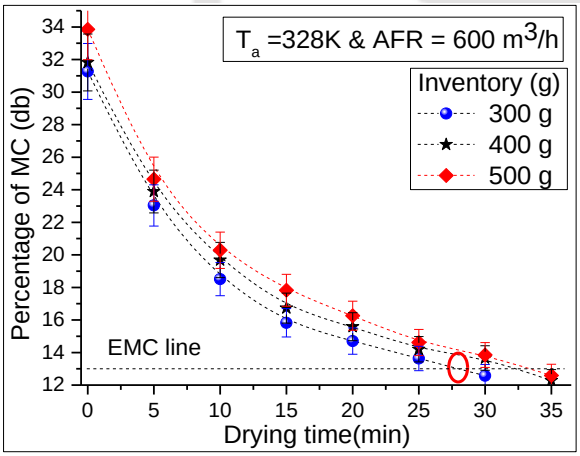

Figure 5.7 Effect of inventory on drying time at T_a = 328 K, and AFR = 600 m^3/h

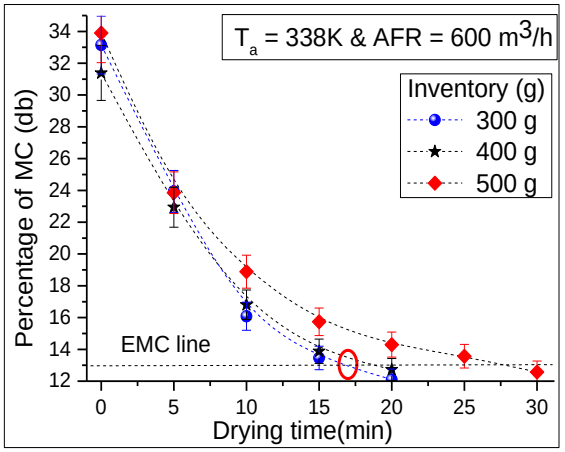

Figure 5.8 Effect of inventory on drying time at T_a = 338 K, and AFR = 600 m^3/h

5.3 COMPARISON OF RFB-SG DRYER WITH AND WITHOUT SLIT

Figures 5.9-5.11 show the comparison of performance of RFB-SG dryer without and with slits dryer, for varying inventory of 300-500 g paddy, at air flow rate of 600 m^3/h, the temperature of 338 K, and drying time.

Figure 5.9 shows that the drying time of 300 g paddy in both the RFB-SG without slit and with slit, at the air temperature of 338 K and air flow rate of 600 m^3/h. It is found that the drying time is found to be 32% lesser in the RFB-SG dryer without slit as compared to RFB-SG dryer with slit at the operating temperature of 338 K, while the drying time for the inventory of 400 g, is observed 23.5% lesser in RFB-SG dryer without slit as compared to RFB-SG dryer with slit as shown in Fig.5.10. In the same way, Fig.5.11 shows that at the operating temperature of 338 K the drying time is reduced by 23% in RFB-SG dryer without slit as compared to RFB-SG dryer with slit.

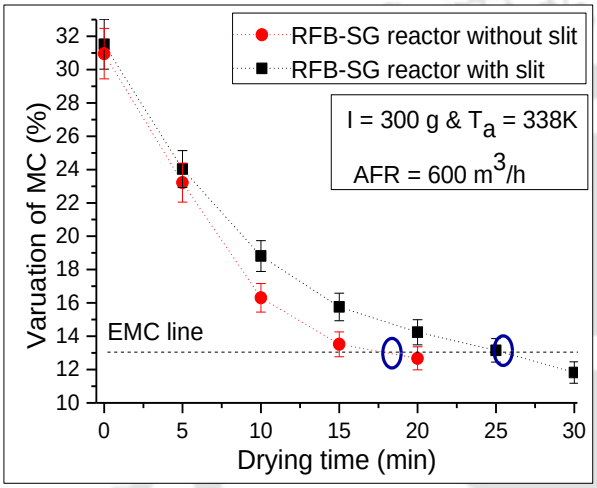

Figure 5.9 Variation of MC for 300 g paddy in RFB-SG dryer without and with slit

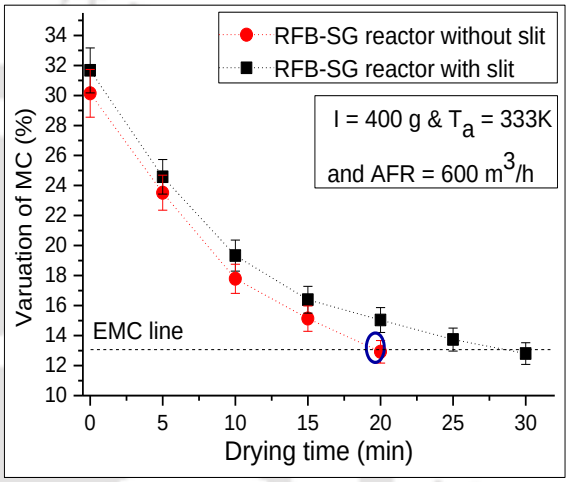

Figure 5.10 Variation of MC for 400 g paddy in RFB-SG dryer without and with slit

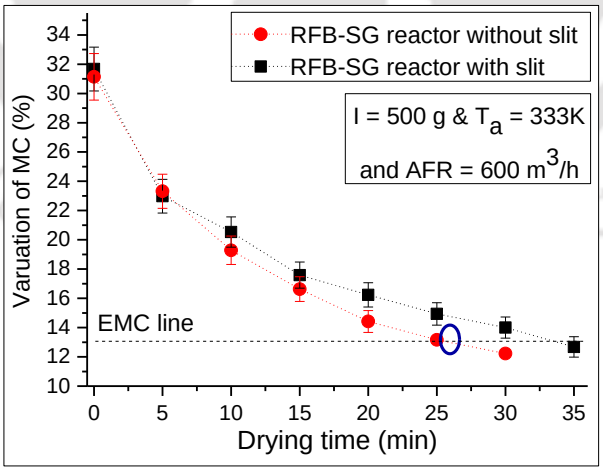

Figure 5.11 Variation of MC for 500 g paddy in RFB-SG dryer without and with slit

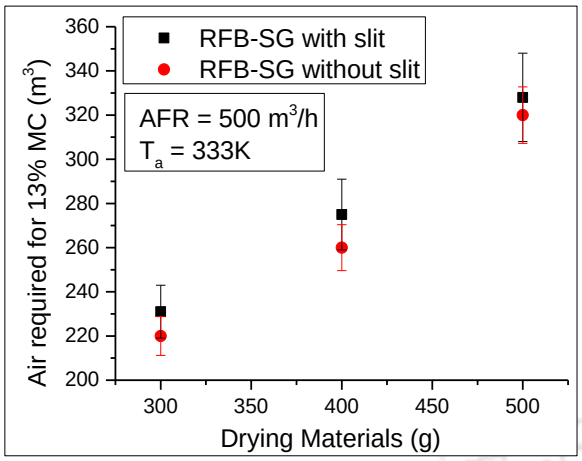

Figure 5.12 Amount of air required for solid loading in RFB-SG dryer without and with slit

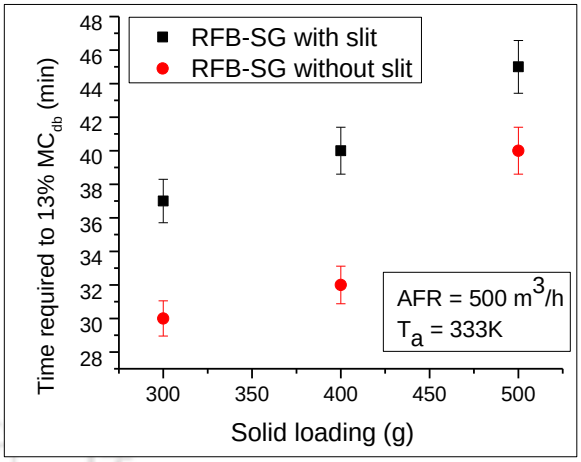

Figure 5.13 Drying time to reach MC (13%) of paddy in RFB-SG dryer without slit and with slit

Figure 5.12 shows the amount of air required in drying of 400 g paddy in RFB-SG dryer without slit and with slit at the drying air temperature of 333K, and the airflow rate of 500 m^3/h. Though the mass, momentum, and heat transfer occur through the chimney outlet in both dryers, the total amount of air required is 5.45% lesser in RFB-SG dryer without slit than the RFB-SG dryer with slit. Figure 5.13 shows the time required to reach the safe moisture content level of paddy in both RFB-SG dryers without slit and with slit at the drying air temperature of 333 K. The drying time taken in the RFB-SG dryer without slit is 21% lesser than the RFB-SG dryer with slit.

5.4 STUDIES OF BEAKAGE OF PADDY GRAINS

The estimation of the fraction of broken particles (paddy grains) concerning time for selected operating conditions, such as air inlet temperature, airflow rate, and inventory loading, as shown in Fig. 5.14. This particle damage is caused by shear and normal stresses, which develop in a rapidly rotating solid-bed and the drying quality test is shown in appendix E. In the 22 minutes of time observation, the particle damage was found to be minimum at a higher airflow rate of 600 m^3/h, while it was observed maximum at a lower airflow rate of 400 m^3/h in 33 minutes. The fast attrition on a higher airflow rate was expected when less particle damage occurred at a higher airflow rate in a shorter time duration.

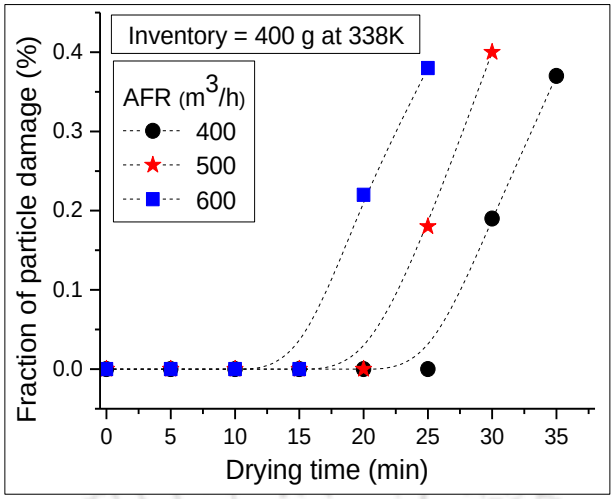

Figure 5.14 Fraction of particle damage at air inlet temperature of 338K and I= 400 g

5.5 EXPERIMENTAL VALIDATION OF RFB-SG UNIT WITHOUT SLIT

The numerical results are validated for three different parameters, such as temperature dissimilarity in the radial direction, variation in heat transfer coefficient with time, and influence of inlet air-velocity on RFB-SG unit fluidization capacity. In the following subsections results of the findings are presented.

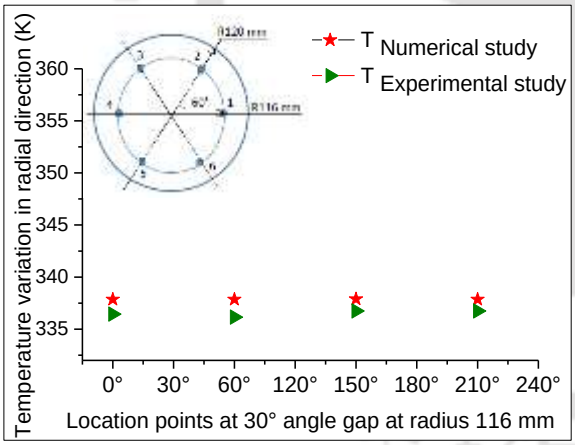

Figure 5.15 Comparison of temperature variation along the radial direction

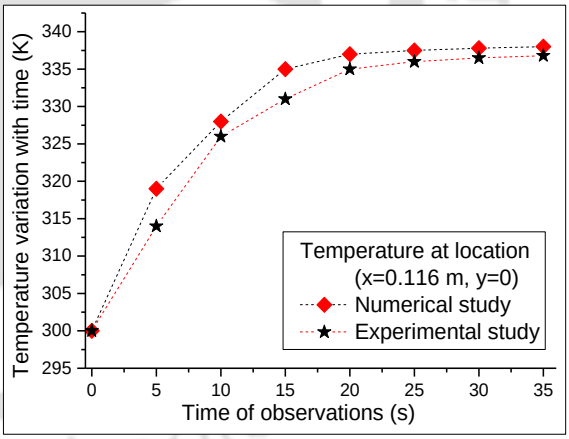

Figure 5.16 Comparison of temperature variation with time

5.5.1 COMPARISON OF TEMPERATURE VARIATION ALONG THE RADIAL DIRECTIONS

Figure 5.15 presents the influence of the air inlet temperature along the radial direction at a radius of 116 mm. The temperature difference in the radial direction is more or less the

same in numerical and experimental investigations. Yet, it is observed comparatively higher (1.55K) at the bottom position of the unit than other locations.

5.5.2. TEMPERATURE DIFFERENCE WITH TIME AT A SELECTED LOCATION POINT

Figure 5.16 shows the variation of temperature with time, at a selected point (x = 0.116 m, y = 0, & z = 0.025 m), in both numerical versus experimental investigations. However, the temperature variation between numerical and experimental investigations found to be very close. However, certain differences in temperature are noticed in different locations of the unit. A maximum deviation of 5.98% (degree-centigrade basis) has been observed at the time of 15 second.

5.5.3 VARIATION OF HEAT TRANSFER COEFFICIENT

Figure 5.17 shows the variation of heat transfer coefficient with time in both the numerical and experimental studies at a location point P_1 in the RFB-SG unit. The maximum difference in the heat transfer coefficient is calculated 7769 W/m²K at time of 15s, which is found to be 17.8% more in experimental results than numerical investigations.

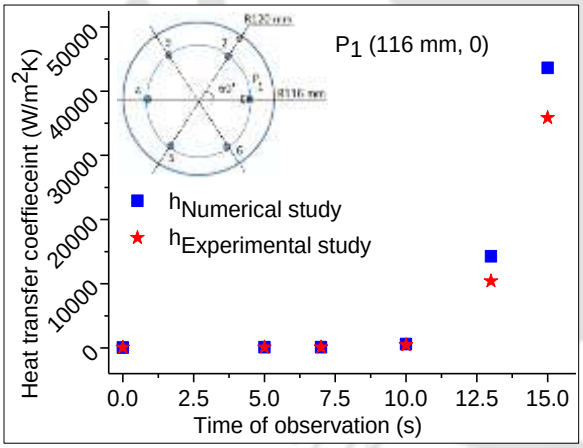

Figure 5.17 Comparison of heat transfer coefficient with time, at a selected point

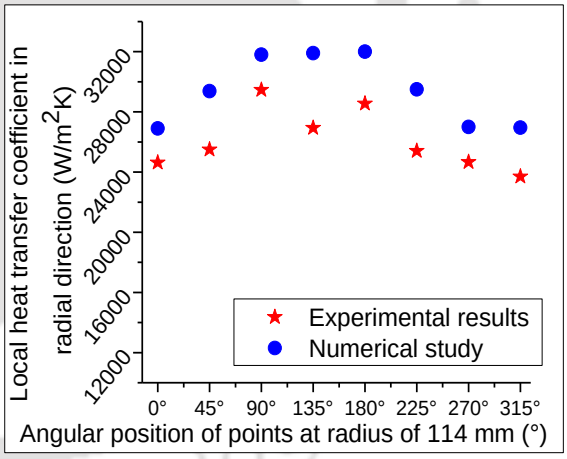

Figure 5.18 Comparison of heat transfer coefficient along radial direction

5.5.4 VARIATION OF HEAT TRANSFER COEFFICIENT IN RADIAL DIRECTION

Figure 5.18 shows the variation of heat transfer coefficient in radial directions at two different radii of 110 mm and 114 mm, respectively. In both curves at radius of 110 mm and 114 mm, the heat transfer coefficient at the top location of the RFB-SG unit is comparatively higher (31800 and 25000 W/m²K) than the other three locations, while it is lowest at the bottom location of the unit.

5.5.5 COMPARISON OF AIR FLOW RATE EFFECT ON LOADING CAPACITY

Figure 5.19 represents the difference in the numerical and experimental results on the effect of air flow rate vs. solid feed capacity. The minimum variation of solid loading capacity between experimental and the numerical studies are obtained at 3.25% for the fluidization air flow rate of 600 m^3/h. However, a maximum difference of the solid loading is found to be 7.72% more at the inlet airflow rate of 500 m^3/h. A good agreement between the numerical and experimental investigations justifies the validation of experimental results with the maximum errors of 0.24%, 17.8%, and 7.72% in the temperature, heat transfer coefficient, and inventory loading measurement, respectively.

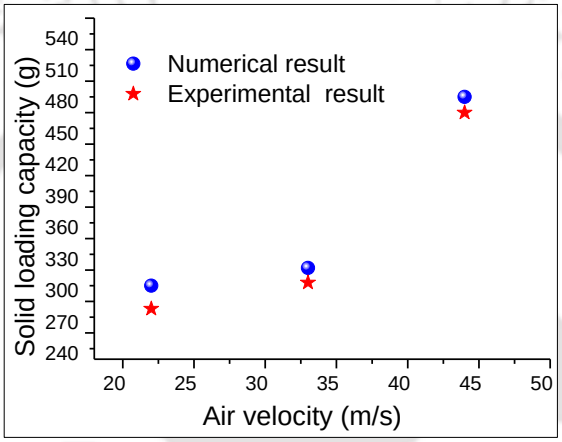

Figure 5.19 Effect of air flow rate on solid inventory

5.6 SCALE-UP OF RFB-SG UNIT WITHOUT SLIT

From the previous results discussed in this chapter it is found that performance of RFB-SG without slit is better than that of the RFB-SG with slits. Hence it is attempted to scale up the RFB-SG unit without slit numerically. To enhance the lab-scale RFB-SG unit's capacity without-slit, the numerical investigations have been conducted for three different lengths to diameter ratio (L/D=0.8, 1.0 and 1.2). Experimental results with L/D =0.2 is compared with the same. The unit diameter, air inlet width, chimney outlet width, and the number of air inlets are 240 mm, 8 mm, 70 mm, and 16, respectively. In the present study, the vortex chamber's length is increased from 50 mm to 300 mm for the dryer's capacity enhancement (500-3370 g), while the drying chamber diameter (240 mm) is fixed. Also, the dimensional details of three-dimensional RFG-SG model are presented in Fig. 5.20 and Table 5.2.

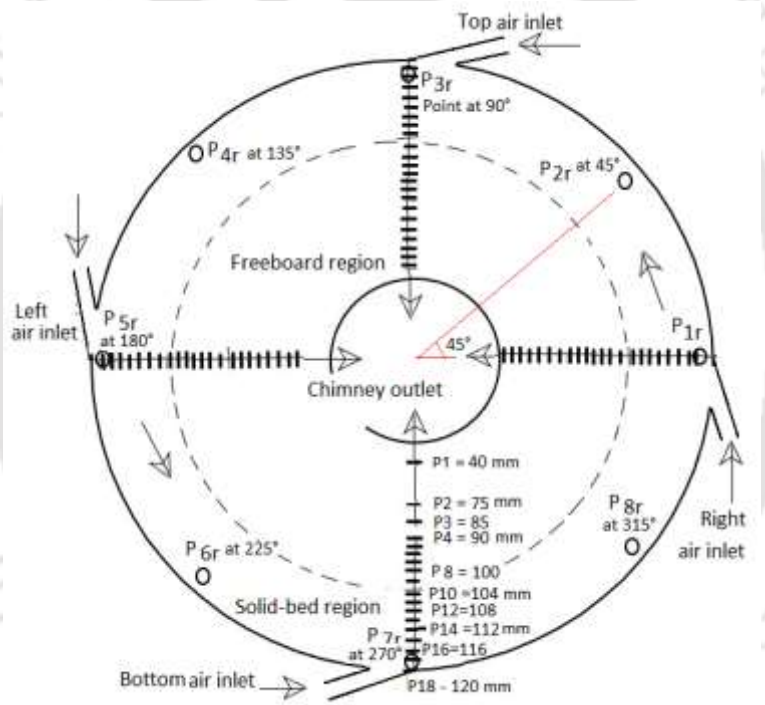

Figure 5.20 Dimensional details of selected locations

Table 5.2 Dimensional details of scale-up unit

L/D	Chamber diameter (D) in mm	Chamber length (L) in mm	Solid loading capacity (g)
0.2	240	50	500
0.8	240	200	2433
1.04	240	250	3041
1.2	240	300	3370

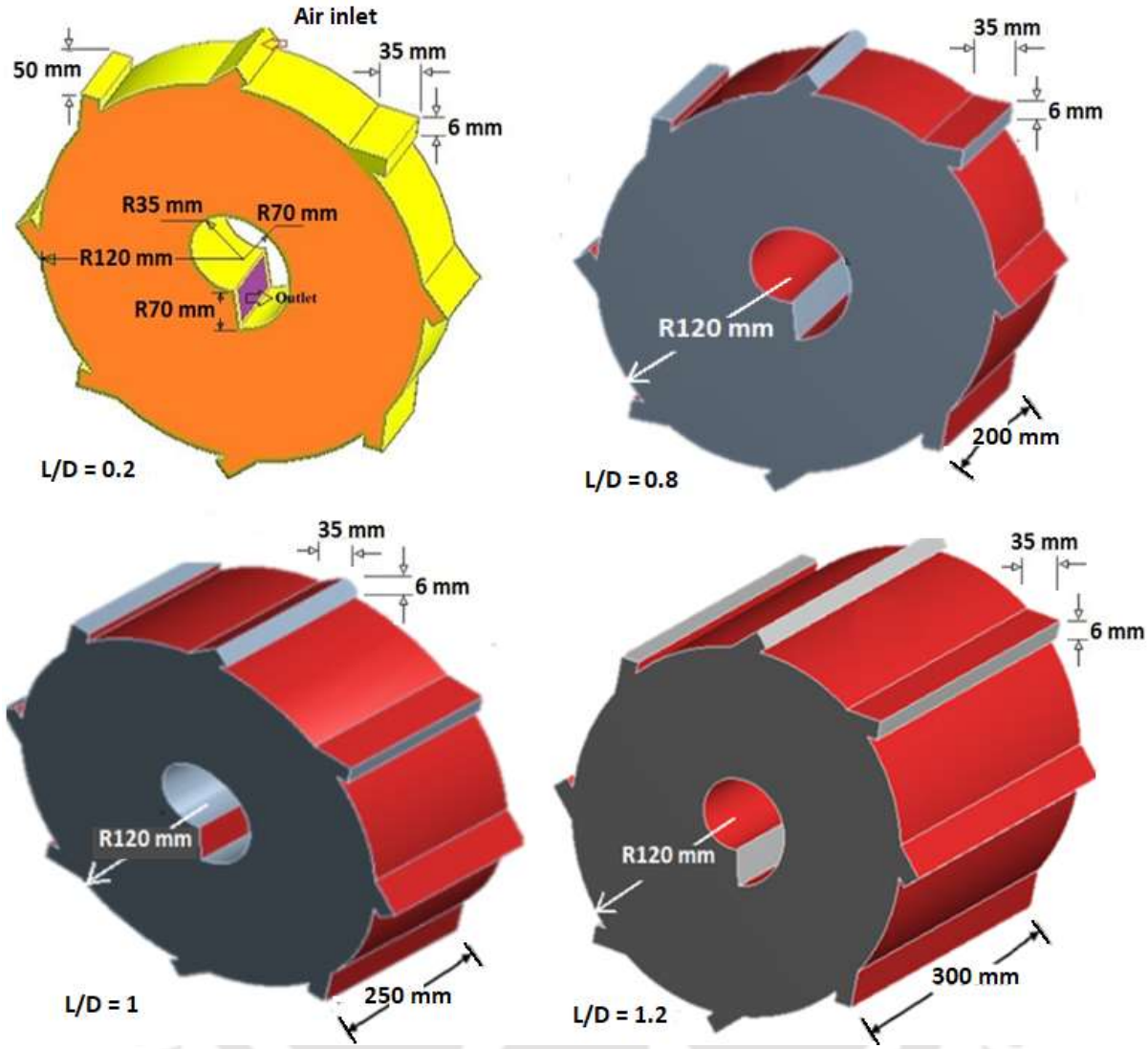

Figure 5.21 Three dimensional view of simulation models used in scale-up

5.6.1 NUMERICAL ANALYSIS ON SCALE-UP OF RFB-SG UNIT WITHOUT SLIT FOR L/D = 0.8

To enhance the fluidization capacity of RGB-SG unit without-slit, a numerical study has been conducted using a commercial software ANSYS FLUENT 14.5, considering the length to diameter ratio of 0.8, as shown in Fig. 5.21. The gas-solid hydrodynamic and heat transfer characteristics of the gas-solid phase in the RFB-SG unit without slits have been investigated considering numerous variables described in the following sub-sections.

5.6.1.1 VARIATION IN THE VOLUME FRACTION OF SOLID (L/D = 0.8)

The volume fraction of solid in four distinct directions is inspected, as shown in Figs. 5.22, and 5.23. It is noticed that the volume fraction of solid first decreases from 0.55-0.32 in the

small bed thickness of 120-118 mm near the air inlet locations. However, the volume fraction variations are symmetric in all directions; still, the maximum (0.11) and minimum (0.8) variations of volume-fraction of solid are noticed at the location point of 112 mm and 116 mm, while it is almost zero in the freeboard region. Also, it is observed that the volume fraction of solid is suddenly decreased near to the air inlets due to the impact of high-velocity air and jet effect is observed at the location of 116 mm.

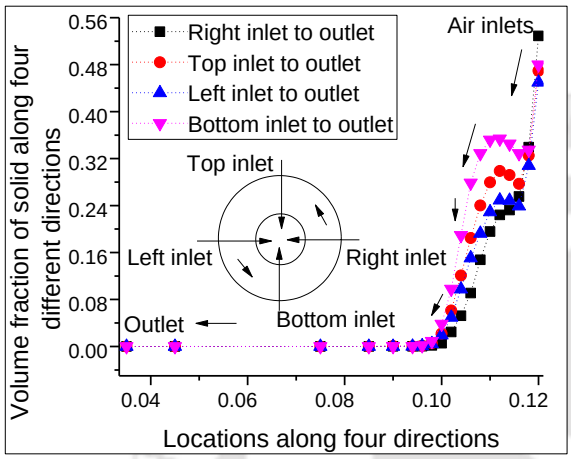

Figure 5.22 Volume fraction of solid in different directions

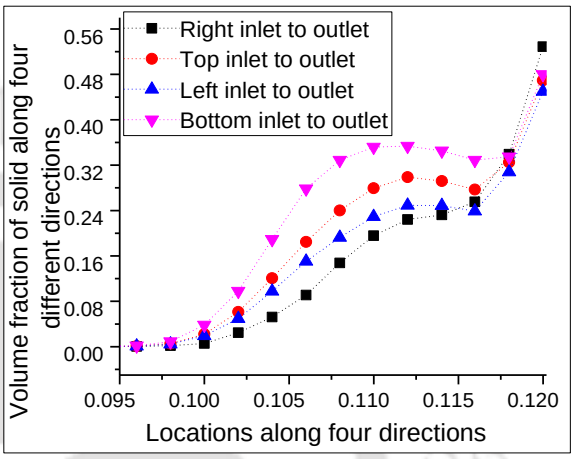

Figure 5.23 Volume fraction of solid in solid bed region

5.6.1.2 PRESSURE DISTRIBUTION AT VARIOUS LOCATIONS SOLID (L/D = 0.8)

Figures 5.24, 5.25 and 5.26 present that the pressure distribution along the right, top, left and bottom air inlet to chimney outlet in the RFB-SG unit without slit. It is observed that the pressure increases from 59-61 kPa in the solid bed region of 120-116 mm when the high velocity air streams enter in the vortex chamber via air inlets. Initially, the higher velocity of air induces to rotate solid particles in the solid-bed thickness of 120-116 mm, and the pressure is reached to its peak value of 61kPa. Further, the pressure decreases in the solid-bed thickness of 116-106 mm and it is almost constant in the location 106-85 mm. The pressure variation in the freeboard region is observed high which is maximum in the right location of the RFB-SG unit chimney outlet, while it is minimum in front of the chimney outlet.

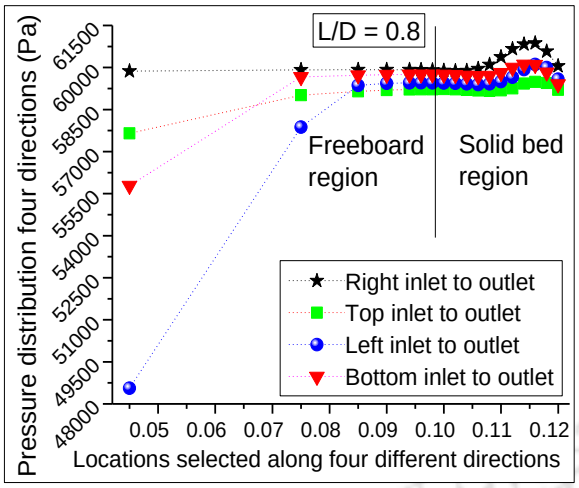

Figure 5.24 Pressure variation in four different directions

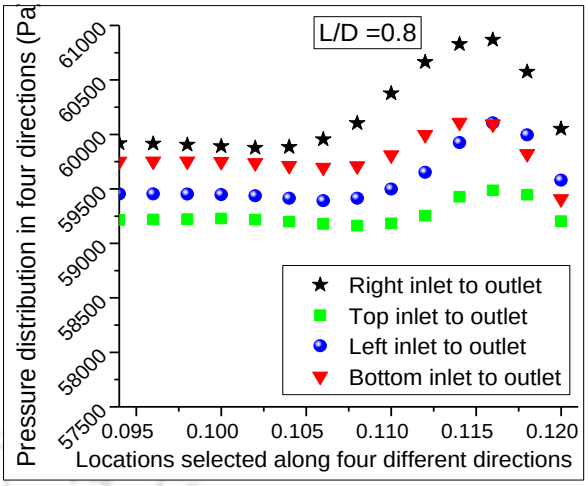

Figure 5.25 Pressure variation in solid bed region

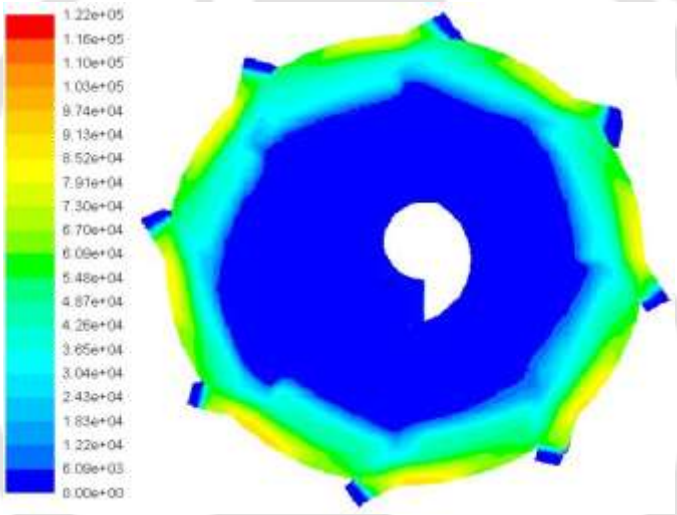

Figure 5.26 Contour of pressure variation in four different directions

5.6.1.3 VARIATION OF AIR VELOCITY IN FOUR DIFFERENT DIRECTIONS SOLID (L/D = 0.8)

Variation of the fluidization air velocity in different four directions is shown in Figs. 5.27, 5.28 and 5.29. It has been observed that the fluidization air velocity in the solid bed region is observed to be maximum of 60 m/s at the selected location point of 116 mm in the right of the RFB-SG unit. Further, the air velocity in the solid bed region start decreasing from 60-14 m/s. However, the variation of fluidization air velocity in all selected directions is similar, but in the freeboard region a major difference is observed in the velocity variations in different directions. The air velocity near to chimney outlet is observed maximum of 75 m/s in bottom location, while it is minimum (14 m/s) in the right side of the unit.

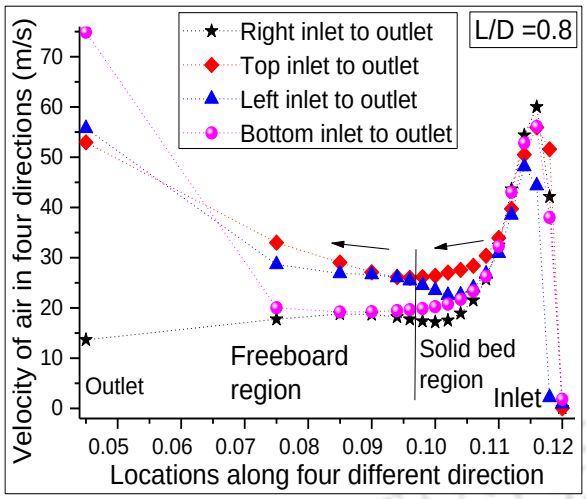

Figure 5.27 Variation of fluidization air velocity in four different directions

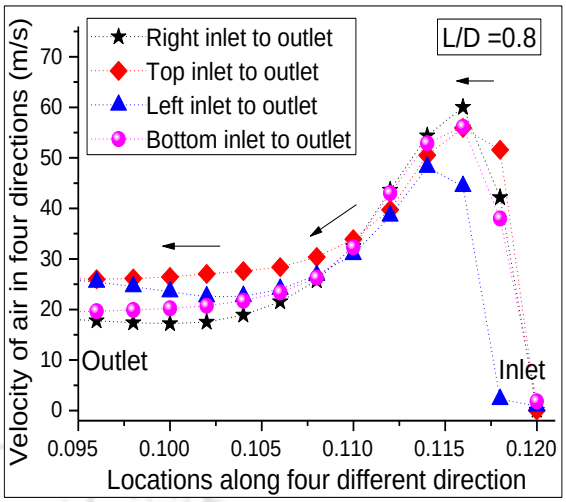

Figure 5.28 Variation of fluidization air velocity in solid bed region

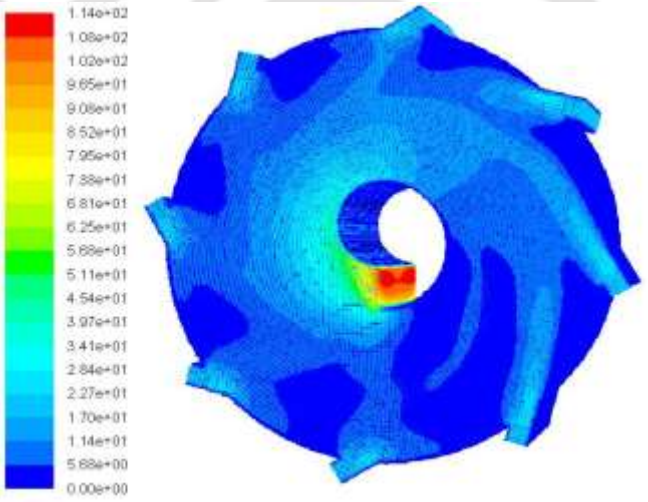

Figure 5.29 Contour of air velocity variation

5.6.1.4 TEMPERATURE DISTRIBUTION ALONG FOUR DIFFERENT DIRECTIONS SOLID (L/D = 0.8)

Temperature distribution along four different (right, top, left, and bottom-inlet to outlet) directions is presented in the Figs. 5.30 and 5.31. while the various location points are selected in each of all four directions at 45, 75, 85, 90, 94, 96, 98, 100, 102, 104, 106, 108, 110, 112, 114, 116, 118, 120 mm, respectively. However, the temperature distribution pattern in all four directions is almost similar. Still, the air temperature along right to chimney outlet direction is comparatively higher than the air temperature in the left to chimney outlet direction. When the air injected into the vortex chamber, the air temperature decreases (337-324 K) rapidly due to dense bed near to the air inlet, especially on the right side (120-106 mm) of the RFB-SG unit as compared to the other three locations of the unit. Further, in the bed-thickness of 106-96 mm the temperature increases from 224-228.5 K.

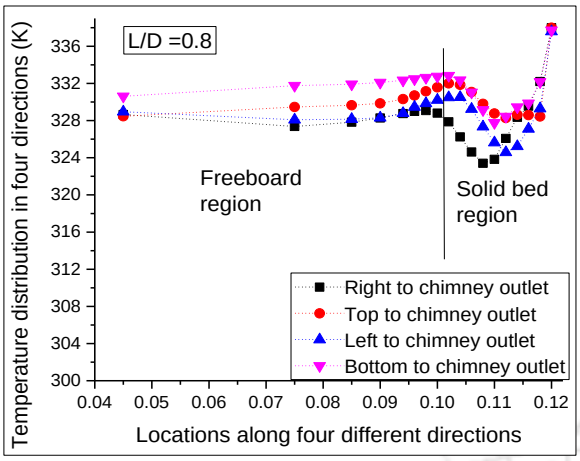

Figure 5.30 Variation of temperature along four different directions

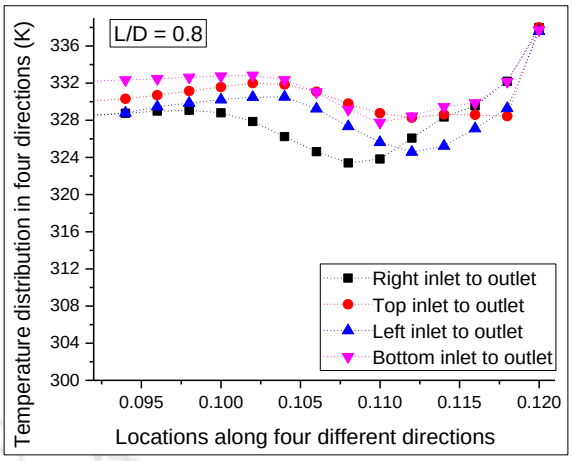

Figure 5.31 Temperature variation in solid-bed region

5.6.2 NUMERICAL ANALYSIS ON SCALE-UP OF RFB-SG UNIT WITHOUT SLIT (L/D= 1)

To increase the RGB-SG unit's fluidization capacity without-slit, a numerical study has been conducted using a commercial software ANSYS FLUENT 14.5, for L/D of 1. The gas-solid hydrodynamic and heat transfer characteristics of the gas-solid phase in the RFB-SG unit without slits have been investigated considering numerous variables described in the following sub-sections.

5.6.2.1 VARIATION IN THE VOLUME FRACTION OF SOLID

The volume fraction of solids in the RFB-SG unit without slit is examined in four different directions, namely right-inlet, top-inlet, left-inlet, and bottom-inlet to the chimney outlet, as shown in Figs. 5.32, 5.33 and 5.34. It is observed that the volume fraction of solid first decreases from 0.55 to 0.33 in the bed-thickness of 118-116 mm due to the impact of air, and the bed-thickness remains constant at 0.33 in the bed-thickness of 116-112 mm, while it decreases 0.03 to 0 in remaining bed thickness of 112-98 mm. It is observed that the variation of volume of solids followed a similar pattern in all four directions of the unit and the density of the solid is observed more stable in the location away from the air inlets.

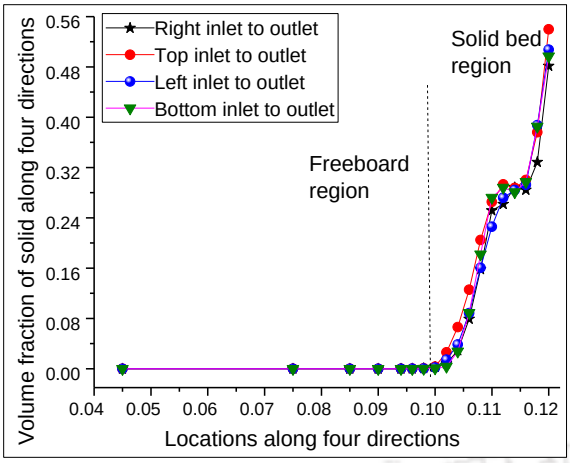

Figure 5.32 Volume fraction of solid in different directions

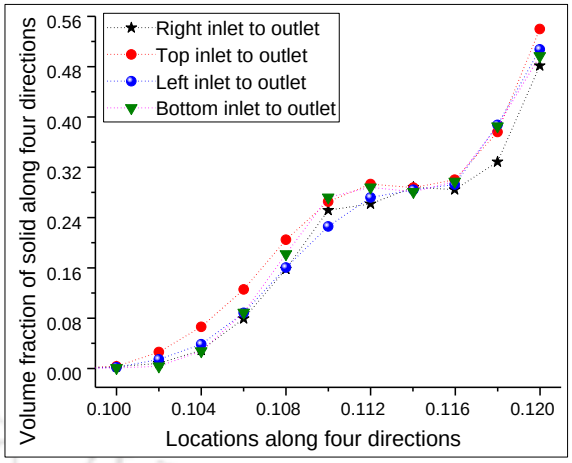

Figure 5.33 Volume fraction of solid in solid bed region

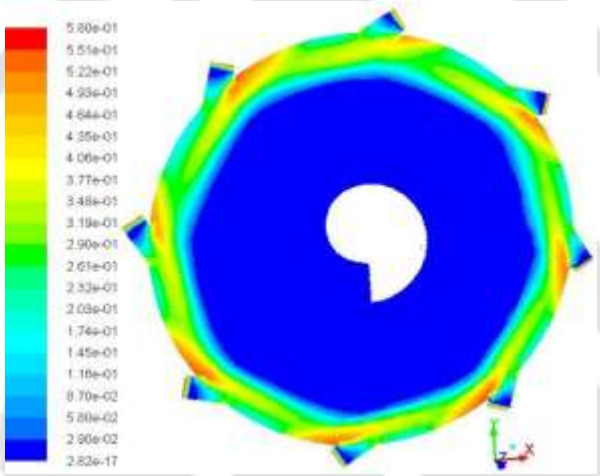

Figure 5. 34 Contour of variation in the volume-fraction

5.6.2.2 PRESSURE DISTRIBUTION AT VARIOUS LOCATIONS

Figures 5.35, through 5.38 present the pressure distribution in solid-bed region in the different directions at various selected locations in the vortex chamber. In each direction, the pressure distribution is investigated at various location points, and pressure contours are shown in Figs. 5.35, 5.36, and contours in Figs. 5.37. Initially, the higher velocity air streams come across the solid particles near to air inlets where pressure seems lower and the high-velocity of air tempts to rotate solid particles in the solid-bed thickness of 4 mm (120-116 mm), and the pressure along right-inlet to outlet direction is reached to a maximum value of 56.5 kPa. Further, the pressure decreases continuously in the solid-bed region from 116-106 mm. However, the pressure variation along right-inlet to outlet

direction is more or less same from the length of 106-40 mm, but the pressure is decreased to 5.25kPa in the bottom-inlet to outlet location.

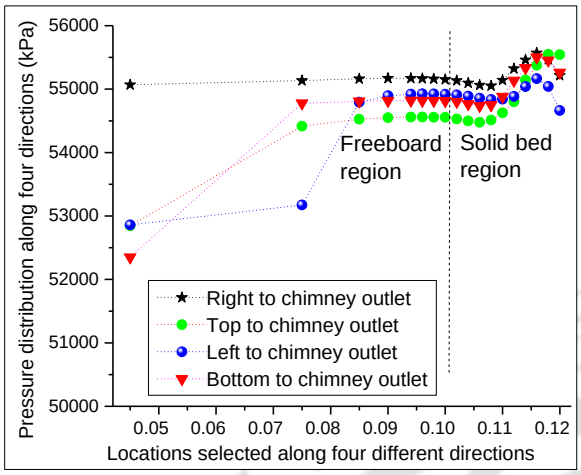

Figure 5.35 Pressure variation in four different directions

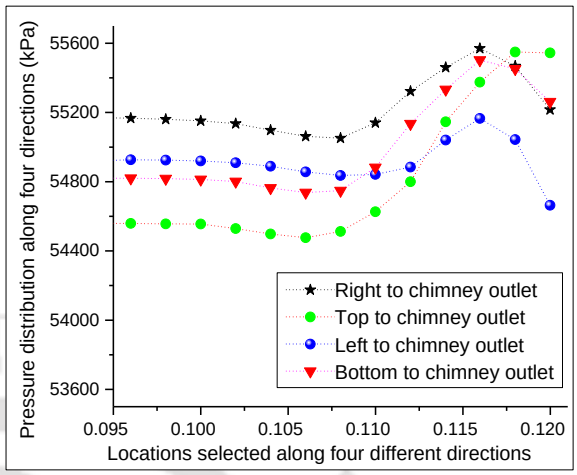

Figure 5.36 Pressure variation in solid bed region

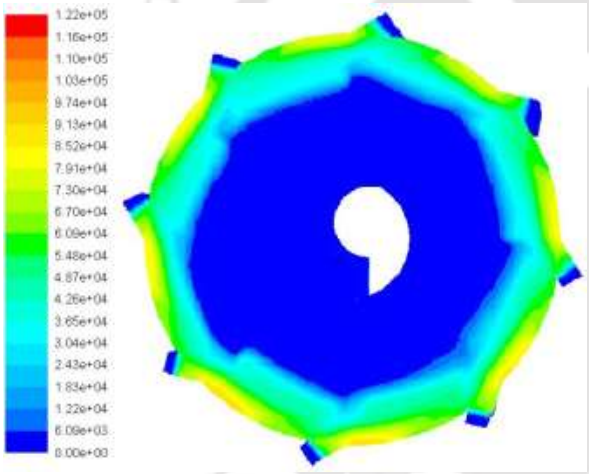

Figure 5.37 Contour of pressure variation

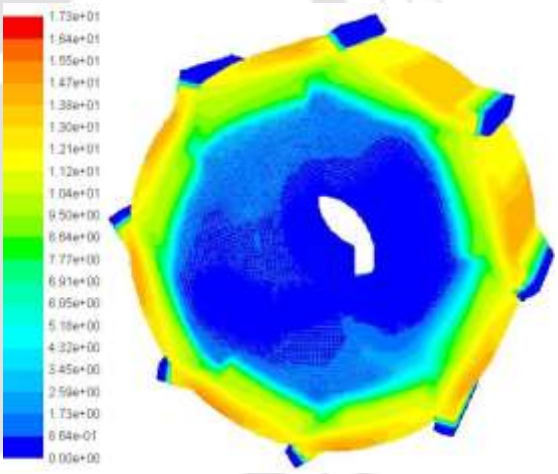

Figure 5.38 Contour of velocity magnitude of solid in 3-D view

5.6.2.3 VARIATION OF FLUIDIZATION AIR VELOCITY IN DIFFERENT FOUR DIRECTIONS

Air velocity distribution in the selected four directions is shown in Figs. 5.39 and 5.40. It has been observed that the fluidization air velocity in the solid bed region is observed the maximum of 55 m/s at the selected location point of 116 mm in the top of the RFB-SG unit. Further, the air velocity in the solid bed region start decreasing from 55-27 m/s. However, the variation of fluidization air velocity in all selected directions is similar, but in the freeboard region a major difference is observed in the velocity variations in different

directions. The air velocity near to chimney outlet is observed maximum (64 m/s) in top location, while it is minimum (13 m/s) in the right side of the unit.

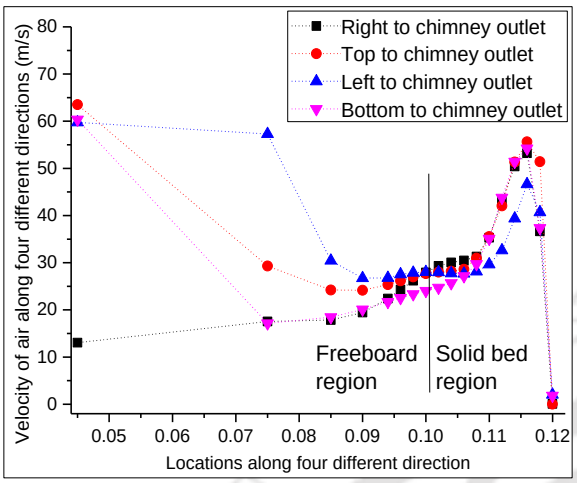

Figure 5.39 Variation of fluidization air velocity in four different directions

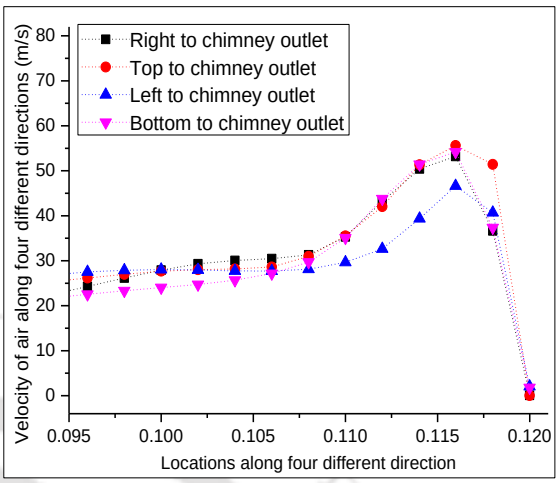

Figure 5.40 Variation of fluidization air velocity in solid bed region

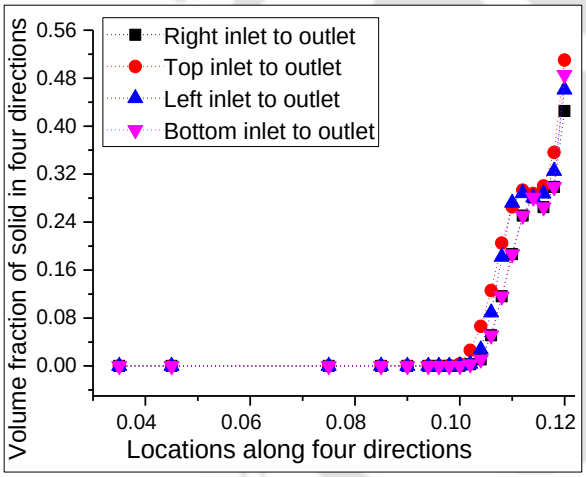

Figure 5.41 Volume fraction of solid in different directions

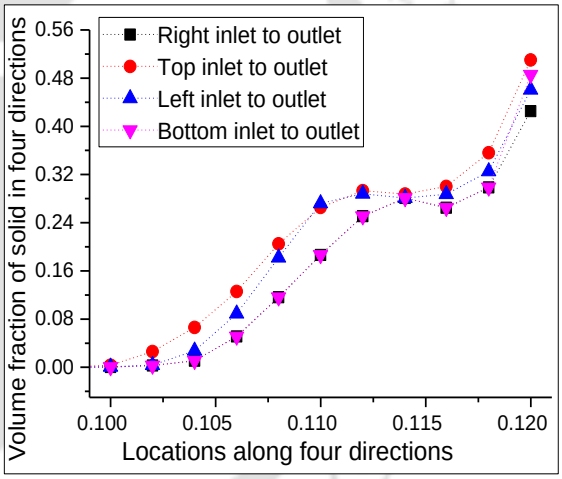

Figure 5.42 Variation of volume fraction of solid in solid-bed region

5.6.3 NUMERICAL ANALYSIS ON SCALE-UP OF RFB-SG UNIT WITHOUT SLIT (L/D=1.2)

To increase the RGB-SG unit's fluidization capacity without-slit, a numerical study has been conducted using a commercial software ANSYS FLUENT 14.5, for length to diameter ratio of 1.2. The gas-solid hydrodynamic and heat transfer characteristics of the gas-solid phase in the RFB-SG unit without slits have been investigated considering numerous variables described in the following sub-sections.

5.6.3.1 VARIATION IN THE VOLUME FRACTION OF SOLID (L/D = 1.2)

The volume fraction of solids in the RFB-SG unit without slit is investigated in four different directions, such as right-inlet, top-inlet, left-inlet, and bottom-inlet into the chimney outlet, as illustrated in Figs. 5.41, and 5.42. It is noticed that the volume fraction of solid decreases from 0.5 to 0.31 in the bed-thickness of 118-116 mm in the top location. Further, the variation of volume-fraction of solid remains unchanged in the bed-thickness of 116-112 mm, and then it decreases again from 0.31-0 in the bed-thickness of 112-98 mm.

5.6.3.2 EFFECT OF INLET AIR TEMPERATURE VARIATION IN FOUR DIRECTIONS

Temperature variation along the right, top, left, and bottom-inlet to outlet) directions are presented in Figs. 5.43 and 5.44. while the various location points are selected in each of all four directions at 40, 75, 85, 90, 94, 96, 98, 100, 102, 104, 106, 108, 110, 112, 114, 116, 118, 120 mm, respectively. However, the temperature distribution pattern in all four directions is almost similar. Still, the air temperature along the right to chimney outlet direction is comparatively higher than the air temperature in the left to chimney outlet direction. When the air is injected into the vortex chamber, the air temperature decreases (337-323 K) rapidly due to the dense bed near to the air inlet, especially on the right side (120-108 mm) of the unit as compared to the other three locations of the RFB-SG unit. Further, in the bed-thickness of 106-96 mm, the temperature increases from 223-333 K.

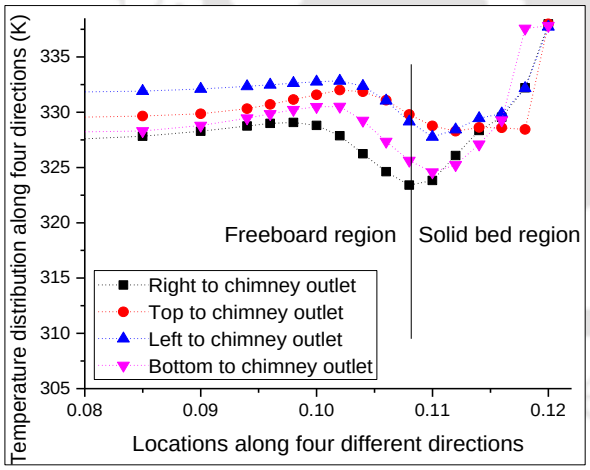

Figure 5.43 Variation of temperature along four different directions

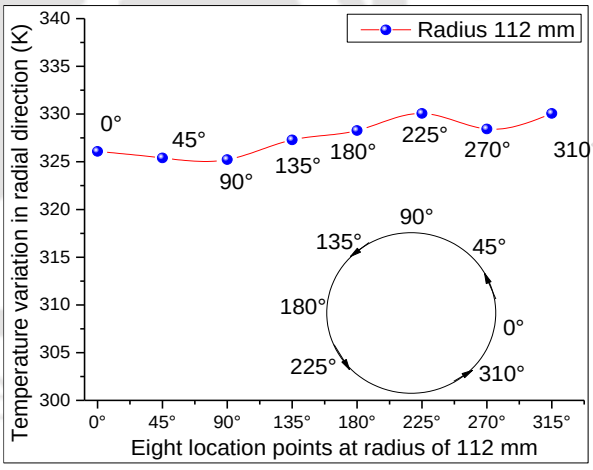

Figure 5.44 Temperature variation along radial direction

The temperature variations in the radial direction at an angular position of 0°, 45°, 90°, 135°, 180°,225°, 270°, and 315° are shown in Fig.5.44. It is observed that the temperature at

selected locations is varying in the range of 325-330K. The maximum and minimum temperatures were observed at the angular position of 225° and 90°, respectively.

5.6.3.3 VARIATION OF HEAT TRANSFER COEFFICIENT IN DIFFERENT FOUR DIRECTIONS

Figure 5.45 shows the variation of heat transfer coefficient among right-inlet, top-inlet, left-inlet, and bottom-inlet to chimney outlet directions. However, the pattern of variation of heat transfer coefficient seems similar in all four directions, but major variations in heat transfer coefficient for a maximum value of 180 W/m²K in the top-inlet location in the solid-bed region at 118 mm. Initially, the heat transfer coefficient increases in all direction in the bed-thickness of 120-112 mm and it decreases from 170-80 W/m²K in the bed-thickness of 112-104 mm. Further, it increases from 80-105 W/m²K in the bed-thickness of 104-94 mm.

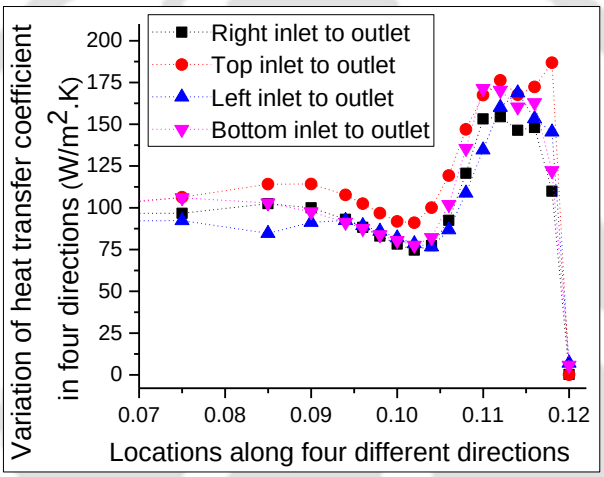

Figure 5.45 Variation of heat transfer coefficient along four directions

5.6.4 COMPARISON OF PRESSURE DISTRIBUTION ALONG RIGHT-INLET TO OUTLET FOR L/D OF 0.2, 0.8, 1, AND 1.2

Figure 5.46 presents the pressure variation in left-inlet to chimney outlet direction for different values of L/D of 0.2, 0.8, 1, and 1.2, respectively. However, the pressure varies symmetrically for each value of L/D, but the pressure intensity in the nearby location of air-inlets is higher for L/D of 1.2 as compared to 0.8, 1, and 1.2. In further bed-thickness of 116-94 mm the pressure variation is observed to be higher for L/D value of 0.8.

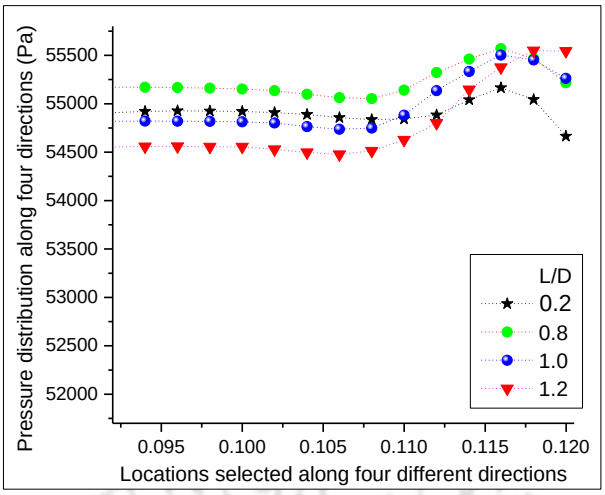

Figure 5.46 Pressure distribution along left-inlet to outlet direction (L/D = 0.2, 0.8, 1, & 1.2)

5.6.5 COMPARISON OF TEMPERATURE DISTRIBUTION IN LEFT-INLET TO OUTLET DIRECTION FOR L/D OF 0.2, 0.8, 1, AND 1.2

Figure 5.47 shows the temperature distribution along left air inlet to chimney outlet for different values of L/D of 0.2, 0.8, 1, and 1.2, respectively. However, the pattern of temperature variation in the solid-bed region seems similar for different length to diameter ratio, but the maximum temperature variation of 6K is observed to be higher at a location point of 0.106 m. Also, it is observed that the temperature for different L/D is varying location-wise which is observed to be higher near the air-inlet for the L/D of 1.2, while it is the value of L/D of 0.8.

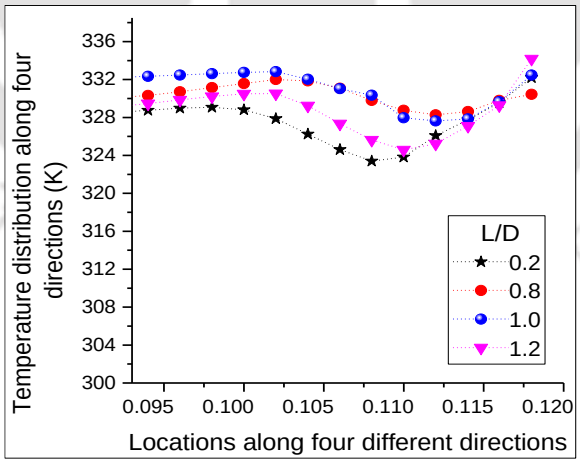

Figure 5.47 Variation of temperature along four different directions

5.6.6 VARIATION OF LOADING CAPACITY, AIR FLOW RATE, AND VOLUME FRACTION OF SOLID FOR L/D OF 0.2, 0.8, 1, AND 1.2

Figures 5.48, 5.49, and 5.50 present the variation of the solid loading capacity of RFB-SG unit, airflow rate, and interpretation of volume fraction of solid with the variation of length to diameter ratio of 0.2, 0.8, 1, and 1.2, respectively. Fig.5.48 shows that the solid-loading capacity increases with the increase of L/D from 0.2-1.2. However, the fluidization capacity increases when L/D increased from 0.2 to 1.2, but further increase of the L/D by more than 1 either causes the solid particles to escape via the chimney outlet or are in solid-bed suspension conditions.

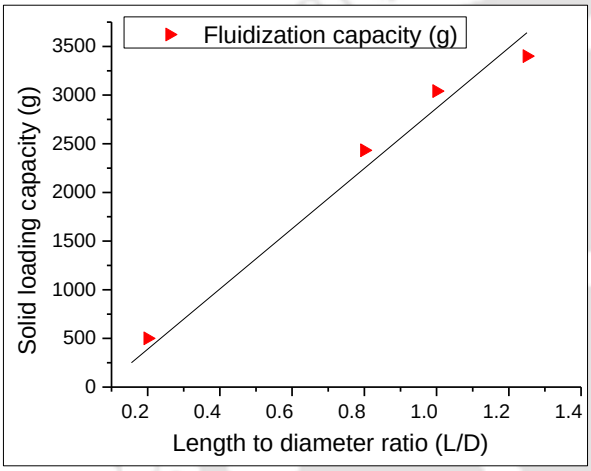

Figure 5.48 Variation of solid capacity

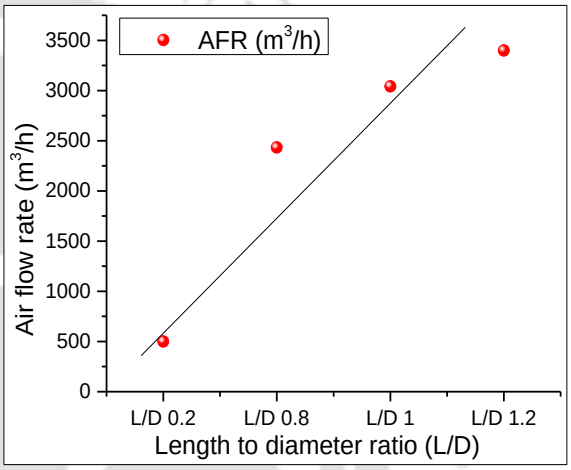

Figure 5.49 Fluidization capacity of the particles for different L/D ratio

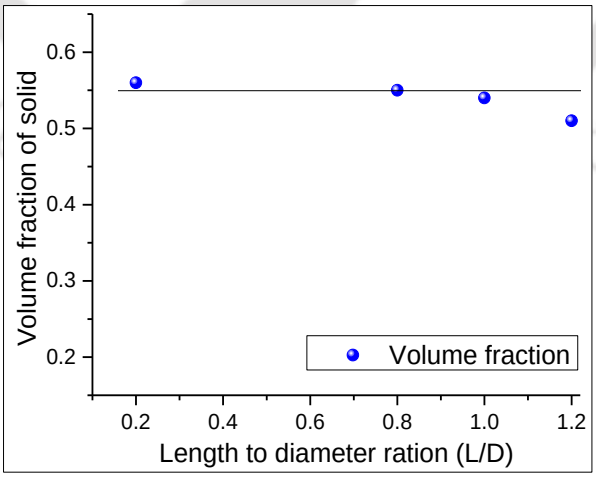

Figure 5.50 Variation of the volume fraction of solid

Figure 5.49 illustrates that for the fluidization of a particular amount of particles in a batch, the airflow rate increases with the increase of the L/D from 0.2 to 1.2. Figure 5.50 shows that a minor variation in volume fraction of solid is observed for L/D of 0.2, 0.8, and 1, but further increase of L/D the volume fraction of solid is decreased. However, the amount of solid in the batch is adopted in the unit of a fixed diameter of 240 mm with varying L/D. The volume fraction is almost the same for L/D of 0.2, 0.8, and 1, but a small variation is observed in the case of L/D of 1.2.

5.7 SUMMARY

In the present chapter, experimental studies on paddy drying have been conducted in the RFB-SG dryer without slit and with-slit. Comparison between experimental results of RFB-SG without slit and with slit has been made. A numerical analysis of better-performing RFB-SG unit without slit has been carried out using commercial software ANSYS FLUENT 14.5. Numerical results obtained without slit has been validated with the experimental results obtained under similar experimental conditions. Furthermore, the RFB-SG unit without slit is scaled-up numerically for three different "length to diameter ratio" of 0.2, 0.8,1, and 1.2, considering various parameters, such as pressure, temperature, the volume fraction of solid, air flow rate, and fluidization capacity of the unit. In the next chapter thermo-economic analysis of the RFB-SG dryer without and with slit are presented.

CHAPTER-6

THERMO-ECONOMIC ANALYSIS

6.1 INTRODUCTION

The energy and exergy analysis of the paddy drying process in the RFB-SG dryer without and with slit are presented in this chapter. Thermodynamic (energy and exergy) and economic analysis were carried out by considering three different cases such as (a) energy used during the drying process for different inventories, (b) drying energy supplied to heat the air, and (c) the energy use ratio. The exergy efficiency of drying air at the dryer inlet and its chimney outlet have been determined. Moreover, the exergy variations at the different dryer locations have also been evaluated for different experiment phases. During the drying operation, several parameters such as atmospheric pressure, drying air temperature, and paddy moisture was recorded in 5 minutes' interval. During the energy and exergy calculations, an average temperature of 5 minutes was taken into account. The atmospheric air is assumed to be constant during the paddy drying operation. The thermodynamic analysis of the RFB-SG dryer is represented in sub-sections 6.2, and the economic analysis of the RFB-SG dryer is represented in subsection 6.3.

6.2. ENERGY ANALYSIS

The energy analysis of a cylindrical-shaped solid beds drying process has been carried out considering the RFB-SG dryer without slit as a thermodynamic system, as illustrated in Also, the energy balance at each inlet and outlet of the system can be achieved by considering the temperature, mass, and heat energy, as shown in Figs. 6.1 and 6.2.

6.2.1 MASS BALANCE EQUATIONS

As shown in Figs. 6.1 and 6.2, the three components, such as drying air, water content, product (granular particles) are considered to be balanced. The mass balance equation of the above-mentioned components can be expressed as [Dincer and Sahin 2004].

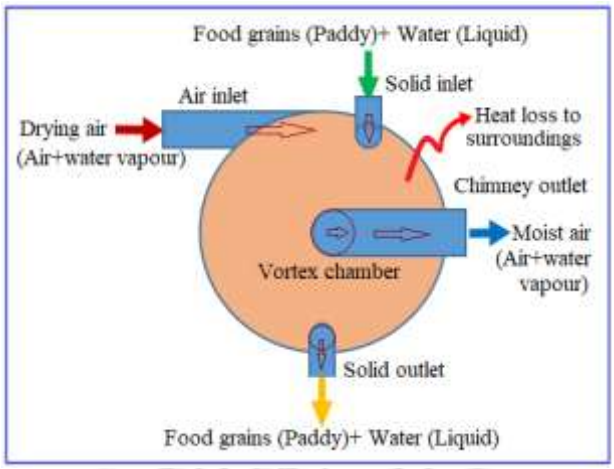

Figure 6.1 Schematic diagram of drying process in RFB-SG dryer without slit

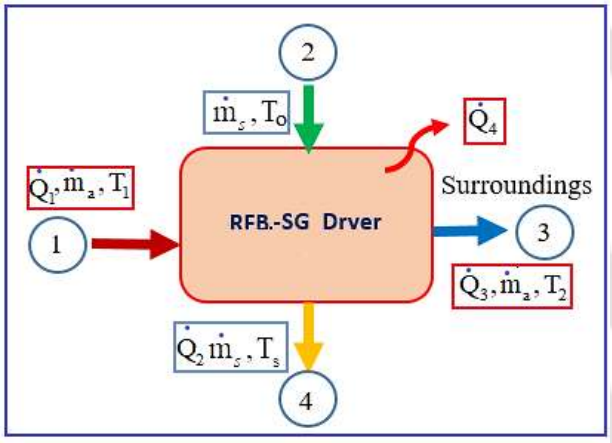

Figure 6.2 The schematic diagram for energy analysis

Drying air: $$(\dot{m}_a)_1 = (\dot{m})_3 = \dot{m}_a \quad (6.1)$$

Water: $$\omega_1 \dot{m}_a + (\dot{m}_{sw})_2 = \omega_3 \dot{m}_a + (\dot{m}_{sw})_4 \quad (6.2)$$

Dried product: $$(\dot{m}_s)_2 = (\dot{m}_s)_4 = \dot{m}_s \quad (6.3)$$

where

m_w : Mass of water

ω : Water vapour

m_a : Mass of air

m_s : Mass of the solid particles

m_{da} : Mass of dry air

Hence, energy estimation of paddy-drying in the RFB-SG dryer can be expressed as in Eq. 6.4 [Celma (2009)]. The relative humidity,

$$\phi = \frac{\omega\, p}{(0.622+\omega)\, p_{sat,T}} \tag{6.4}$$

where $p_{sat,T,}$ ω and p, are saturated vapour-pressure of air, specific humidity, and atmospheric pressure, respectively. The enthalpy of the drying air corresponding to the temperature of the drying air can be expressed as in Eq. (6.5). The equation has made the enthalpy calculations of the drying air;

$$h = Cp_{da}\, T + \omega\, h_{sat,T} \tag{6.5}$$

where C_p, da, T and $h_{sat,T}$ are the specific heat of the drying air, air temperature, and enthalpy of saturated vapour. The energy gained by drying air can be written as;

$$Q_{da,eg} = m_{da} Cp_{da} (T_i - T_0) \tag{6.6}$$

The energy utilized by the RFB-SG dryer without slit,

$$Q_{d,eu} = m_{da} (h_{ida,T} - h_{oda,T}) \tag{6.7}$$

where, subscript i, o and 0 represent the inlet, outlet and ambient conditions.

6.2.2 ENERGY UTILIZATION RATIO (EUR)

The ratio of drying energy utilized by the dryer to the energy gained by the drying air is also called the energy utilization ratio (EUR).

$$EUR = \frac{m_{da} (h_{ida,T} - h_{oda,T})}{m_{da} Cp_{da} (T_i - T_0)} \tag{6.8}$$

6.2.3 ENERGY UTILIZED IN RFB-SG DRYER WITHOUT SLIT

Figure 6.3 presents the value of energy utilized in the drying of varying inventory of 300-500 g, at the airflow rate from 400 to 600 m^3/h at the air temperatures of 328, 333, and 338 K, respectively. The bar diagrams are plotted for three different inlet air temperatures, maintaining 5 K increments. The maximum energy utilization value was 3.52 kJ/s at an air inlet temperature of 338 K, drying air mass flow rate of 600 m^3/h, and inventory of 0.5 kg paddy. The minimum value of energy utilization was 0.4 kJ/s at air temperature 328 K, drying air mass flow rate 400 m^3/h and inventory of 0.4 kg paddy. Energy use is high at a higher air flow rate. The inlet air temperature contributes to the adequate absorption of heat energy by the drying material (paddy), resulting in significant moisture removal.

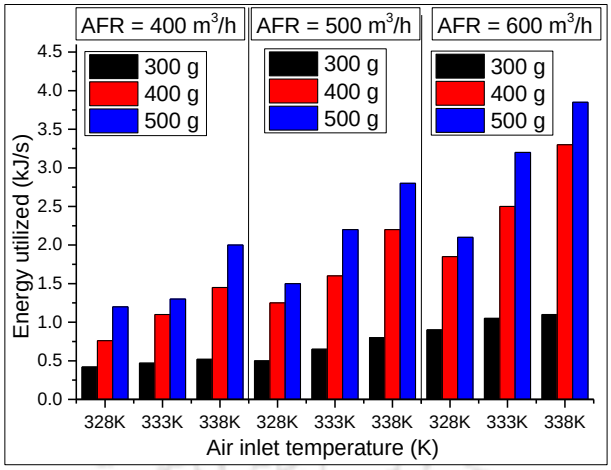

Figure 6.3 Variation of energy utilization with air temperatures, inventory and airflow rates

6.2.4 ENERGY UTILIZATION RATIO IN RFB-SG DRYER WITHOUT SLIT

Figures 6.4, 6.5, and 6.6 show the value of energy utilization ratio in the drying of varying inventory of 300-500 g, at the airflow rate of 400 to 600 m^3/h, at the air temperatures of 328, 333, and 338 K, respectively. The energy utilization ratio is found to be lowest (0.075) at the operating temperature of 328 K, at an air flow rate of 400 m^3/h, and inventory of 300 g paddy. In contrast, it is found to be a maximum (0.332) for paddy drying of 500 g, at an operating temperature of 338 K and an air flow rate of 600 m^3/h. It is observed that the fixed inventory more energy is used at higher air temperature and air flow rate as increasing both the heat and mass transfer rates.

Fast-drying and uniform drying in the RFB-SG dryer has been observed at higher superficial velocity of the air due to higher turbulence. Further, drying air is more effectively utilized at higher inlet air temperature, air flow rate, and inventory loading.

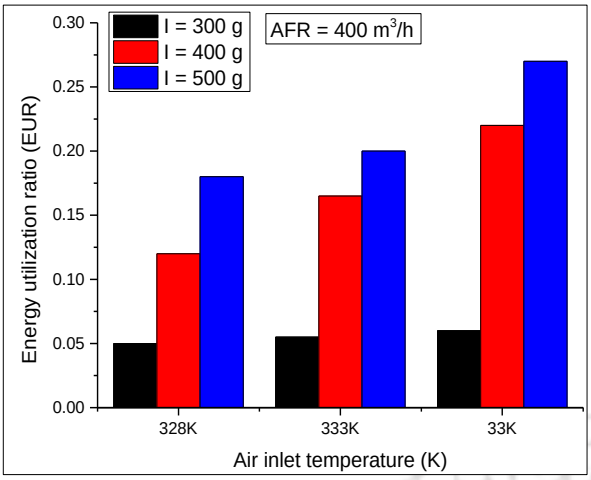

Figure 6.4 Variation of EUR with inventory and temperature, at AFR = 400 m³/h

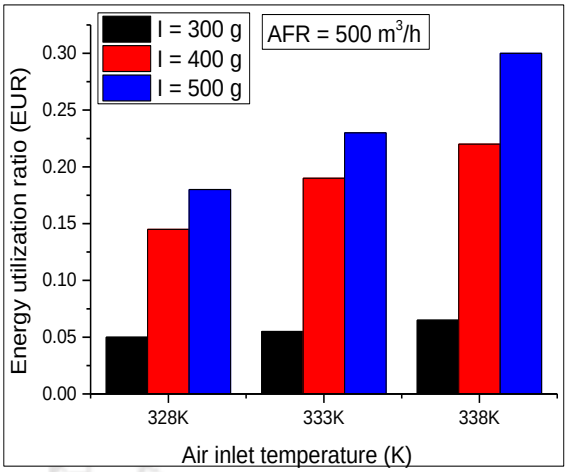

Figure 6.5 Variation of EUR with inventory and temperature, at AFR = 500 m³/h

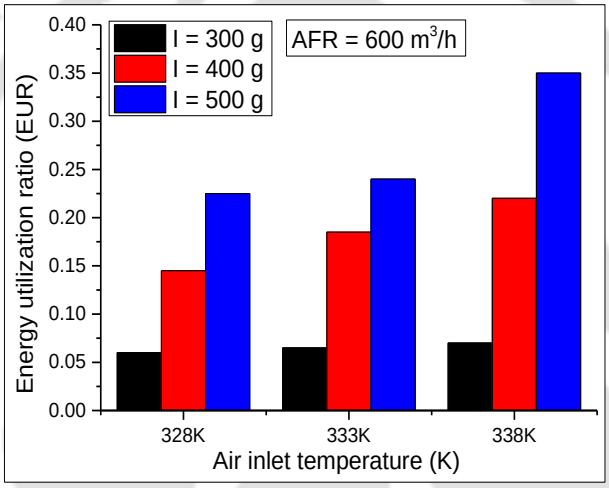

Figure 6.6 Variation of EUR with temperature, and inventory at AFR = 600 m³/h

6.3 EXERGY ANALYSIS

Exergy analysis is concerned with evaluating available energy at various RFB-SG dryer locations, as shown in Fig. 6.7 and the experimental matrix for exergy analysis is given in Table 6.1. This analysis is accomplished by applying the second law of thermodynamics. The expressions for exergy calculations at inlet and outlet of RFB-SG are given in Eq. (6.9) through Eq. (6.12) [Nag (2008)].

$$E_x = \dot{m}_{da} Cp_{da} \left[(T_1 - T_0) - T_0 \ln \frac{T_1}{T_0} \right] \quad (6.9)$$

$$\dot{E}x_{i,d} = \dot{m}_{da} Cp_{da} \left[(T_{i,da} - T_0) - T_0 \ln \frac{T_{i,da}}{T_0} \right] \quad (6.10)$$

$$\dot{E}x_{o,d} = \dot{m}_{da} Cp_{da} \left[(T_{o,da} - T_0) - T_0 \ln \frac{T_{o,da}}{T_0} \right] \quad (6.11)$$

where $T_{i,d} = T_1$, and $T_{o,d} = T_3$ are the inlet air and outlet air temperature of the drying dryer, respectively. Hence, the exergy utilized can be calculated as

$$\sum \dot{E}_U = \sum \dot{E}x_{i,d} - \sum \dot{E}x_{o,d} \quad (6.12)$$

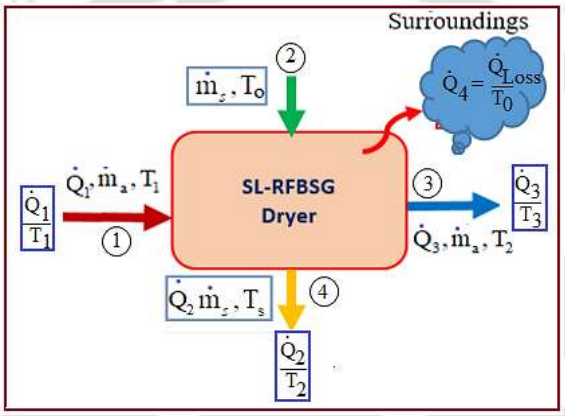

Figure 6.7 Schematic diagram for exergy analysis

Table 6.1 Experimental matrix for exergy analysis

Sl. No.	Inventory (g)	Airflow rate (m^3/h)	Air inlet temperature K)
1	300	400, 500, 600	328, 333, 338
2	400	400, 500, 600	328, 333, 338
3	500	400, 500, 600	328, 333, 338

6.3.1 EXERGY UTILIZED IN DRYING PROCESS

Appendix F presents the exergy inflow and outflow at various air inlet temperature and the airflow rates for paddy drying operation in the RFB-SG dryer without slit. Figures 6.8-6.10 present exergy utilized of paddy drying in different drying conditions. Air inlet temperature, airflow rate, and different loadings are observed in the exergy analysis. It is observed that the exergy utilization increases with an increase in air inlet temperature, airflow rate, and different loading.

Figures 6.8-6.10 present the exergy utilized for airflow rate from 400 to 600 m^3/hat various air temperatures of 328, 333, and 338 K, respectively. The bar diagrams are plotted for three different inlet air temperatures, maintaining 5 K increments. The exergy used is maximum (0.32 kJ/s) at an inventory of 500 g, an airflow rate of 600 m^3/h, and an inlet air temperature of 338K. In comparison, it is found to be the lowest (0.04) kJ/s, at an airflow rate of 400 m^3/h, inventory 300 g, and the temperature 328 K. The following exergy usage value specifies that only a small amount of exergy is used through the outlet of the dryer, leaving a sufficient amount of energy. Hence, there is scope to improve both the drying capacity and drying efficiency, minimizing energy loss.

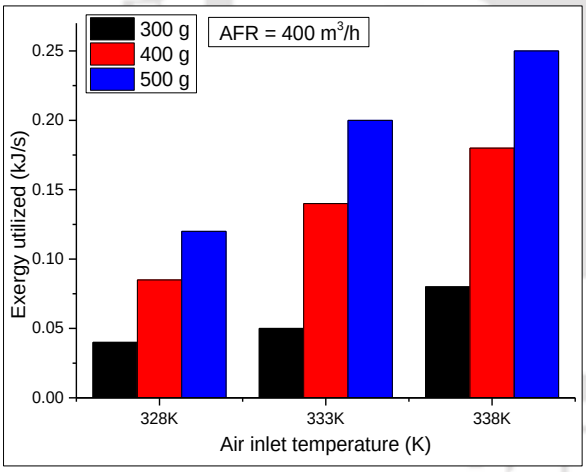

Figure 6.8 Variation of exergy utilization with temperature, inventory, and AFR of 400 m^3/h

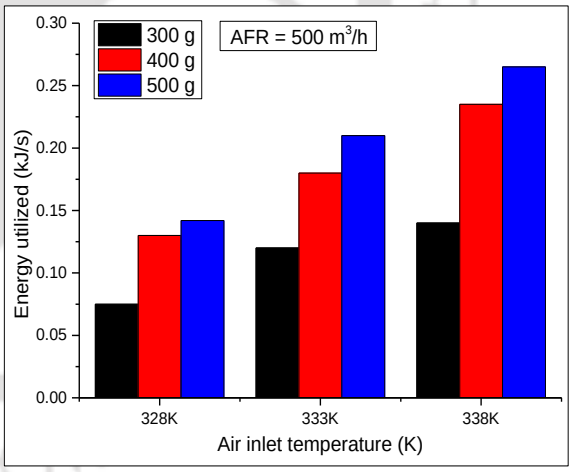

Figure 6.9 Variation of exergy utilization with temperature, inventory and AFR of 500 m^3/h

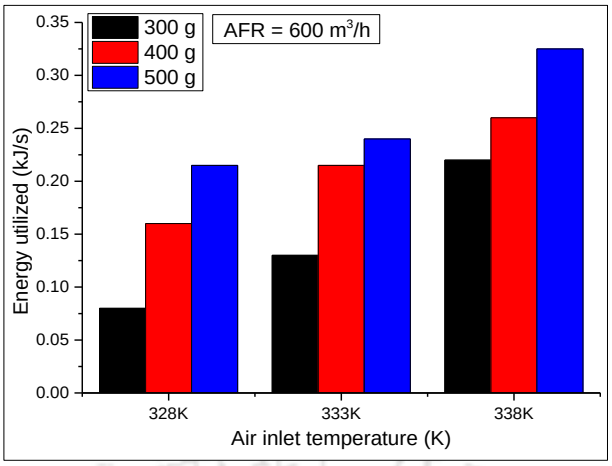

Figure 6.10 Variation of exergy use with temperature and inventory at AFR of 600 m³/h

6.3.2 EXERGY EFFICIENCY

The exergy efficiency can be defined as the ratio of exergy used in the dryer and the exergy supplied to the dryer for the drying process [Dincer and Sahin, (2004)].

$$\eta_{Ex} = \frac{\text{Exergy utilized in moisture removal of the product}}{\text{Exergy supplied to the drying air}} \qquad (6.13)$$

Figures 6.11, 6.12 and 6.13 show the influence of inlet temperature and airflow rate on the exergy efficiency. It has been observed that the exergy efficiency increases with the inlet temperature, airflow rate, and inventory. This is attributed to the better heat and mass transfer mechanism prevailing in RFB-SG dryer. For the inventories of 300, 400, and 500 g paddy, the exergy efficiencies are found to be maximum and minimum at the airflow rates of 600 m³/h and 400 m³/h, respectively.

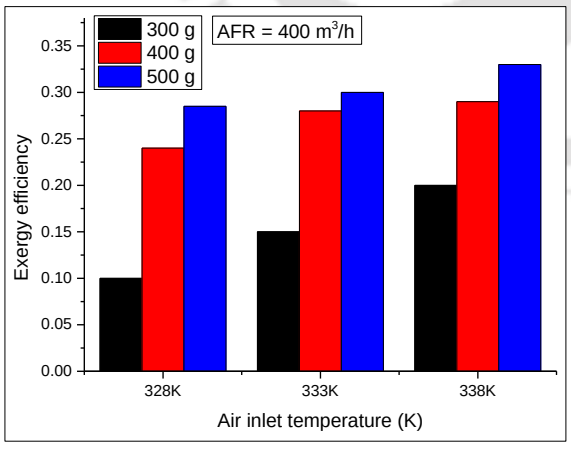

Figure 6.11 Variation of exergy with varying inventory and air temperatures, at AFR of 400 m³/h

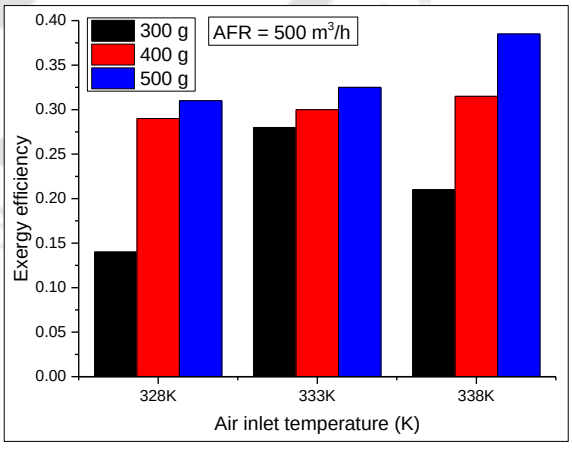

Figure 6.12 Variation of exergy with varying inventory and air temperatures, at AFR of 500 m³/h

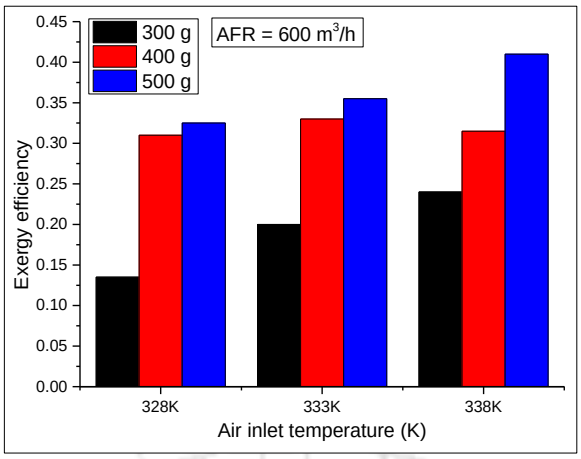

Figure 6.13 Variation of exergy with inventory and air temperatures, at AFR of 600 m³/h

6.4 COMPARATIVE ENERGY ANALYSIS OF RFB-SG DRYER WITHOUT AND WITH SLIT

Figure 6.14 shows the energy utilized in paddy drying in RFB-SG dryer without slit and with slit at different inlet air temperatures, inventories of paddy, and airflow. For an inventory of 300 g, the maximum airflow rate in both the dryers viz. RFB-SG dryer without slit and RFB-SG dryer with slit is maintained at 600 m³/h. The maximum value of energy used for RFB-SG dryer with slit was found to be maximum (3.65 kJ/s) at the air flowrate of 600 m³/h at an operating temperature of 338 K, while the minimum energy (0.95 kJ/s) was utilized at the inlet air temperature of 328 K and airflow rate of 400 m³/h. Similarly, the maximum value of energy used for RFB-SG dryer without slit was found to be maximum (3.52 kJ/s) at the air flowrate of 600 m³/h at an operating temperature of 338 K, while the minimum energy (0.4 kJ/s) was utilized at an inlet air temperature of 328 K, and an airflow rate of 400 m³/h. For the same air inlet temperature, the energy utilization increases fast in RFB-SG dryer with slit, as compared to RFB-SG dryer without slit.

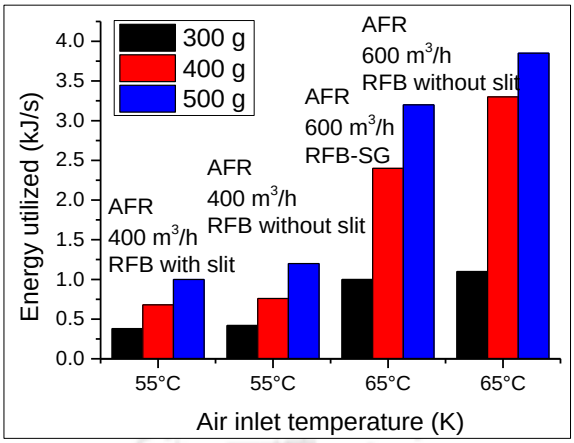

Figure 6.14 Energy used at different temperature and inventory at AFR of 400 and 600 m³/h in RFB-SG dryer without slit.

6.5 COMPARISON OF EXERGY EFFICIENCY

Figures 6.15, 6.16, and 6.17 show the influence of drying air temperature, the air flowrate, and solid loading, respectively. It is observed that exergy efficiency of RFB-SG dryer without slit is comparatively higher than that of RFB-SG dryer with slit. Fig.6.15 shows that on increasing inlet air temperature, the exergy efficiency of the RFB-SG dryer without slit and RFB-SG dryer with slit increased by 50% and 34.6%, respectively. It is seen from Fig. 6.16 that with an increase of 66.6% inventory, the exergy efficiency for RFB-SG without slits and RFB-SG dryer with slit is increased by 50% and 46.5%, respectively. Similarly, it is observed from Fig.6.17 that as the airflow rate increases by 50%, the efficiency of RFB-SG without slit and RFB-SG dryer with slit increases by 52% and 47%, respectively.

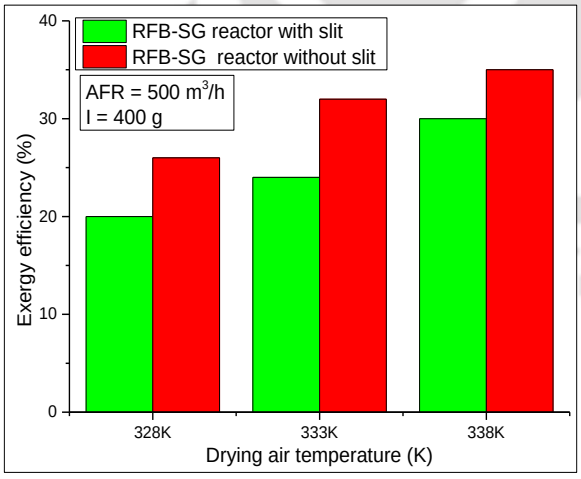

Figure 6.15 Variation of exergy efficiency with air temperature for inventory of 400 g

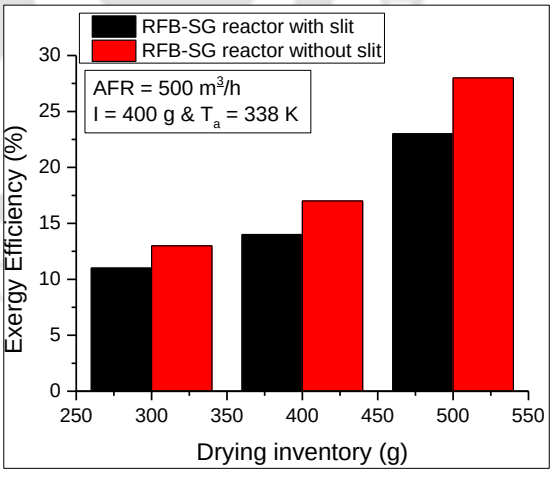

Figure 6.16 Variation of exergy efficiency with inventory at temperature of 338 K

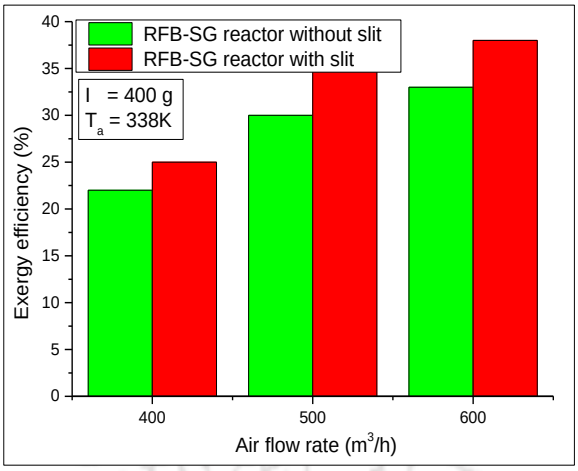

Figure 6.17 Variation of exergy efficiency with airflow rate, at T_a = 338 K and I =400 g

6.6 ECONOMIC ANALYSIS OF RFB-SG DRYER WITH AND WITHOUT SLITS

A RFB-SG drying dryer without slit offers several advantages over conventional drying such as protected drying throughout night and rain, maintenance of food grain (paddy) quality, capacity enhancement, fast-drying, protection from insects, easy control to handle, and cost-effective. This dryer functions with high gravitational force and the volume of RFB-SG dryer is relatively smaller compared to other dryers. An economic assessment of RFB-SG dryer without slit and with slit have been stated in the following subsections.

6.6.1 COST OF DRYING

The cost of drying includes fixed costs and variable costs. The fixed costs are comprising the cost of the rate of interest, depreciation, the cost of repair, and opportunity cost, while the variable cost is concerned with electricity, fuels, and labour costs. The cost of drying can be expressed either as a per-unit cost of weight or as annual cost, depending on the goal of drying as shown in appendix G. In the present calculation, the cost of drying is assumed to as one metric-ton of food grain (paddy). The total cost of drying has been determined as given below:

$$C_D = C_F + C_V \tag{6.14}$$

where C_D, C_F, and C_V are total cost, fixed cost, and variable cost, respectively.

In order to determine the cost of drying, the numerical value of the input measurement is required in addition to the fixed cost and variable cost.

6.6.2 INPUT PARAMETERS AND ASSUMPTIONS FOR ECONOMIC ANALYSIS OF DRYING

For acceptability of the developed methodology economic analysis is performed. While doing the analysis cost associated with repair and maintenance of the setup were not considered. Some assumptions for the cost of paddy-drying calculation are shown in Table 6.2.

Table 6.2 Assumptions for drying cost calculation of paddy

Calculation parameters	RFB-SG dryer without slit	RFB-SG with slit
Dryer service life	10 year	10 year
Capacity per day	21.45 kg	17.6 kg
Drying time for 500 g paddy	26 minutes	32 minutes
Dryer utilization	300 days/year (paddy)	300 days/ year
Initial MC (db) (paddy)	65%	65%
Final controlled MC (db)	13-14%	13-14%
Wet Paddy per 100kg (price)	1300/- (INR)	1300/- (INR)
Dry Paddy per 100kg (price)	2200/- (INR)	2200/- (INR)
Repair and maintenance	2.5% of investment	2.5% of investment
Price per kWh	2.60/- (INR)	2.60/- (INR)
Unskilled Labour wage/day	283/- (INR) (https://clc.gov.in/clc/node/557)	283/- (INR)

6.6.3 FIXED COST

$$C_F = C_{system} + C_{instrum} + C_{depr} + C_{other} \quad (6.15)$$

where

C_F = Fixed cost [Rs/kg]

C_{system} = Cost of the system [Rs/kg]

C_{instr} = Cost of the instrumentation [Rs/kg]

C_{depr}= Cost of the depreciation [Rs/kg]

C_{others} =others cost [Rs/kg]

The average rate of interest per annum is calculated as Rs 3,780

The fixed cost of the dryer is estimated as Rs. 22 per day.

Estimated drying cost per kg is Rs 31.30

6.6.4 VARIABLE COST

The variable cost is an operating cost of the drying system, which consists of several expenses such as labour cost, fuel cost, electricity cost, and other minor costs at which are unforecastable.

$$C_V = C_{labor} + C_{electricity} + C_{others} \tag{6.16}$$

where

$C_{variable}$ = variable cost [Rs/kg]

C_{labour} = labour cost [Rs/kg]

$C_{electricity}$=Electricity cost [Rs/kg]

C_{other}= other cost [Rs/kg]

6.6.5 COST OF ENERGY

$$C_{energy} = \frac{EC.\ C_U}{m_{da}} \tag{6.17}$$

where

EC = Energy consumption [units/batch]

C_u = Cost of electricity per unit [Rs/unit]

m_{dry} = Weight of dried grain per batch [1 kg/batch]

Hence, cost of energy consumed is Energy = Rs. 8.60/kg.

6.6.6 BREAK-EVEN POINT

The break-even point per year in batches is estimated as

$$BEP = \frac{C_F}{m_{day}\left(\Delta P - C_v\right)} \tag{6.18}$$

where ΔP = Price difference of wet and dried grain [Rs/year] .

The detailed calculations of economic analysis are presented in the appendix G.

6.7 COMPARISON OF ECONOMIC ANALYSIS OF DRYER

In the economic analysis of paddy drying, all the related calculations such as drying cost and payback period for both RFB-SG dryers without slit and with slit are presented in Table 6.3. It is seen that both the cost of drying per kg of paddy and the BEP for RFB-SG dryer without slit are lower than that of the RFB-SG dryer with slit. The BEP is observed to

be seven months higher in RFB-SG dryer with-slit than RFB-SG dryer without slit, while the drying cost per kg of paddy is Rs 5.60 higher in RFB-SG dryer with slit than RFB-SG without slit.

Table 6.3 Drying cost per kg and payback period in the year, are described

Dryer	Paddy	
	Payback Period (years)	Drying cost per kg (Rs)
RFB-SG dryer without slit	5/12	11.70
RFB-SG dryer with slit	11/12	14.60

6.8 SUMMARY

In this chapter, thermo-economic analysis of paddy drying process in RFB-SG dryer without and with slit have been carried out. The present chapter highlights the various calculations, such as the energy used, energy utilization ratio (EUR), the exergy utilization, and the exergy efficiency of drying. Based on the experiments it has been observed that RFB-SG dryer without slit is more energy-efficient than the RFB-SG dryer with slit. From the economic point of view, it has been found that the drying cost is lower in RFB-SG dryer without slit as compared to RFB-SG dryer with slit. In the next chapter, summary of the research findings and scope for future work are presented.

CHAPTER-7

CONCLUSIONS AND SCOPE FOR FUTURE WORK

7.1 BRIEF SUMMARY OF THE INVESTIGATION

The present research work focuses on the development of a RFB-SG dryer without slit to minimize the post-harvest losses of food grains (paddy) with importance to maintain the grain quality. RFB-SG dryer without slit has been developed at CFB Lab, IIT Guwahati, according to fluidization capacity and the heat transfer characteristics from the predictions made in the numerical study. The performance of the RFB-SG dryer with and without slits was evaluated experimentally, and comparison was made between them. As the RFB-SG dryer without slit is found better than RFB-SG dryer, hence the fluidization capacity is enhanced numerically in terms of length to diameter ratio. Parametric studies on paddy drying in the RFB-SG dryer without slit and RFB-SG with slit have been carried out to decrease the initial moisture content (IMC) of the food grain 29±4% to 13±0.8%. The quality of the product (particle damage) was tested in terms of milling index. Furthermore, thermo-economic analysis of RFB-SG dryer without and with slit has been carried out to find its appropriateness of launching in rural areas.

7.2 EXPERIMENTAL STUDY OF PADDY DRYING IN RFB-SG DRYER WITH AND WITHOUT SLIT

- The drying time was increased when the air inlet temperature, inventory, and air flow rate increased. To achieve the safe moisture content 13±0.8%), the drying time was observed to be 17 min in RFB-SG without slit and 27 minutes in RFB-SG with slit at the inlet air temperature of 338K, airflow rate 600 m^3/h, and inventory 300 g. In contrast, the initial moisture content of fresh paddy was 29-32% (wb) for the experiments.
- The drying time required to reach MC of 13% was reduced by 15 minutes (37.5 %) in RFB-SG without slit when the air temperature was reduced from 328 to 338 K at the airflow rate of 400 m^3/h for an inventory of 300 g.
- The drying time in RFB-SG without slit is reduced by 10 minutes (30%) with an increase in inlet air temperature from 328 to 338 K at air flow rate of 400 m^3/h for an inventory of 400 g.

- The drying time is found to be increased by 12 minutes (34%) when inventory increased from 300 g to 500 g, inlet temperature of 338 K, and airflow of 400 m^3/h.
- For the inventory of 400 g paddy, at the drying air temperature of 338K and airflow rate of 600 m^3/h the drying time is found to be 19% in RFB-SG dryer without slit than the RFB-SG dryer developed by Pati et al. (2016) which resulted in a reduction of the drying air as well as energy requirement significantly, hence drying efficiency is improved by 20.4%.
- The drying time is assumed to be significantly reduced by increasing the air inlet temperature and the airflow rate. In contrast, degradation of product quality is seen when the air temperature rises above 338 K.

7.3 COMPARISON OF RFB-SG DRYER WITH AND WITHOUT SLITS

- RFB-SG dryer without slit is observed to be an efficient, less complex, and low cost dryer for granular drying in which a sensitive and cost effective element slit is reduced in order to make the dryer simple, easy to handle with improved performance as compared to the RFB-SG dryer with slit.
- Drying time of 500 g paddy at an inlet air temperature of 338K is 23% lesser in RFB-SG dryer without slit than RFB-SG dryer, while the drying time of 300 g paddy is observed 32% lesser in RFB-SG dryer without slits as compared to RFB-SG with slit.
- Though the mass, momentum, and heat transfer occur through the chimney outlet in both dryers, the total amount of air required is 6.47% lower in the RFB-SG dryer than the RFB-SG dryer with slit.
- The drying time of paddy in the RFB-SG dryer without slit is 23% lesser than the RFB-SG dryer with slit, at the air flow rate of 600 m^3/h and air temperature of 338K. Hence, the efficiency of the RFB-SG dryer without slit is higher than RFB-SG with slit due to the reduction of drying time and the amount of air required.

7.4 NUMERICAL STUDY ON RFB-SG DRYER WITHOUT SLIT AND EXPERIMENTAL VALIDATION

- A good agreement between the numerical and experimental results justified the validation of experimental results with the maximum error 0.24%, 17.8%, and 7.72% in the temperature, heat transfer coefficient, and inventory loading measurement, respectively.

7.5 SCALE-UP RFB-SG DRYER WITHOUT SLIT (L/D = 0.2, 0.8, 1 and 1.2)

- Scale-up of RFB-SG dryer is carried out for various length to diameter ratio (L/D) of 0.8, 1, and 1.2, considering a reference of L/D of 0.2.
- Scale-up of the lab-scale RFB-SG dryer without slit has been carried out for the solid loading capacity of 500 g, 1210 g, 2420 g, 3370 g, considering different length to diameters ratios of 0,2, 0,8, 1, and 1.2, respectively.
- On increasing L/D from 0.2 to 1.2, the fluidization capacity is increased. However, L/D above 1.2 was indicating escape of solid particles from the bed. Hence, further increase of loading capacity is not preferred for L/D of more than 1.2.

7.6 SCOPE FOR FUTURE WORK

In the present study, various drying parameters are considered to evaluate the drying performance of the dryers. Extensive research conclusions are discussed. However, there is great scope for further research on the RFB-SG dryer without slit. Some of the works that can be done in the future are given below:

- A scaled-up commercial model of RFB-SG dryer without slit experimentally and a physical extension will be novel research.
- A variety of food grains may be attempted to dry in the RFB-SG dryer without slit with small modifications.
- Grain stabilization may be studied for effective drying and storage.

REFERENCES

Abdollahi, M., Guy, C. and Chaouki, J., 2010. Biomass gasification in rotating fluidized bed. The 13th International Conference on Fluidization -New Paradigm in Fluidization Engineering, May 16-21, Advanced Institute of Science and Technology, Chungnam National University, Korea.

Ahmadzadeh, A., Arastoopour, H., Teymour, F. and Strumendo, M., 2008. Population balance equations' application in rotating fluidized bed polymerization reactor. *Chemical Engineering Research and Design*, *86*(4), pp.329-343.

Akpinar, E., Midilli, A. and Bicer, Y., 2003. Single layer drying behaviour of potato slices in a convective cyclone dryer and mathematical modeling. *Energy conversion and management*, *44*(10), pp.1689-1705.

Ambrosio-Ugri, M.C.B. and Taranto, O.P., 2007. Drying in the rotating-pulsed fluidized bed. *Brazilian Journal of Chemical Engineering*, *24*(1), pp.95-100.

Amer, B.M.A., Hossain, M.A. and Gottschalk, K., 2010. Design and performance evaluation of a new hybrid solar dryer for banana. *Energy conversion and management*, *51*(4), pp.813-820.

Anderson, T.B. and Jackson, R., 1967. Fluid mechanical description of fluidized beds. Equations of motion. *Industrial & Engineering Chemistry Fundamentals*, *6*(4), pp.527-539.

Anwar, S.I. and Tiwari, G.N., 2001. Convective heat transfer coefficient of crops in forced convection drying–an experimental study. *Energy conversion and management*, *42*(14), pp.1687-1698.

Ayensu, A., 1997. Dehydration of food crops using a solar dryer with convective heat flow. *Solar energy*, *59*(4-6), pp.121-126.

Bakker-Arkema, F.W. and Salleh, H.M., 1986. In-store drying of grain: the state of the art. ACIAR Proc. Preserving Grain Quality by Aeration & In-store Drying, 15, 24-30

Basunia, M.A. and Abe, T., 2001. Thin-layer solar drying characteristics of rough rice under natural convection. *Journal of food engineering*, *47*(4), pp.295-301.

Bena, B. and Fuller, R.J., 2002. Natural convection solar dryer with biomass back-up heater. *Solar energy*, *72*(1), pp.75-83.

Celma, A.R. and Cuadros, F., 2009. Energy and exergy analyses of OMW solar drying process. *Renewable Energy*, *34*(3), pp.660-666.

Chakravety, A., 1975. Effects of various drying air temperatures, exposure time and moisture levels of paddy on milling quality. *J. Agric. Engg.*, *12*(2), pp.1-6.

Chakraverty, A.,1981. Post-harvest technology of cereals, pulses and oilseeds. Oxford and IBH, Third Edition.

Chakraverty A. 1994. Post-harvest technology of cereals, pulses and oilseeds. Oxford and IBH, Third Edition.

Chapman S., and Cowling T.G., 1970. The Mathematical Theory of Non-uniform Gases. *Cambridge, 2e éd. I*, *952*, pp.354-356.

Chapman, S., Cowling, T.G. and Burnett, D., 1990. The mathematical theory of non-uniform gases: an account of the kinetic theory of viscosity, thermal conduction and diffusion in gases. *Cambridge university press*.

Chen, X. and Wang, J., 2014. A comparison of two-fluid model, dense discrete particle model and CFD-DEM method for modeling impinging gas–solid flows. *Powder technology*, *254*, pp.94-102.

Chen, Y.M., 1987. Fundamentals of a centrifugal fluidized bed. *AIChE journal*, *33*(5), pp.722-728.

Chen, G., Wang, X. and Li, X., 2014. *Fundamentals of complex networks: models, structures and dynamics*. John Wiley & Sons.

Chokphoemphun, S. and Chokphoemphun, S., 2018. Moisture content prediction of paddy drying in a fluidized-bed drier with a vortex flow generator using an artificial neural network. *Applied Thermal Engineering*, *145*, pp.630-636.

Darvishi, H., Khoshtaghaza, M.H. and Minaei, S., 2015. Effects of fluidized bed drying on the quality of soybean kernels. *Journal of the Saudi Society of Agricultural Sciences*, *14*(2), pp.134-139.

Daud, W.R.W., 2008. Fluidized bed dryers—Recent advances. *Advanced Powder Technology*, *19*(5), pp.403-418.

De Wilde, J. and de Broqueville, A., 2007. Rotating fluidized beds in a static geometry: experimental proof of concept. *AIChE Journal*, *53*(4), pp.793-810.

De Wilde, J. and de Broqueville, A., 2008. Experimental investigation of a rotating fluidized bed in a static geometry. *Powder Technology*, *183*(3), pp.426-435.

De Broqueville, A. and De Wilde, J., 2009. Numerical investigation of gas-solid heat transfer in rotating fluidized beds in a static geometry. *Chemical Engineering Science*, *64*(6), pp.1232-1248.

De Wilde, J. and de Broqueville, A., 2010. A rotating chimney for compressing rotating fluidized beds. *Powder technology*, *199*(1), pp.87-94.

De Wilde, J., 2014. Gas–solid fluidized beds in vortex chambers. *Chemical Engineering and Processing: Process Intensification*, *85*, pp.256-290.

Diamante, L.M. and Munro, P.A., 1993. Mathematical modelling of the thin layer solar drying of sweet potato slices. *Solar energy*, *51*(4), pp.271-276.

Dincer, I. and Sahin, A.Z., 2004. A new model for thermodynamic analysis of a drying process. *International Journal of Heat and Mass Transfer*, *47*(4), pp.645-652.

Dong, L. and Zhihuai, M., 2003. Experimental study on the microscopic structure of stress cracks of rice kernel after sun drying. In *2003 ASAE Annual Meeting* (p. 1). American Society of Agricultural and Biological Engineers.

Dongbang, W., Pirompugd, W. and Triratanasirichai, K., 2010. The drying kinetics of chilies using a rotating fluidized bed technique. *American Journal of Applied Sciences*, *7*(12), pp.1599-1606.

Dutta, A., Ekatpure, R.P., Heynderickx, G.J., De Broqueville, A. and Marin, G.B., 2010. Rotating fluidized bed with a static geometry: Guidelines for design and operating conditions. *Chemical Engineering Science*, *65*(5), pp.1678-1693.

Dutta, S., Loha, C., Chatterjee, P.K., Sadhukhan, A.K. and Gupta, P., 2018. Numerical investigation of gas-particle hydrodynamics in a vortex chamber fluidized bed. *Advanced Powder Technology*, *29*(12), pp.3357-3367.

Ekatpure, R.P., Suryawanshi, V.U., Heynderickx, G.J., De Broqueville, A. and Marin, G.B., 2011. Experimental investigation of a gas–solid rotating bed reactor with static geometry. *Chemical Engineering and Processing: Process Intensification*, *50*(1), pp.77-84.

El-Sebaii, A.A., Aboul-Enein, S., Ramadan, M.R.I. and El-Gohary, H.G., 2002. Experimental investigation of an indirect type natural convection solar dryer. *Energy conversion and management*, *43*(16), pp.2251-2266.

Eliaers, P. and De Wilde, J., 2013. Drying of biomass particles: Experimental study and comparison of the performance of a conventional fluidized bed and a rotating fluidized bed in a static geometry. *Drying technology*, *31*(2), pp.236-245.

Eliaers, P., Pati, J.R., Dutta, S. and De Wilde, J., 2015. Modeling and simulation of biomass drying in vortex chambers. *Chemical Engineering Science*, *123*, pp.648-664.

Ergun, S., 1952. Fluid flow through packed columns. *Chem. Eng. Prog.*, *48*, pp.89-94.

Ertekin, C. and Yaldiz, O., 2004. Drying of eggplant and selection of a suitable thin layer drying model. *Journal of food engineering*, *63*(3), pp.349-359.

Forson, F.K., Nazha, M.A.A., Akuffo, F.O. and Rajakaruna, H., 2007. Design of mixed-mode natural convection solar crop dryers: Application of principles and rules of thumb. *Renewable Energy*, *32*(14), pp.2306-2319.

Froment, G.F., Bischoff, K.B. and De Wilde, J., 1990. *Chemical reactor analysis and design* (Vol. 2). New York: Wiley.

Fudholi, A., Sopian, K., Ruslan, M.H., Alghoul, M.A. and Sulaiman, M.Y., 2010. Review of solar dryers for agricultural and marine products. *Renewable and sustainable energy reviews*, *14*(1), pp.1-30.

Gbaha, P., Andoh, H.Y., Saraka, J.K., Koua, B.K. and Toure, S., 2007. Experimental investigation of a solar dryer with natural convective heat flow. *Renewable Energy*, *32*(11), pp.1817-1829.

Geldart, D., 1973. Types of gas fluidization. *Powder technology*, *7*(5), pp.285-292.

Geldart, D. and Abrahamsen, A.R., 1978. Homogeneous fluidization of fine powders using various gases and pressures. *Powder Technology*, *19*(1), pp.133-136.

Gidaspow, D., 1994. *Multiphase flow and fluidization: continuum and kinetic theory descriptions*. Academic press.

Golmohammadi, M., Assar, M., Rajabi-Hamaneh, M. and Hashemi, S.J., 2015. Energy efficiency investigation of intermittent paddy rice dryer: Modeling and experimental study. *Food and bioproducts processing*, *94*, pp.275-283.

Gunn, D.J., 1978. Transfer of heat or mass to particles in fixed and fluidised beds. *International Journal of Heat and Mass Transfer*, *21*(4), pp.467-476.

Hacıhafızoğlu, O., Cihan, A. and Kahveci, K., 2008. Mathematical modelling of drying of thin layer rough rice. *food and bioproducts processing*, *86*(4), pp.268-275.

Hardy, B., De Wilde, J. and Winckelmans, G., 2019. A penalization method for the simulation of weakly compressible reacting gas-particle flows with general boundary conditions. *Computers & Fluids*, *190*, pp.294-307.

Henderson, S. M., 1957. Milled rice yields. California Agriculture 11(6)15.

Hendorson, S.M., 1961. Grain drying theory (I) temperature effect on drying coefficient. *Journal of Agricultural Engineering Research*, *6*(3), pp.169-174.

Hustrulid, A., 1962. Comparative drying rates of naturally moist, remoistened, and frozen shelled corn. (1962): 64-0067.

Hustrulid, A., 1963. Comparative drying rates of naturally moist, remoistened, and frozen wheat. *Transactions of the ASAE*, *6*(4), pp.304-0308.

Imoudu, P.B. and Olufayo, A.A., 2000. The effect of sun-drying on milling yield and quality of rice. *Bioresource Technology*, *74*(3), pp.267-269.

Jain, D. and Tiwari, G.N., 2004. Effect of greenhouse on crop drying under natural and forced convection I: Evaluation of convective mass transfer coefficient. *Energy conversion and Management*, *45*(5), pp.765-783.

Jangam, S.V., 2011. An overview of recent developments and some R&D challenges related to drying of foods. *Drying Technology*, *29*(12), pp.1343-1357.

Karbassi, A. and Mehdizadeh Z., 2008. Drying Rough Rice in a Fluidized Bed Dryer. J. Agric. Sci. Technol. Vol. 10: 233-241.

Kochetov, L.M., Sazhin, B.S. and Karlik, E.A., 1969. Experimental determination of the optimal ratios of structural dimensions in the whirl chamber for drying granular materials. *Chemical and Petroleum Engineering*, *5*(2), pp.106-108.

Kovacevic, J.Z., Pantzali, M.N., Niyogi, K., Deen, N.G., Heynderickx, G.J. and Marin, G.B., 2015. Solids velocity fields in a cold-flow gas–solid vortex reactor. *Chemical Engineering Science*, *123*, pp.220-230.

Kudal, H.N., Pangavhane, D.R. and Parishwad, G.V., 2009. Study of Photovoltaic Powered Forced Circulation Solar Tunnel Bagasse Dryer. *International Journal of Engineering Studies, ISSN*, pp.0975-6469.

Kulkarni, S.R., Vandewalle, L.A., Gonzalez-Quiroga, A., Perreault, P., Heynderickx, G.J., Van Geem, K.M. and Marin, G.B., 2018. Computational fluid dynamics-assisted process intensification study for biomass fast pyrolysis in a gas–solid vortex reactor. *Energy & fuels*, *32*(10), pp.10169-10183.

Kunii D. and Levenspiel O.,1969. Fluidization Engineering. John Wiley, 8, 44-5

Kuipers, J.A.M., Prins, W. and Van Swaaij, W.P.M., 1992. Numerical calculation of wall-to-bed heat-transfer coefficients in gas-fluidized beds. *AIChE Journal*, *38*(7), pp.1079-1091.

Kunze, O.R. and Prasad, S., 1978. Grain fissuring potentials in harvesting and drying of rice. *Transactions of the ASAE*, *21*(2), pp.361-0366.

Laohavanich, J. and Wongpichet, S., 2009. Drying characteristics and milling quality aspects of paddy dried with gas-fired infrared. *Journal of food process engineering*, *32*(3), pp.442-461.

Lavrich, Z., Wagner, D.R., Taie, Z., Halliday, D. and Hagen, C.L., 2018. Design considerations for small scale rotating fluidized beds in static geometry with screens for fine particles. *Chemical Engineering Research and Design*, *137*, pp.89-100.

Luangmalawat, P., Prachayawarakorn, S., Nathakaranakule, A. and Soponronnarit, S., 2008. Effect of temperature on drying characteristics and quality of cooked rice. *LWT-Food Science and Technology*, *41*(4), pp.716-723.

Lun, C.K.K., Savage, S.B., Jeffrey, D.J. and Chepurniy, N., 1984. Kinetic theories for granular flow: inelastic particles in Couette flow and slightly inelastic particles in a general flowfield. *Journal of fluid mechanics*, *140*, pp.223-256.

Madhlopa, A. and Ngwalo, G., 2007. Solar dryer with thermal storage and biomass-backup heater. *Solar energy*, *81*(4), pp.449-462.

McLeod, R., 1999. *Improved drying of high moisture grains* (No. 434-2016-33639).

Mohapatra S.S and Mahanta P, 2011. Experimental investigation of an indirect type of natural convection dryer for thin layer paddy drying. *International Journal of Mechanical Engineering and Research*, vols. 1, pp 47-54.

Mohapatra, S.S. and Mahanta, P., 2012, January. Thermodynamic evaluation of natural convection paddy dryer. In *2nd International Conference on the Developments in Renewable Energy Technology (ICDRET 2012)* (pp. 1-4). IEEE.

Moon, S.J., Kevrekidis, I.G. and Sundaresan, S., 2006. Particle simulation of vibrated gas-fluidized beds of cohesive fine powders. *Industrial & engineering chemistry research*, *45*(21), pp.6966-6977.

Mujumdar, A.S., 2007. Book Review: Handbook of Industrial Drying, Third Edition, Drying Technology 25 1133–1134.

Nag P.K, 2008. Power plant Engineering, Tata, McGrow Hill, Third edition.

Nakamura, K., Baba, M., Ajmal Khan, M., Du, W., Sasase, M., Hara, K.O., Usami, N., Toko, K. and Suemasu, T., 2013. Lattice and grain-boundary diffusions of boron atoms in BaSi2 epitaxial films on Si (111). *Journal of applied physics*, *113*(5), p.053511.

Ndukwu, M.C., 2009. Effect of Drying Temperature and drying air Velocity on the Drying Rate and Drying constant of Cocoa Bean. Agricultural Engineering International: the CIGRE journal Manuscript 1091.

Niyogi, K., Torregrosa, M.M., Pantzali, M.N., Heynderickx, G.J. and Marin, G.B., 2017. Experimentally validated numerical study of gas-solid vortex unit hydrodynamics. *Powder Technology*, *305*, pp.794-808.

Nygaard D. and Pellett P.L., eds., 1986. Dry Area Agriculture, Food Science and Human Nutrition. New York: Pergamon Press.

Ogawa, S., Umemura, A. and Oshima, N., 1980. On the equations of fully fluidized granular materials. *Zeitschrift für angewandte Mathematik und Physik ZAMP*, *31*(4), pp.483-493.

Padhi, R.K., Dora, D.T.K., Mohanty, Y.K., Roy, G.K. and Sarangi, B., 2016. Hydrodynamics of three-phase fluidization of homogeneous ternary mixture in a conical conduit—Experimental and statistical analysis. *Chinese Journal of Chemical Engineering*, *24*(10), pp.1335-1343.

Pangavhane, D.R., Sawhney, R.L. and Sarsavadia, P.N., 2002. Design, development and performance testing of a new natural convection solar dryer. *Energy*, *27*(6), pp.579-590.

Pati, J.R., Dutta, S., Eliaers, P., Mahanta, P., Chatterjee, P.K. and De Wilde, J., 2016. Experimental study of paddy drying in a vortex chamber. *Drying Technology*, *34*(9), pp.1073-1084.

Pawar, R.S., Takwale, M.G. and Bhide, V.G., 1995. Solar drying of custard powder. *Energy conversion and management*, *36*(11), pp.1085-1096.

Pourbagher, R., Rahmati, M.H. and Alizadeh, M.R., 2016. Air temperature and final grain moisture effects on drying time and milling quality in two types of fluidized bed dryer. *Agricultural Engineering International: CIGR Journal*, *18*(2), pp.449-456.

Prasad, J., Vijay, V.K., Tiwari, G.N. and Sorayan, V.P.S., 2006. Study on performance evaluation of hybrid drier for turmeric (Curcuma longa L.) drying at village scale. *Journal of Food Engineering*, *75*(4), pp.497-502.

Quevedo, J., Pfeffer, R., Shen, Y., Dave, R., Nakamura, H. and Watano, S., 2006. Fluidization of nanoagglomerates in a rotating fluidized bed. *AIChE journal*, *52*(7), pp.2401-2412.

Özbey, M. and Söylemez, M.S., 2005. Effect of swirling flow on fluidized bed drying of wheat grains. *Energy conversion and management*, *46*(9-10), pp.1495-1512.

Rong, D., Mikami, T. and Horio, M., 1999. Particle and bubble movements around tubes immersed in fluidized beds–a numerical study. *Chemical Engineering Science*, *54*(23), pp.5737-5754.

Sankat, C.K., 2006. Drying technologies for Caribbean agro-industry using solar energy. *Solar Assisted Drying Systems Innovative Technologies for Agricultural and Marine Products, ISESCO, Rabat*, pp.229-54.

Savage, G.P., Dutta, P.C. and Rodriguez-Estrada, M.T., 2002. Cholesterol oxides: their occurrence and methods to prevent their generation in foods. *Asia Pacific journal of clinical nutrition*, *11*(1), pp.72-78.

Schaeffer, D.G., 1987. Instability in the evolution equations describing incompressible granular flow. *Journal of differential equations (Print)*, *66*(1), pp.19-50.

Shih, T.H., Liou W.W., Shabbir A., Yang Z., and Zhu J., 1995. A new k–e eddy-viscosity model for high Reynolds number turbulent flows—model development and validation. Computers & Fluids 24 (3), 227–238.

Sobrino, C., Almendros-Ibáñez, J.A., Santana, D. and De Vega, M., 2008. Fluidization of Group B particles with a rotating distributor. *Powder Technology*, *181*(3), pp.273-280.

Soponronnarit, S., Swasdisevi, T., Wetchacama, S. and Wutiwiwatchai, W., 2001. Fluidised bed drying of soybeans. *Journal of Stored Products Research*, *37*(2), pp.133-151.

Sreekumar, A., Manikantan, P.E. and Vijayakumar, K.P., 2008. Performance of indirect solar cabinet dryer. *Energy Conversion and Management*, *49*(6), pp.1388-1395.

Syamlal, M. and O'brien, T.J., 1988. Simulation of granular layer inversion in liquid fluidized beds. *International Journal of Multiphase Flow*, *14*(4), pp.473-481.

Syamlal, M. and Gidaspow, D., 1985. Hydrodynamics of fluidization: prediction of wall to bed heat transfer coefficients. *AIChE Journal*, *31*(1), pp.127-135.

Syamlal, M. and O'Brien, T.J., 1989, January. Computer simulation of bubbles in a fluidized bed. In *AIChE Symp. Ser* (Vol. 85, No. 1, pp. 22-31). Publ by AIChE.

Syamlal, M., Rogers, W. and OBrien, T.J., 1993. *MFIX documentation theory guide* (No. DOE/METC-94/1004). USDOE Morgantown Energy Technology Center, WV (United States).

Tabassum, M.A. and Jindal, V.K., 1992. Effect of drying conditions on moisture removal rate and head yield of Basmati-370. *Pakistan Journal of Agricultural Research*, *13*(4), pp.312-319.

Thompson, J.B., 1955. The thermodynamic basis for the mineral facies concept. *American Journal of Science*, *253*(2), pp.65-103.

Tiris, C., Ozbalta, N., Tiris, M. and Dincer, I., 1994. Experimental testing of a new solar dryer. *International Journal of Energy Research*, *18*(4), pp.483-491.

Toğrul, İ.T. and Pehlivan, D., 2002. Mathematical modelling of solar drying of apricots in thin layers. *Journal of Food Engineering*, *55*(3), pp.209-216.

Triratanasirichai, K., Dongbang, W. and Pirompugd, W., 2011. Mathematical modeling of drying characteristics of chilies in a rotating fluidized bed technique. *American Journal of Applied Sciences*, *8*(10), p.979-983.

Trujillo, W.R. and De Wilde, J., 2012. Fluid catalytic cracking in a rotating fluidized bed in a static geometry: a CFD analysis accounting for the distribution of the catalyst coke content. *Powder technology*, *221*, pp.36-46.

Tsuji, T., Ito, A. and Tanaka, T., 2008. Multi-scale structure of clustering particles. *Powder Technology*, *179*(3), pp.115-125.

Vasquez, S., 2000. A phase coupled method for solving multiphase problems on unstructured mesh. In *ASME 200 Fluids Engineering Division Summer Meeting*.

Volchkov, É.P., Dvornikov, N.A., Lukashov, V.V., Borodulya, V.A., Teplitskii, Y.S. and Pitsukha, E.A., 2012. Study of swirling gas-dispersed flows in vortex chambers of various structures in the presence and absence of combustion. *Journal of Engineering Physics and Thermophysics*, *85*(4), pp.856-866.

Waldo, R.T., and De Wilde J., 2012. Fluid catalytic cracking in a rotating fluidized bed in a static geometry: a CFD analysis accounting for the distribution of the catalyst coke content. Powder Technology, Vol.221, pp. 36–46.

Weber, J.M., Stehle, R.C., Breault, R.W. and De Wilde, J., 2017. Experimental study of the application of rotating fluidized beds to particle separation. *Powder Technology*, *316*, pp.123-130.

Wen, C.Y. and Yu, Y.H., 1966. A generalized method for predicting the minimum fluidization velocity. *AIChE Journal*, *12*(3), pp.610-612.

Wimberly, J.E., 1983. *Technical handbook for the paddy rice postharvest industry in developing countries*. Int. Rice Res. Inst.

Wongpornchai, S., Dumri, K., Jongkaewwattana, S. and Siri, B., 2004. Effects of drying methods and storage time on the aroma and milling quality of rice (Oryza sativa L.) cv. Khao Dawk Mali 105. *Food chemistry*, *87*(3), pp.407-414.

Yadollahinia, A.R., Omid, M. and Rafiee, S., 2008. Design and fabrication of experimental dryer for studying agricultural products. *Int. J. Agri. Biol*, *10*, pp.61-65.

Zaman, M.A., and Bala B.K., 2001. Thin layer solar drying of rough rice. Journal of Food Eng. 47(4). 295-301.

Zhang, Q., Yang, W., Howard, L. and Earp, C.F., 2003. Tracing fissure information by scanning electron microscopy characterization of naturally fissured surfaces of rice kernels. *Transactions of the ASAE*, *46*(6), p.1583.

Zhang, W., 2009. A review of techniques for the process intensification of fluidized bed reactors. *Chinese Journal of Chemical Engineering*, *17*(4), pp.688-702.

APPENDICES

APPENDIX-A

SELECTION OF PARTICLE SIZE

For proper liquefaction of granular particles, the density of the particle bed should be more or less the same everywhere, in the vortex chamber. According to the behaviour of the particle fluidization, these are of four types, as represented in Table A1 [Geldart (1973), Geldart and Abrahamsen (1978)]. Also, Kunii and Levenspiel (1969) stated that the classification of the particle depends on the equivalent mean diameter of the solid particle and an apparent density $(\rho_s - \rho_g)$.

Table A1: Geldart classification of the particles according to their size

Particle Size	Class	Descriptions
0-30 μm	C	These are very fine and most cohesive powder. The fluidization behaviour of these powders is hugely influenced by inter-particle forces
20-100 μm	A	The bed expands before the bubbles appeared, particulate fluidization.
40-1000 μm	B	The particle size falls in between, aggregative fluidization. Bubbles form at the beginning of the fluidization.
>400 μm	D	Fluidization is possible with an unstable particle bed. Even the fluidization is vital for too large particle size.

APPENDIX-B

CALIBRATION OF THERMOCOUPLE

Screw feeder is used to inject paddy into the vortex chamber of the RFB-SG dryer. There are various dosage parameters for feeding paddy grain per second. The Chromel-Alumula (K-Type) thermocouples were calibrated before use in the drying experimentation as shown in Fig.B1 The calibration of thermocouples is made using the oil heater calibration machine. The ambient temperature is taking as reference temperature. The temperature variation of the circulating bath is measured by the thermocouple, while the ambient temperature is assumed as the reference temperature.

Table B.1 Variation of voltage and temperature

Sl. No.	Voltage in mV (Y_1)	Oil temperature °C	Reference temperature °C	Temperature difference (Y_1)
1	0.062	24	19	5
2	0.06	28	19	9
3	0.10	30	19	11
4	0.28	36	19	17
5	0.48	38	19	19
6	0.70	44	19	25
7	0.91	52	19	33
8	1.12	58	19	39
9	1.32	60	19	41
10	1.40	68	19	49
11	1.55	72	19	53
12	1.78	75	19	56
13	1.91	82	19	63
14	2.0	88	19	69
15	2.25	96	19	77
16	2.4	100	16	84
	∑Yi = 18.122			∑ Xi = 650

Also, ∑ Xi2 = 43112.67, ∑ Yi2 = 18.122, (∑ Xi)2 = 422500, (∑ Yi)2 = 328.4,

∑ XiYi = 1029, N = 16 data points

Using regression analysis,

$a = N \sum Xi\ Yi - (\sum Xi \times \sum Yi) / N \sum Xi2 - (\sum Xi)2 = 0.033$

$b = \sum Yi \times \sum Xi2 - (\sum Xi\ Yi \times \sum Xi) / N \sum Xi2 - (\sum Xi)2 = -0.165$

As $Y = a X + b$, $Y = 0.033 X - 0.165$

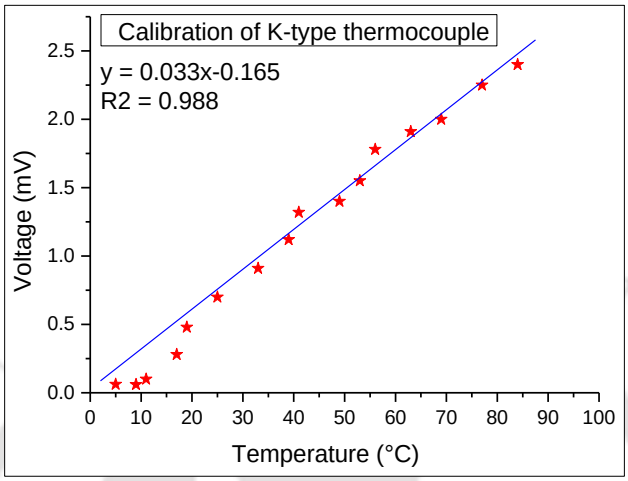

Fig. B.1 Calibration of thermocouple

APPENDIX-C

LIST OF EQUIPMENT/INSTRUMENTS USED

- ✓ Compressor: Capacity- 225 liters, maximum operating pressure-12.30 kg/cm^2., driven by a motor of 3 HP (Manufactured by Ingersoll, Model:7S-01480),
- ✓ Twin Lobe Blower: Capacity-1275 M3/HP, speed-1300 rpm, pressure- 2000 MMWC driven by a 3- phase motor at 1400 rpm, 20 HP, 28.5 amp (Model:710)
- ✓ Data acquisition system with multiplexer: Agilent 34970A
- ✓ Weighing balance: Operating range 0.04-15 kg with error of 2 g (Manufactured by Shyam Switchgears Pvt. Ltd., Model: SP/p1s-15-FLP)
- ✓ Thermocouple calibrator with a constant temperature bath (Make: Julabo)
- ✓ Thermocouple sensor [Chromel-Alumel K-Type]
- ✓ Water-tube manometer board – In-house fabrication
- ✓ Installation of Orifice plate with the U-tube water filled manometer- In-house fabrication

APPENDIX-D

UNCERTAINTY ANALYSIS

The experimental error in drying operation has been determined in terms of the percentage of uncertainty. Accuracy of measuring apparatuses based on the specification given by the manufacturer and seen during experiments are given in the Table D.1. Also, the detail explanation has been given in the appendix D.

Calculation of moisture content of paddy

The percentage of moisture content (MC) available in paddy is calculated using Eqs. (D.1) and (D.2) given by [Zaman and Bala 2001], IRRI [2005].

Moisture content wet basis is

$$MC_{w.b.} = \frac{M_i - M_f}{m_i} X\ 100\ \% \tag{D.1}$$

$$MC_{d.b.} = \frac{M_i - M_f}{m_f} X\ 100\ \% \tag{D.2}$$

where M_i, M_f, MC_{wb} and MC_{db} are initial weight of paddy, final weight of paddy, moisture content of paddy (wet basis) and moisture content of paddy (dry basis), respectively. It can be written as the moisture content (MC) is the function of independent variables.

$$MC_{w.b.} = f\,(W_i, W_f) \tag{D.3}$$

Hence, uncertainty in the measurement of the MC available in the granular material [Bekweith et al. 2003].

$$= \frac{Error}{MC_{db}} X\ 100\ \% \tag{D.4}$$

Percentage of uncertainty

$$= \pm \sqrt{\left(\frac{a_1}{w_f}\right)^2 + \left(\frac{a_2}{w_i}\right)^2}\ X\ 100\ \% \tag{D.5}$$

where a_1 is uncertainty associated with independent variable w_f and a_2 is uncertainty associated with independent variable w_i.

For 500 g of food grain (Paddy)

$$w_f = 290 \pm 7g \qquad \text{where } a_1 = \pm 7g$$

$$w_i = 500 \pm 10g \qquad \text{where } a_2 = \pm 10g.$$

Therefore, the percentage of uncertainty of MC available in food grain (Paddy) is

$$= \pm \sqrt{\left(\frac{7}{290}\right)^2 + \left(\frac{10}{500}\right)^2} \text{ X } 100\ \% = \pm 2.001\%. \qquad \text{(D.6)}$$

Table D.1 Measured value of uncertainty for different experimental parameters

Uncertainty (%)		
Experimental parameters	RFB-SG dryer without slit	RFB-SG dryer with slit
Temperature	± 4.4	± 5
Solid loading	± 5.1	± 4.8
Air flow rate	± 4.8	± 4.6
Initial MC	± 4	± 4
Final MC	± 0.8	± 0.8

APPENDIX-E

DRYING QUALITY TEST OF PADDY

In the context of the present investigation, the nutritional value, protein, fat, fiber, and carbohydrate found in paddy were examined before drying and after drying, in three sequential time intervals of 10, 20, and 30 minutes, as shown in Table E1. In this investigation, the nutritional contents such as carbohydrate, protein, fiber, and fat in the paddy grains have been examined using the anthrone, Kjeldahl, crude fiber estimation, and soxhlet extraction methods. Examination of nutrients of all nutrients has been observed that during the drying process of paddy, the percentage of almost all nutrients decreases with increasing drying time, due to biological changes during the drying process macronutrient content of paddy found to be reduced. Due to the occurrence of a chemical reaction (Maillard reaction), the percentage of carbohydrates and protein is reduced. In addition, the percentage of protein in grains decreases due to oxidation that occurs during the drying operation, as reported by [Savage et al. (2002)].

Table E.1 Nutritional value in paddy samples collected at a drying time interval of 10 minutes

Sample type	Normal	10 (minutes)	20 (minutes)	30 (minutes)
% of Carbohydrate	81.5	78.8	77	76
% of Protein	14	13.7	12.5	12.4
% of Fiber	2.75	2.45	1.9	1.8
% of Fat	2.4	1.9	1.53	1.48

MILLING QUALITY OF PADDY

The milling quality of the paddy dried in the RFB-SG dryer without slit is examined, at the drying air temperature of 333 K and airflow rate of 400 m^3/h. The milling quality has been estimated by using equations E.1 and E.2. The weight of milled-rice is the sum of the weight of broken rice and head rice in the sample collected sample [Padhi et al. (2016)]. A sample of 100 g paddy was taken from RFB-SG dryer without slit to examine the milling

quality in which around 78% of milled rice obtained, while the percentage of head rice and broken rice are found 67% and 10%, respectively.

$$\text{Percentage of head rice} = \frac{\text{weight of whole grain after milling}}{\text{weight of paddy sample}} \text{ X } 100\ \% \quad \text{(E.1)}$$

$$\text{Percentage of broken rice} = \frac{\text{weight of broken grain after milling}}{\text{weight of paddy sample}} \text{ X } 100\ \% \quad \text{(E.2)}$$

$$\text{Percentage of head rice} = \frac{\text{weight of milled rice}}{\text{weight of paddy sample used}} \text{ X } 100\ \% \quad \text{(E.3)}$$

APPENDIX- F

EXERGY INFLOW AND OUT FLOW FOR RFB-SG DRYER WITHOUT SLIT

The exergy inlet and out flow in the dryer have been calculated using formula given below.

$$E_x = \dot{m}_{da} Cp_{da} \left[(T_1 - T_0) - T_0 \ln \frac{T_1}{T_0} \right] \quad (F.1)$$

where E_x, m_{da}, C_p, T_1, and T_o are exergy of the system, mass of dry air, specific heat of drying air, temperature of drying air, and the atmospheric temperature, respectively.

Table F.1 Exergy inflow at various inlet air temperature and air flow rate.

Air flow rate (m^3/h)	Exergy inflow (kJ/s)			Exergy outflow (kJ/s)		
	328 K	333 K	338 K	328 K	333 K	338 K
400	0. 165	0.230	0.310	0.137	0.198	0.236
500	0.206	0.287	0.387	0.155	0.275	0.312
600	0.247	0.345	0.465	0.187	0.308	0.335

EXERGY INFLOW AND OUT FLOW FOR RFB-SG DRYER WITH SLIT

Table F.2 Exergy inflow at various inlet air temperature and air flow rate.

Air flow rate (m^3/h)	Exergy inflow (kJ/s)			Exergy outflow (kJ/s)		
	328 K	333 K	338 K	328 K	333 K	338 K
400	0. 167	0.228	0.314	0.135	0.200	0.238
500	0.209	0.288	0.390	0.156	0.277	0.315
600	0.248	0.347	0.468	0.185	0.310	0.341

APPENDIX-G

ECONOMIC ANALYSIS OF PADDY DRYING IN RFB-SG DRYER WITHOUT SLIT

Table G.1. Economic analysis of paddy drying in RFB-SG dryer without and with slit

Parameters	RFB-SG dryer without slit	RFB-SG dryer with slit
Wet paddy	1300/-	1300/-
Dry paddy rate	1800/-	1800/-
Electricity kWh	2.60/-	2.60/-
Unskilled labour for 4 dryers	Rs. 283 per day	Rs. 283 per day
Rate of interest	13.50% of investment	13.50% of investment
Repair and Maintenance	2.5% of investment	2.5% of investment
Dryer utilization	300 days	300 days
Dryer cost	Rs 18000	25000
Instrumentation	Rs 10000	10000
Drying of paddy per day	21.45 kg per day	17.6 kg per day

The calculation of electric heater power and blower mass flow rate are described as:

CFM = 1,75 x (Watt per temperature difference) (G.1)

(www.agmark.nic.in, www.botanical.com)

ECONOMIC ANALYSIS OF PADDY DRYING IN RFBSG DRYER WITHOUT SLIT

The calculation of total electricity used per hour in RFB-SG dryer = 3 kW

Total cost of dryer = Rs 18,000 + Rs. 10,000 = Rs 28,000

Considerable total lifetime of dryer = 10 years

The total interest of investment per year at 13.50% = 3,780.

Fixed cost instalment per year = Fixed cost/year + yearly rate of interest

= Rs 2,800 + Rs 3,780 = Rs 6,580

Annual repairing and maintenance at 2.5% of initial investment = Rs 700

Table G.2 One-day expenditure of paddy drying in RFB-SG dryer without slit

Expenditures	Cost
Fixed cost per day	Rs 22
Maintenance cost per day	Rs 2.35
Electricity cost per day	Rs.156
Unskilled labour per day per dryer	Rs 70.75
Total expenditure at 1 dryer per day	Rs 151

Expenditure of paddy drying of 21.45 kg = Rs. 251.10.

The cost of drying per kg of paddy = Rs. 11.70

Total weight of dried paddy is 15 kg from wet paddy of 21.45 kg.

Selling of 1 kg dry paddy is collected by extra = Rs. 30

Total collected money for paddy of 15 kg = Rs. 15x30 = Rs. 450

Profit = Selling price of paddy – Expenditure for paddy drying

Profit = Rs. 450 – Rs. 251 = Rs 199 per day

Yearly profit for 300 days = Rs. 199×300 = Rs. 59700

BREAK EVEN POINT

The break-even point per year in batches is estimated as

$$BEP = \frac{C_F}{S}$$

where S is net annual saving (profit), and C_F is capital cost (investment).

BEP = (Rs 28,000/Rs 60225) = 5 Months**.**

The cost of one kg wet paddy and BEP for RFB-SG dryer without slit are Rs. 11.70 and 6 months, respectively.

SIMILARLY, THE ECONOMIC ANALYSIS OF PADDY DRYING IN RFB-SG DRYER WITH SLIT

The calculation of total electricity used per hour in RFB-SG dryer = 3 kW

Total cost of dryer = Rs 25,000 + Rs. 10,000 = Rs 31,000

Considerable total lifetime of dryer = 10 years

The total interest of investment per year at 13.50% = 4185.

Fixed cost instalment per year = Fixed cost/year + yearly rate of interest

= Rs 3,500 + Rs 4,185 = Rs 7,685

Annual repairing and maintenance at 2.5% of initial investment = Rs 775

Table G.3 One-day expenditure of paddy drying in RFB-SG dryer with slit

Expenditures	**Cost**
Fixed cost per day	Rs 27.5
Maintenance cost per day	Rs 2.5
Electricity cost per day	Rs.156
Unskilled labour per day per dryer	Rs 70.75
Total expenditure per day	Rs 256.75

Expenditure of paddy drying of 17.6 kg = Rs 256.75

The cost of drying per kg of paddy = Rs 14.60

Total weight of dried paddy is 12.30 kg from wet paddy of 17.6 kg.

Selling of 1 kg dry paddy is collected by extra Rs 30.

Total collected money for paddy of 12.30 kg = Rs 12.30 x 30 = Rs 369

Profit = Selling price of paddy – Expenditure for paddy drying

Profit = Rs 369 – Rs 256.75 = Rs 112 per day

Yearly profit for 300 days = Rs 112 ×300 = Rs 33,675

BREAK EVEN POINT

The break-even point per year in batches is estimated as

$$BEP = \frac{C_F}{S}$$

where S is net annual saving (profit), and C_F is capital cost (investment).

BEP = (Rs 31,000/Rs 33,675) = 11/12 year

The cost of one kg wet paddy and BEP for RFB-SG dryer are Rs 14.60 and 11 months, respectively.

LIST OF PUBLICATIONS

Journals

1. P. Singh, Mahanta, P. and Kalita, P., 2020. Numerical study on the gas-solid hydrodynamics and heat transfer in a rotating fluidized bed with static geometry dryer. ***International Journal of Heat and Mass Transfer,*** *153*, p.119666.

2. Singh, P., Kalita, P. and Mahanta, P., 2020. Numerical study of the hydrodynamics and heat transfer characteristics of gas–solid in a slit-less rotating fluidized bed in static geometry. ***Journal of Thermal Analysis and Calorimetry***, *141*(6), pp.2647-2656.doi.org/10.1007/s10973-020-10070-w.

3. Singh, P., Kalita, P. and Mahanta, P., 2020. Experimental study of food grain drying in a gas–solid vortex reactor. ***Drying Technology***, pp.1-13. Dio:10.1080/07373937.2020.1835948.

4. Singh, P., Mahanta, P. and Kalita, P., 2021. A comparative analysis and scale-up of a novel slit-less gas-solid vortex reactor dryer with spiral chimney versus conical chimney outlet. ***International Communications in Heat and Mass Transfer,*** *121*, p.105112.doi.org/10.1016/j.icheatmasstransfer.2021.105112.

5. Singh, P.**,** Kalita, P., and Mahanta, P., 2021. A novel slit-less gas-solid vortex reactor dryer: Experimental validation and scale-up. ***Journal of the Taiwan Institute of Chemical Engineers*** (2020). doi.org/10.1016/j.jtice.2021.01.017.

6. Singh, P., Mahanta, P and Kalita, P., 2021. Energy perspective of granular drying in a rotary fluidized bed dryer in static geometry without slit: an application in granular drying. ***International Communications in Heat and Mass Transfer*** (under review).

7. Singh, P., Mahanta, P and Kalita, P., 2021 Numerical investigation of fluid flow and heat transfer in a gas-solid vortex reactor without slit: Scale-up and optimization. ***International Communications in Heat and Mass Transfer*** (Under review).

8. Singh, P., Mahanta, P and Kalita,P. 2021. Thermo-economic analysis of gas-solid vortex reactor dryer with and without slit. ***Innovative Food Science & Emerging Technologies*** (communicated).

Book Chapters

9. Singh, P., Kalita, P., Mahanta, P. and Das, H.J., 2021. Study of Granular Food Material Drying in a Pilot-Scale Rotating Fluidized Bed with Static Geometry Dryer. In ***Recent Advances in Mechanical Engineering*** (pp. 555-562). Springer, Singapore.

10. Singh, P., Kalita, P. and Mahanta, P., 2019. Study of agricultural product drying in a rotating fluidized bed with static geometry. ***Post-Harvest Technology and Value Addition***, *1*, pp.1-8.

Conferences

11. Singh, P., Mahanta, P., and Kalita, P., 2020. Study of agricultural product drying in a slit-less rotating fluidized bed dryer with static geometry. ***International Conference on Thermal Engineering and Management Advances (ICTEMA-2020)***, 27-28 June 2020 Jalpaiguri Government Engineering College, Jalpaiguri, West Bengal 735102, India.

12. Singh, P., Mahanta, P., and Kalita, P., 2020. Study of agricultural product drying in a rotating fluidized bed with static geometry dryer with and without slits. ***International Conference on Recent Trends in Developments of Thermo-fluids and Renewable Energy (TFRE-2020)*** 24-26th June 2020, at National Institute of Technology Arunachal Pradesh, India.

13. Singh, P., Kalita, P., and Mahanta, P., 2019. Numerical study of the hydrodynamics and heat transfer of a gas-solid rotating fluidized bed in static geometry dryer. The ***2nd International Mechanical Engineering Conference (IMEC) - 2019*** to from 29th November to 1st December 2019, at National Institute of Technology, Tiruchirappalli, Tamil Nadu.

14. Singh, P., Mahanta, P., and Kalita, P., 2020. Numerical study of gas-solid vortex reactor with spiral chimney. ***1st online National Conference on Recent Trend in Thermal Sciences and Alternate Energy Resources (RTTSAER2020)*** on 1st July 2020, at Government college of Technology, Coimbatore and National Institute of Technology, Arunachal Pradesh.
15. Singh, P., Purkayastha, R., Kalita, P., Mahanta, P., 2018. Development and performance evaluation of an efficient and user-friendly rotating fluidized bed in static geometry (RFBSG) dryer, ***National conference on Waste to Energy Conversion (WEC-2018)***, December 28-29, 2018, NIT Mizoram, Mizoram.